Analysis of Ventricular Depolarisation and Repolarisation Using Registration and Machine Learning

by

Filip Karisik

Bachelor of Engineering (Electrical and Electronic Engineering) with First Class Honours,
The University of Adelaide, Australia, 2018

Bachelor of Finance,
The University of Adelaide, Australia, 2018

Thesis submitted for the degree of

Doctor of Philosophy

in

School of Electrical and Electronic Engineering
The University of Adelaide, Australia

November, 2022

Supervisors:

Associate Professor Mathias Baumert, The University of Adelaide

Professor Prashanthan Sanders, The University of Adelaide

In honour of my loving grandmother Zlatana

THE UNIVERSITY
of ADELAIDE

Abstract

Our understanding of cardiac diseases has greatly advanced since the advent of electrocardiography (ECG). With the increasing influx of available data in recent times, significant research efforts have been put forth to automate the study and detection of cardiac conditions. Naturally, the focus has progressed toward studying dynamic changes in ventricular depolarisation and repolarisation across serial recordings - as complex beat-to-beat changes in morphology manifest over time. Manual extraction of diagnostic and prognostic markers is a laborious task. Hence, automated and accurate methods are required to extract markers for the study of ventricular lability and detection of common diseases, such as myocardial ischemia and myocardial infarction.

The aim of this thesis is to improve automated marker extraction and detection of diseases for the study of ventricular depolarisation and repolarisation lability in ECG. As such, two novel template adaptation methods capable of capturing complex beat-to-beat morphological changes are proposed for three-dimensional and two-dimensional data, respectively. The proposed three-dimensional template adaptation method provides an inhomogeneous method for transforming template vectorcardiogram (VCG) by exploiting registration-inspired parametrisation and an efficient kernel ridge regression formulation. Analysis across simulated data and clinical myocardial infarction data demonstrates state-of-the-art results. The two-dimensional template adaptation method draws from traditional registration-based techniques and treats the ECG as a two-dimensional point set problem. Validation against previously employed simulated data and a gold-standard annotated clinical database demonstrate the highest level of performance. Subsequently, frameworks employing the proposed template adaptation techniques are developed for the automated detection of ischemic beats and myocardial infarction. Furthermore, a small study analysing ventricular repolarisation variability (VRV) in non-ischemic cardiomyopathy (CM) is considered, utilising markers of cardiac lability proposed in the development of the three-dimensional template adaptation system.

In summary, this thesis highlights the necessity for custom template adaptation methods for the accurate measurement of beat-to-beat variability in cardiac data. Two novel state-of-the-art methods are proposed and extended to study myocardial ischemia, myocardial infarction and non-ischemic CM.

Statement of Originality

I certify that this work contains no material which has been accepted for the award of any other degree or diploma in my name, in any university or other tertiary institution and, to the best of my knowledge and belief, contains no material previously published or written by another person, except where due reference has been made in the text. In addition, I certify that no part of this work will, in the future, be used in a submission in my name, for any other degree or diploma in any university or other tertiary institution without the prior approval of the University of Adelaide and where applicable, any partner institution responsible for the joint award of this degree.

The author acknowledges that copyright of published works contained within the thesis resides with the copyright holder(s) of those works.

I give permission for the digital version of my thesis to be made available on the web, via the University's digital research repository, the Library Search and also through web search engines, unless permission has been granted by the University to restrict access for a period of time.

I acknowledge the support I have received for my research through the provision of an Australian Government Research Training Program Scholarship.

Signed

Date

Acknowledgments

I would like to express the sincerest of appreciation for my supervisor and mentor Associate Professor Mathias Baumert. Mathias provided me with unconditional support, absolute academic freedom and every opportunity to succeed. I am immensely thankful for the fact that Mathias entertained all my ideas, reasonable or not, permitting me to explore new paths whilst simultaneously ensuring my success. It was a true pleasure working alongside Mathias and watching our relationship evolve over the course of my candidature. I would also like to thank my co-supervisor Professor Prashanthan Sanders for providing me with exposure to multidisciplinary research practices early on in my tenure.

I would like to extend great thanks to my collaborator Dr. Martin Schmidt (Technische Universität Dresden) for his constant availability and willingness to share data. Additionally, I would like to extend my sincerest appreciations for my Italian collaborators from Università degli Studi di Milano, Professor Alberto Porta and Dr. Beatrice Cairo. Alberto afforded me with a truly unique opportunity for which I am eternally grateful. I thank the former the Head of School, Associate Professor Wen Soong, for taking the time to provide me with guidance before undertaking my doctoral studies, and with a subsequent offer of study. I would also like to thank Associate Professor Withawat Withayachumnankul for his never-ending compassion and support throughout my candidature. Similarly, a great thanks to the support staff and all my other colleagues within the School of Electrical and Electronic Engineering. Thank you to Madhu and Simon. Seldom do you meet the same type of odd-ball as yourself, but I was fortunate enough to have that opportunity twice. I am forever grateful for their support and friendship.

I extend a great thanks to all my friends over the years who were able to distract me from my academic pursuits and various ruts. Just to name a few - Marko, Aleksa, Milos, Joe, Narayan, Gian and most recently Stan. There is a plethora of other names not on that list, to whom I am eternally indebted.

Finally, I would like to thank all my family for their support. Mum and dad, I don't know where I'd be without all your sacrifices. I can't imagine what it would've felt like uprooting your life and moving to a foreign planet. Thank you for doing so again when I moved to Melbourne. I am sure that I could write a thesis on all your sacrifices alone. To my cousin, thank you for always being supportive and believing in me more than I ever could. This

Acknowledgments

Conventions

This thesis is typeset using the MiKTeX software - where Texmaker was used as the text editor. Matlab®/RStudio were utilised for figure generation and statistical analysis. Harvard style referencing is employed throughout this thesis.

Publications

Journals

Karisik, F. and Baumert, M. (2019), 'Inhomogeneous Template Adaptation of Temporal Quasi-Periodic Three-Dimensional Signals', *IEEE Transactions on Signal Processing* **67**, pp. 6067–6077.

Karisik, F. and Baumert, M. (2021), 'Template Adaptation of 2D Quasi-Periodic Data Using a Soft-Assign Localized Correspondence Matrix', *IEEE Transactions on Signal Processing* **69**, pp. 826–836.

Karisik, F. and Baumert, M. (2022), 'Template Adaptation of 2D Quasi-Interpretable Classification of Cardiac Ischemic Beats Using Correspondence Based Template Adaptation', unpublished manuscript.

Conference papers

Karisik, F., Schmidt, M. and Baumert. M (2019), 'Beat-to-Beat Analysis of Vectorcardiogram by Inhomogeneous Template Adaptation', *2019 41st Annual International Conference of the IEEE Engineering in Medicine and Biology Society (EMBC)*, pp. 83–86.

Karisik, F. and Baumert. M (2019), 'A Long Short-Term Memory Network to Classify Myocardial Infarction Using Vectorcardiographic Ventricular Depolarization and Repolarization', *2019 Computing in Cardiology (CinC)*, pp. 1–4.

Schmidt, M., Karisik, F., Zausender, S., Linke, A., Malberg, H. and Baumert. M (2021), 'Evaluation of Ventricular Repolarization Variability in Patients With Nonischemic Dilated Cardiomyopathy From Vectorcardiography *2021 Computing in Cardiology (CinC)*, pp. 1–4.

Patents

The University of Adelaide, (2021), 'Template Adaptation Method for Analysing 2D Quasi-Periodic Biomedical Signals', *AUS Patent Application Ser. No. 2020904577* (filed 2020-09-12). PCT stage.

Contents

List of Figures

List of Figures

List of Tables

List of Tables

Acronyms

AF	atrial fibrillation
AHA	American Heart Association
AM	amplitude modulation
ANN	artificial neural network
ANS	autonomic nervous system
AV	atrioventricular
AWGN	additive white Gaussian noise
BIDMC	BIDMC PPG and Respiration
BW	baseline wander
CAD	coronary artery disease
CCTA	coronary computed tomography angiogram
CM	cardiomyopathy
CNN	convolutional neural network
CULM	Complex Upper-Limb Movements
CVD	cardiovascular disease
DALY	disability adjusted life years
DEFINITE	Defibrillators in Non-Ischemic Cardiomyopathy Treatment Evaluation
DTW	dynamic time warping
DV	distance variability
ECG	electrocardiography
ECHO	echocardiogram
EM	electrode movement
EST-T	European ST-T
FFD	free form deformations

GOFR	generalised orthogonal forward regression
HCM	hypertrophic cardiomyopathy
HPC	high performance computing
HR	heart rate
HRV	heart rate variability
ICD	implantable cardioverter-defibrillator
IDT	inverse Dower transform
kNN	k-nearest neighbour
LDA	linear discriminant analysis
LSTM	long short-term memory
LV	left ventricular
LVEF	lower ventricular ejection fraction
MA	muscle artefact
MIT-BIH Arrhythmia	MIT-BIH Arrhythmia
MLL	mean loop length
MRI	magnetic resonance imaging
PCA	principal component analysis
PD	panic disorder
PPG	photoplethysmogram
PTB	Physikalisch-Technische Bundesanstalt
QTDB	QT Database
QTV	QT variability
QTV_i	QT variability index
REM	rapid eye movement
RNN	recurrent neural network
SA	sinoatrial

SCD	sudden cardiac death
SD	standard deviation
SDQT	standard deviation of QT
SNR	signal-to-noise ratio
SVD	singular value decomposition
SVM	support vector machine
TCRT	total cosine R to T
THEW	Telemetric and Holter ECG Warehouse
TPS	thin plate splines
VA	ventricular tachyarrhythmia
VCG	vectorcardiogram
VRV	ventricular repolarisation variability
VT	ventricular tachycardia

Introduction

CARDIAC health is critical for the function of all human physiological processes and sustenance of life. Ventricular depolarisation and repolarisation lability can be observed in electrocardiography (ECG) and employed to study heart disease. Thus, the development of accurate systems capable of automatically extracting cardiac markers and detecting disease is critical for the advancement of biomedical science related to cardiac health. This chapter describes the motivations for the research conducted on automated cardiac analysis in this thesis. Additionally, the original contributions of this thesis are presented.

1.1   Introduction

In a 2007 essay for The New York Review (Dyson, 2007), Freeman Dyson, a pioneer of twentieth century physics and avid futurist, predicted that "the twenty-first century will be the century of biology". His self-admitting realisation that "biology is now bigger than physics", paved the way for his belief that the domestication of biotechnology will revolutionise our lives over the next fifty years. Dyson's outlook, which echoes both purist elements of scientific realism and optimism, has already begun across the broad range of research and applications defined under biotechnology. In this context, computer vision and machine learning extend themselves as natural processes in enabling automated diagnosis and scientific progress in biomedical research. However, the application of such technologies is at its infant stages of being realised and will require a concerted effort to be solidified as foundational tools in this new age.

Heart arrhythmia and disease have been long studied due to their quality-of-life, mortality and socio-economic implications. Globally, cardiovascular disease (CVD) is the leading cause of mortality and a large contributing factor to disability (Roth *et al.*, 2020). Furthermore, CVD impacts are continuing to increase across all countries with the exception of high-income countries (Roth *et al.*, 2020). Likewise, disability adjusted life years (DALY), which is a cumulative measure of the number of years lost due to ill-health, disability or early death, has also seen an increasing trend over the last three decades (Roth *et al.*, 2020). To estimate the financial burden, a recent American Heart Association (AHA) report indicated that medical and productivity costs associated with CVD stood at \$555 billion in 2015 and are expected to rise to \$1.1 trillion by 2035 (Dunbar *et al.*, 2018). The culmination of these startling trends and figures highlights the importance of increased efforts in research and policy related to CVD.

The ECG and the closely related vectorcardiogram (VCG) have been previously studied to identify markers of CVD and arrhythmia. The ECG represents variations in the summed electrical potential generated by heart muscle (Clark and Kruse, 1990). Similarly, VCG is a method of recording both the magnitude and direction of the summed electrical forces generated by the cardiac cycle across time. Subtle variations due to physiological changes manifest as morphological deviations in the ECG and vary across different cardiac conditions. In the case of myocardial infarction, more commonly known as heart attack, the changes have been shown to be observable in beat-to-beat QT variability (QTV) of the ECG (Schmidt *et al.*, 2014, 2018a) and VCG (Hasan *et al.*, 2012a). Similarly, for myocardial ischemia - which refers to the obstruction by a partial or complete blockage of

a coronary artery from plaque, morphological changes are known to arise in the ST-interval of the ECG (Alpert *et al.*, 2000; Thygesen *et al.*, 2007, 2012, 2018). In a position statement, Baumert *et al.* (2016a) proposed that more sophisticated tools for the analysis of subtle morphological changes are required to study QTV and other markers. This thesis focuses on the development of tools capable of accurately capturing such subtle variations in two-dimensional and three-dimensional ECG. Similar to other areas of research where template matching (or correspondence matching) is employed (e.g. biomedical computer vision), image registration inspired methods are utilised to achieve this.

The development of automated tools capable of capturing morphological changes may provide more accurate analysis and classification methods. Ultimately, the purpose of automation in biomedical applications is three-fold: (a) to reduce the manual labour required by medical practitioners, (b) to decrease human error by such laborious manual efforts and (c) to minimise the variability in assessment by different medical practitioners (i.e. have an unbiased consensus). The extraction of morphological features in ECG has been well studied with evidence suggesting template adaptation tools yield superior results to their counterparts (Baumert *et al.*, 2012). However, for the three-dimensional representation of summed electrical activity in the heart, sophisticated methodologies for feature extraction are sparse. Hence, in this thesis, we propose an inhomogeneous template adaptation method for VCG. Conversely, numerous ECG-specific tools have been proposed to extract important morphological features in the analysis of ventricular depolarisation and repolarisation variability (Porta *et al.*, 1998; Zifan *et al.*, 2005; Vullings *et al.*, 1998; Dubois *et al.*, 2007; Rincón *et al.*, 2011; Martinez *et al.*, 2004), however, these methods have been shown to yield lower accuracy compared to template matching techniques across simulated data (Baumert *et al.*, 2012) and annotated clinical data (Schmidt *et al.*, 2014). Although having demonstrated superior performance to their counterparts, template matching techniques share common drawbacks such as strictly performing homogeneous adaptations (Berger *et al.*, 1997; Starc and Schlegel, 2006) or not addressing the correspondence problem (Schmidt *et al.*, 2014, 2018a). More specifically, the correspondence problem relates to finding corresponding samples between two sets of data. In this thesis, for the case of the ECG, we incorporate mathematically smooth inhomogeneous adaptations with correspondence assignment to provide a more robust solution. To evaluate the performance of the proposed template adaptation methods in automated detection of myocardial ischemia and myocardial infarction, we combine our novel adaptation methods with traditional classifiers. Lastly, a study assessing ventricular repolarisation variability (VRV) in non-ischemic cardiomyopathy (CM)

is assessed using the proposed three-dimensional template adaptation technique. The remainder of this chapter provides an overview of the research questions addressed and the novel contributions to cardiac data processing produced by this thesis.

1.2 Contextual statement

The ECG has long been used to study physiological markers of lability related to heart disease. Analysis of pathophysiology in cardiac conditions has been employed to study complex patterns (Hasan *et al.*, 2012a; Baumert *et al.*, 2016a; Shaffer and Ginsberg, 2017; Ramírez *et al.*, 2019; Vogel *et al.*, 2019). In particular, markers of ventricular depolarisation and repolarisation have been studied, e.g. - QTV (Baumert *et al.*, 2016a), T-wave shape variability (Baumert *et al.*, 2016a; Hekkanen *et al.*, 2020) and ST-elevation (Channer and Morris, 2002). These markers have previously been linked to myocardial infarction, myocardial ischemia, sudden cardiac death and many other conditions. Although morphological features are rich in information, the extraction of such features is plagued by limited clinical resources. Manual delineation of the ECG by clinical experts is not only a cumbersome but error prone process, which is further amplified in the age of big data. Furthermore, manual diagnosis and prognosis in the study of cardiac conditions is extremely laborious and opinions vary amongst practitioners. With the computer revolution, great research efforts have been expended towards developing automated methods in cardiac analysis and classification. The focus of this this is the development of inhomgeneous feature extraction tools and their application to the analysis and classification of cardiac disease and lability.

Previous works on beat-to-beat VCG feature extraction via template adaptation are sparse. Continuing on from the works of Schmidt *et al.* (2014, 2018a) and the conclusions of Baumert *et al.* (2012), an inhomogeneous template adaptation method for accurate VCG feature extraction is developed. The method addresses the shortcomings of traditional methods, which are unable to capture subtle morphological beat-to-beat variations, combined with evidence that template adaptation methods perform better compared to their counterparts (Baumert *et al.*, 2012; Schmidt *et al.*, 2014). The proposed model demonstrated superior performance compared to current methods across simulated data and a myocardial infarction study. To illustrate the potential of the proposed method for other physiological data applications, a supplementary gallery of adaptations across a three-dimensional upper-limb movement database is provided.

Research efforts in ECG template adaptation have recently made great strides. Initial works utilised homogeneous adaptations, which provided a novel approach, but lacked the technical complexity to capture subtle variations in data. More recently, inhomogeneous template adaptations were proposed to account for this, however, the limitation of these works is that they assume a one-to-one correspondence between sample points. Although, these inhomogeneous methods have yielded state-of-the-art results for minor variations in signal, they are unsuitable for capturing larger morphological deformations. Generally, the signal processing domain has not focused on the correspondence problem. The correspondence problem stems from image registration and computer vision where a correspondence needs to be established between two sets of unordered data. To provide a more robust, generalised and complete solution, a non-binary correspondence based template adaptation is developed. The performance of the proposed method yields an improvement in QTV measurement across synthetic data and a myocardial infarction study. Furthermore, the algorithm yielded state-of-the-art results in terms of ECG feature extraction against the gold-standard database for QTV. To demonstrate the potential general application of the algorithm beyond ECG analysis, a small dicrotic notch extraction analysis was performed and benchmarked against a previously proposed work. The work in this thesis demonstrated a significantly higher accuracy.

Few automated methods exist for classifying ischemic beats using beat-specific annotations. Initial methods used simplistic thresholding inspired by manual annotation rules (Papaloukas *et al.*, 2001). Subsequent methods utilised a variety of interpretable (Goletsis *et al.*, 2003, 2004; Exarchos *et al.*, 2006, 2007; Tsipouras *et al.*, 2007) and neural network approaches (Papaloukas *et al.*, 2002a,b). However, previously proposed interpretable efforts have neglected to utilise state-of-the-art feature extraction techniques, such as template adaptation. Additionally, black-box models lack the transparency and interpretability for widespread use. The classification framework in this work utilises the correspondence-based template adaptation combined with an interpretable classifier, k-nearest neighbour (kNN). Improved statistical sensitivity and specificity measures are observed compared to previous proposed methods. Furthermore, a more robust analysis of the sensitivity and specificity is performed to highlight the limitation of previous works using subject-wise evaluation and to provide a more representative measure of performance.

The evaluation of automated myocardial infarction systems has been studied extensively, however, research has neglected to focus on beat-to-beat dynamics and dependencies.

Furthermore, research has suggested that the VCG has superior diagnostic abilities compared to the standard ECG in myocardial infarction assessment (Chou, 1986). In this thesis, an long short-term memory (LSTM) framework is implemented utilising the aforementioned three-dimensional inhomogeneous template adaptation method. The performance of the method is evaluated against a popular database for the analysis of myocardial infarction - the Physikalisch-Technische Bundesanstalt (PTB) database. The sensitivity and specificity of the method are comparable to previous works, especially VCG based methods. However, further research is required to develop a more sophisticated LSTM network architecture.

VRV has been shown to have predictive value in patients with ischemic heart disease, where the suspected mode of death is malignant ventricular arrhythmia. Furthermore, previous works studying patients with non-ischemic CM have suggested that the potential for risk stratification remains unclear (Baumert *et al.*, 2016a). To evaluate potential risk stratification in non-ischemic CM using VRV, the aforementioned three-dimensional inhomogeneous template adaptation technique is employed in conjunction with two-dimensional template adaptation.

1.3   Overview of Thesis

This thesis consists of eight chapters: the introduction, the literature review, five chapters of research contribution and the conclusion. The five main chapters can be separated into three primary chapters, stemming from three modified journal submissions, and two secondary chapters arising from conference submissions. The chapter outline is as follows:

Chapter 1 provides an introductory narrative describing the focus and key research questions addressed in this thesis.

Chapter 2 contains the literature review related to the research topic of this thesis. The literature review describes important physiological information pertaining to heart health. Next, foundational concepts in registration and machine learning are described in conjunction with previously proposed automated tools for the assessment of ventricular depolarisation and repolarisation lability.

Chapter 3 describes the three-dimensional inhomogeneous template adaptation technique developed as part of this thesis. The description contains an in-depth mathematical derivation of the methodology followed by an evaluation of algorithmic performance.

Chapter 4 describes the correspondence based two-dimensional template adaptation technique developed as part of this thesis. The chapter contains a rigorous algorithmic description and evaluation of the developed framework.

Chapter 5 represents the automated ischemic beat detection framework developed as part of this thesis. In this chapter a detailed description of the algorithm is provided alongside a robust validation process.

Chapter 6 is a mini-chapter describing an LSTM framework employing the method from Chapter 3. It is an applications chapter demonstrating the potential usage of the proposed method in Chapter 3. The chapter provides a description of the framework and an evaluation of system performance.

Chapter 7 is a mini-chapter utilising the algorithm introduced in Chapter 3. In this chapter VRV is used to assess non-ischemic dilated CM.

Chapter 8 provides a summary of the findings arising from the original contributions of this thesis. To conclude, a discussion regarding future research directions is provided.

1.4   Statement of original contribution

This thesis consists of two peer-reviewed first-author manuscripts, a third manuscript under review, one first-author conference paper and a co-author conference paper. Additionally, Appendix A contains a third conference paper. All software related to the contents of this thesis, including statistical analysis, was implemented in MATLAB®/RStudio. Furthermore, Bash/Slurm were utilised to enable high performance computing (HPC) for computationally demanding tasks. The author contribution in each study consisted of hypothesis formulation, methodology development and hypothesis testing.

1.5   Data

A combination of publicly available, synthetically generated and online datasets were used in this thesis. The PTB database, Complex Upper-Limb Movements (CULM) database, QT Database (QTDB) and European ST-T (EST-T) database were sourced from PhysioNet. Additionally, the dataset labelled E-HOL-03-0401-017 was sourced from the Telemetric and Holter ECG Warehouse (THEW); the data stems from the Defibrillators in Non-Ischemic Cardiomyopathy Treatment Evaluation (DEFINITE) study. An in-depth description of the datasets employed in this thesis is given below.

1.5.1 Clinical

The PTB database (Bousseljot *et al.*, 1995), available on PhysioNet (Goldberger *et al.*, 2012), was employed in Chapter 3 for the analysis of myocardial infarction using three-dimensional template adaptation. Furthermore, this dataset was utilised in Chapter 4 for the evaluation of the two-dimensional template adaptation framework. Lastly, this dataset was used for the development and evaluation of the LSTM network in Chapter 6. Specifically, the PTB database contains 79 patients with acute myocardial infarction (22 female, mean age 63 ± 12 years; 57 male, mean age 57 ± 10 years) and 69 control subjects (17-female, 42 ± 18 years; 52 male, 40 ± 13 years). Approximately two minutes of data are available for each recording. Each subject is represented by one to five records; and, each recording contains fifteen simultaneously observed signals, consisting of: the standard 12 leads in conjunction with the three orthogonal Frank leads. Each signal is digitised at 1000 samples per second, with a 16 bit resolution. The data were obtained using a non-commercial prototype recorder with the specifications available on PhysioNet.

In Chapter 3 the CULM database (Miranda *et al.*, 2018) was utilised to generate a visual gallery of template adaptation results. The data consists of ten healthy subjects (7 males; 26.4 ± 4.52 years of age; 9 right-handed) who were asked to perform a variety of upper-limb motor tasks. The data was collected using a camera-based motion capture system (VICON, Oxford UK) and was preprocessed with internal system software to map trajectories. The data is four dimensional, containing: three spatial dimensions and one temporal dimension.

The QTDB (Laguna *et al.*, 1997) was utilised in the analysis of the correspondence-based framework proposed in Chapter 4. This database is the gold-standard for the assessment of ECG methods. The database consists of 105 fifteen-minute recordings; each recording contains two leads. Furthermore, 30 to 50 selected beats in each recording contain annotations for the onset, peak and end markers of the P, QRS, T and U waves. Each signal is digitised at 250 samples per second. To ensure an adequate level of physiological variability, the database was compiled using several other datasets including: MIT-BIH Arrhythmia (MIT-BIH Arrhythmia) database (Moody and Mark, 2001), EST-T database (Taddei *et al.*, 1992) and ECG databases collected at Boston's Beth Israel Deaconess Medical Center.

In Chapter 5 the EST-T database (Taddei *et al.*, 1992) was used for the development of an ischemic beat detector. The EST-T database contains 90 ECG recordings from 79 ambulatory ECG with each being two hours in length. The subjects were 9 women (aged 55-71) and 70 men (aged 30-84). Furthermore, the data were digitised at 250 samples per second with a 12-bit resolution ($20m$V input range). In this study, only the raw ECG

were utilised. Alternative annotations for normal, ischemic and noisy beats were obtained from Papaloukas *et al.* (2001). The annotations were independently marked by three clinicians. For ambiguous regions in the recordings, a subsequent joint decision was made. Across the subset of the database, 20 ischemic ST-segment episodes and 20 ischemic T-wave episodes were present. The resultant selection yielded 86 384 cardiac beats of which 6 754 were deemed noisy. Thus, of the 76 989 remaining beats, 37 663 (48.92%) were labelled as ischemic and the rest as normal.

In Chapter 4 visual adaptations are presented to provide a qualitative assessment of correspondence based template adaptation in photoplethysmogram (PPG). The publicly available BIDMC PPG and Respiration (BIDMC) database (Pimentel *et al.*, 2017; Goldberger *et al.*, 2012) was employed. This database contains 53 eight minute recordings of PPG sampled at 125 Hz. In this thesis, 5 cycles for seven subjects were extracted from the BIDMC database.

Finally, the E-HOL-03-0401-017 dataset was sourced from the THEW and used in Chapter 7 to study the predictive value of VRV in patients with non-ischemic dilated CM. This database contains 393 recordings from 236 patients (67 women, age 60 ± 14 years; 168 men, age: 58 ± 12 years; 1 record not specified) enrolled in the DEFINITE study. The data contains 24 hour Holter 3-lead (Frank lead configuration) ECG, digitised at 500 samples per second with an amplitude resolution of 1 μV Rashba *et al.* (2006). ECG recording was performed at enrolment and again up to 5 years later. The all-cause mortality during the follow-up period was 4.8%.

1.5.2 Synthetic

For the purpose of algorithm evaluation in Chapter 3, a synthetic dataset was generated. The simulated data contains a set of non-linear morphological variations and common noise sources, including: baseline wander (BW), muscle artefact (MA), electrode movement (EM) and additive white Gaussian noise (AWGN). The noise was incorporated into the data via an equally weighted combination of the four sources and across four levels of signal-to-noise ratio (SNR). Additionally, the VCG was generated via a Frank lead transformation using the standard eight lead ECG configuration from Sameni *et al.* (2007). Morphological variations were introduced by varying the T-wave amplitude and polarity in leads V1-V3 of the simulated 8-lead ECG. Under this configuration, an additional non-linear and randomly seeded T-wave variation was introduced at the T-wave onset and offset. At each T-wave

amplitude 30 seconds of noisy synthetic data were generated. Thus, yielding 300 seconds of data across the four SNR ratios.

In Chapter 4, simulated data from Porta *et al.* (1998) was employed to assess the QTV measurement performance of the proposed method. Briefly, a single ECG beat from a healthy subject (26 year old) was extracted from lead VII and digitised at 1000 samples per second with a 12-bit amplitude resolution. The T-wave amplitude was then lowered in steps of 10% of the amplitude. The ten cardiac beats were each respectively appended 500 times to generate an ECG sequence, thus forming 10 different recordings. Each recording maintained a QTV of zero, however, contained different T-wave amplitudes. Next three sources of noise were independently introduced into the recordings - BW, AWGN and amplitude modulation (AM). Thus, the resultant database contained thirty 500-second recordings in total. The aim of the simulation was to generate ECG with varying morphology and noise levels; and zero QTV. Thus, an ideal automated method would yield a QTV of zero.

Lastly, in 4 a simulated PPG dataset was generated to quantitatively assess dicrotic notch detection via correspondence based template adaptation. Earlier works have used the dicrotic notch to improve systolic blood pressure estimation Gu *et al.* (2008) and to study athletic differences Wang *et al.* (2015). Briefly, a set of PPG cycles were replicated to generate sequences of 210 seconds sampled at 500 Hz using a previously proposed simulation tool (Charlton *et al.*, 2019). Next, common noise sources (AM, BW and AWGN) were introduced into the simulated data. The distortions were imposed across 29 physiologically plausible RR intervals, resulting in 87 recordings in total. Due to the intra-recording RR interval being constant in the developed database, the true dicrotic notch variability across any given recording was zero. Thus, similar to the ECG simulated data, an ideal system would return a dicrotic notch variability of zero.

Literature review

C ARDIAC function is critical for the operation of human physiological processes and sustenance of life. The role of the heart is to distribute blood and oxygen throughout the body via the circulatory system, and deliver waste products back to the lungs for removal. A healthy cardiac system is directly correlated to a functional lifestyle and prolonged life-expectancy. This chapter describes various state-of-the-art techniques used for assessing debilitating heart conditions via ECG methods. Furthermore, the foundational workings of registration and machine learning are described - providing a high-level description of the algorithmic methods proposed in this thesis. Through feature extraction techniques and classification methods, temporal sequences relating to defective time series can be detected.

2.1   Physiological Background

The cardiac cycle is a pseudo-periodic bio-process that is essential for the sustenance of human life. Great efforts have been undertaken to understand cardiac physiology and pathophysiology. The focus of this thesis is on robust information extraction from heart data. Thus, in the following section an overview of the cardiac cycle, modes of measurement and related biomedical signal morphologies are described. Additionally, previously proposed methods for the detection of cardiac conditions are described.

2.1.1   Heart Function and Disease

The primary purpose of the heart is to enable adequate blood and oxygen flow to be distributed throughout the body. Blood consists of red blood cells to carry oxygen, white blood cells to facilitate the immune system, platelets to assist in clotting and plasma to serve as a transport medium (Dean, 2005). The heart is the driving force of blood distribution amongst most animal lifeforms and has evolved over the period of some 500 million years (Stephenson *et al.*, 2017). A functional cardiac system is imperative to a prolonged and functional lifestyle, with a plethora of links to both cardiac and non-cardiac phenomena. Scientifically, functional cardiac operation is evaluated by a series of proper physiological flows and electrical processes. The flow of blood through arteries, veins and capillaries is one such consideration. Similarly, electrical conduction and timing across appropriate pathways in heart muscle is deemed important.

Myocardial ischemia pertains to the phenomena where blood flow to the heart is reduced by a partial or complete obstruction of a coronary artery (Shimokawa and Yasuda, 2008). The link between myocardial ischemia and myocardial infarction has long been studied. It is known that myocardial infarction is attributable to prolonged myocardial ischemia - resulting from insufficient oxygen supply to the myocardium (DeFilippis *et al.*, 2019; Thygesen *et al.*, 2018). Pathologically, myocardial infarction is defined as myocardial cell death from prolonged ischemia (Thygesen *et al.*, 2018). Silent myocardial infarction, where individuals suffer death of myocardial cells without knowledge, has been found to be prevalent in sudden cardiac death (SCD) victims (Vähätalo *et al.*, 2019). Similarly, SCD has been found to account for $\sim 50\%$ of mortality after myocardial infarction (Waks and Buxton, 2018). The impacts of myocardial infarction extend to abnormalities in the autonomic nervous system (ANS), which have been linked to the genesis of sudden cardiac death (Zipes and Wellens, 1998). A link between SCD and various other heart arrhythmia/disease

have been established. For instance, it is known that ventricular tachyarrhythmia (VA) are a major cause of SCD; particularly ventricular tachycardia (VT) (Israel, 2014). Ventricular tachyarrhythmias are also commonly observable in the early stages of myocardial ischemia (Bhar-Amato *et al.*, 2017); highlighting the complex and interrelated interactions between pathophysiologies. Pertaining to cardiomyopathy studies, diseased patients have been found to represent the second largest group who experience SCD. In at least 80% of SCD patients, coronary artery disease (CAD) is present (Zipes and Wellens, 1998); CAD is caused by plaque build-up in the wall of arteries supplying blood to the heart. The importance of this is highlighted by the fact that in most patients with ischemic heart disease, the cause of myocardial ischemia is a reduction in coronary blood flow due to CAD (Steenbergen and Frangogiannis, 2012). Extensive research in the field has helped improve the understanding of heart physiology and pathophysiology but many interactions are still unclear. By and large, the association between varying heart defects and biomedical data are not sufficiently understood. Similarly, the complex beat-to-beat interaction and causality between different heart conditions is still unclear. However, several established markers exist in clinical practice, including: lower ventricular ejection fraction (LVEF), long QT syndrome, short QT syndrome and ion channelopathies. Thus, providing a foundation and promise for further study of biomedical data.

Cardiac function can be assessed via a number of modalities. The most commonly employed tool is ECG, which is described in the ensuing section. Alternative techniques include the echocardiogram (ECHO), nuclear cardiac test, coronary angiogram, magnetic resonance imaging (MRI) and coronary computed tomography angiogram (CCTA). ECHO is a commonly employed medical imaging technique used to detect tissue damage, valve functionality, pumping capacity and other structural information. Similarly, nuclear cardiac testing, coronary angiogram, MRI and CCTA are other imaging modalities that offer rich structural information. Imaging based techniques are solely employed in clinical and controlled settings due to the immobile and expensive nature of medical imaging equipment. Furthermore, it is expensive and impractical to employ imaging tests for regular and continuous monitoring of cardiac conditions. Additionally, PPG can be employed to track heart rate variability (HRV) by optically measuring volumetric changes in blood.

2.1.2 Biomedical Signals

In this section, important biomedical signals employed in the study of cardiac diseases are presented, namely: ECG, VCG and PPG. A detailed explanation of the electrode configuration for ECG and VCG is provided. Furthermore, the specific bio-processes that generate waveform segments and sub-segments are introduced.

ECG Background

Electrocardiography, the process of producing a recording of the heart's electrical activity can be dated to the 19th century works of Carlo Matteucci. His efforts showed that an electrical current accompanied each cardiac contraction (Fye, 1994). Soon after, the German physiologist Emil DuBois-Reymond, the father of electrophysiology described an "action potential" that accompanied muscular contraction and confirmed Matteucci's discovery of electrical activity in the frog heart. Dutch physicist William Einthoven's attendance at the First International Congress of Physiologists permitted him the opportunity to see Waller's demonstration of recording the heart's electrical impulse (Waller, 1887). The demonstration inspired Einthoven and several other physiologists of the time to pursue further investigation; their line of research included improvements in apparatus via the use of an electric arc light and a higher-resolution projecting microscope. The improvements permitted the investigating group to identify three distinct deflections, which were later classified as the P, QRS and T waves. Waller's earlier works had only identified two separate deflections (Bayliss *et al.*, 1892). Einthoven's further attempts to enhance the capillary electrometer led him to conclude that the device had limited use in cardiac electrophysiology due to a poor frequency response; he proceeded to focus his attentions on galvanometers. Subsequently, Einthoven's modifications to the galvanometer yielded a device capable of capturing 1 mm deflections on the abscissa, representing 0.04 seconds, which still serves as the foundation for ECG devices today.

Present day guidelines pertaining to the digital recording of ECG suggest minimum sampling and resolution frequencies. According to AHA guidelines (Kligfield *et al.*, 2007), the bulk of diagnostic information contained in an ECG recording is contained below 100 Hz in adults and 250Hz for infants. Thus, in contemporary studies high sampling rates are often observed ranging between 250-1000 Hz. Furthermore, studies (Zywietz *et al.*, 1986; Berson and Pipberger, 1967) have suggested that a sampling rate of 500 Hz is required to reduce the amplitude error to roughly 1% in adults; further demonstrating the importance of high sampling rates.

Table 2.1. Depolarisation rates (adapted from Sampson and McGrath (2015).

Conduction Area	Depolarization Rate (beats per minute)
SA node	60-100
AV node	40-60
His-Pukinje system	20-40

Cardiac Electrophysiology

ECG is considered a non-invasive method which records from the body surface the temporal changes in summed electric potential created by heart muscle cells (Clark and Kruse, 1990). The ECG projects the heart's conduction system as a temporal signal. Specifically, the electrical impulse from which the heart beat is regulated stems from the sinoatrial (SA) node; a discrete patch of electrical cells located in the right atrium (Sampson and McGrath, 2015). In their resting state, cardiac cell membranes are negatively charged and depolarize upon cardiac activity (Becker, 2006). The SA node serves as the heart's primary natural pacemaker because it has the quickest rate of depolarisation. In the event of SA node failure, the next quickest pacemaker regulates the depolarization rate (see Table 2.1). This variability in depolarisation rate serves two purposes: 1) it permits the atria to complete contraction before the signal pulsates to the ventricles; 2) serves as a fail-safe (albeit at a slower rate) in the event of SA node failure. From the SA node the electrical signal spreads across both atria (inducing depolarisation) and also arrives at the atrioventricular (AV) node, where conduction is considerably slower ($\sim$10 times) (Klabunde, 2012), compared to the surrounding muscle. Next, the electrical impulse travels from the AV node to the bundle of His, which in a healthy heart serves as the only path for electrical conduction between the atria and ventricles. The bundle of His carries the electrical signal into the two ventricles (left and right) via the left and right bundle branches, thus inducing ventricular depolarisation. This set of bio-processes manifests as different waveforms in the ECG. The P-wave is generated by the depolarisation of the atria. Similarly, the QRS wave represents the depolarisation of the ventricles. Lastly, the ST, T and U waves depict the ventricular repolarisation process.

ECG Configuration

To observe the strength of the extracellular electric field, two electrodes across varying locations on the body are required. In the standard configuration, the frontal plane ECG is

measured from the supine patient by the attachment of an electrode to each of the four extremities (LA - left arm, RA - right arm, LL - left leg, RL - right leg) (Walker, H Kenneth and Hall, W Dallas and Hurst, 1990). In this system, bipolar lead I is defined as the potential difference between the left arm (positive pole) and the right arm - wherein a positive deflection in the recording is observed as current passes from right to left. Lead II represents the potential difference between the right arm and left leg (positive pole). Lead III records the potential difference between the left arm and left leg (positive pole). Three augmented leads record the difference in potential between the right arm, left arm and left leg, respectively, with a ground lead formed by the summation of the remaining two unused limb leads. For augmented leads, the positive pole is defined by the designated limb. The described leads form the cardiac electrical vectors through the entire 360 degrees of the frontal plane (Walker, H Kenneth and Hall, W Dallas and Hurst, 1990).

Conversely, vectors radiating across the horizontal plane are observed in the precordial leads (V_1 - V_6) (Walker, H Kenneth and Hall, W Dallas and Hurst, 1990). For these leads, the electrodes are placed on the anterior and left lateral chest. Specifically, the V_1 electrode is placed on the fourth right intercostal area adjacent to the sternum. Similarly, the V_2 electrode is located in the fourth left intercostal area adjacent to the sternum. The V_3 electrode is defined at the midpoint of the line connecting the electrode location for V_2 and the electrode location for V_4; the V_4 electrode is positioned in the fifth left intercostal space in the midclavicular line. Similarly, the V_5 electrode location is positioned in line with V_4 on the anterior axillary line. The V_6 electrode is located in line with the electrode positions of V_4 and V_5 but on the midaxillary line. In the case of precordial leads, the electrode is defined as the positive pole. The negative pole is defined by forming an electrical connection between all the limb leads such that an electrical current moving toward any given precordial lead will manifest as an upward deflection on the recording (Walker, H Kenneth and Hall, W Dallas and Hurst, 1990). The combination of the six frontal and six horizontal plane leads defines the standard 12-lead ECG recording, as shown in Fig. 2.1.

Non-standard ECG configurations exist and are primarily used to investigate specific and localised diseases. For example, in this thesis, the EST-T database is employed to study myocardial ischemia for which the original investigators used non-standard ECG leads (Taddei *et al.*, 1992). Traditionally, such configurations are discouraged unless a particular reason exists for doing so (Jowett *et al.*, 2005). Furthermore, it is standard practice to accurately document any such modifications to alert future users to the limitations of the study (Jowett *et al.*, 2005).
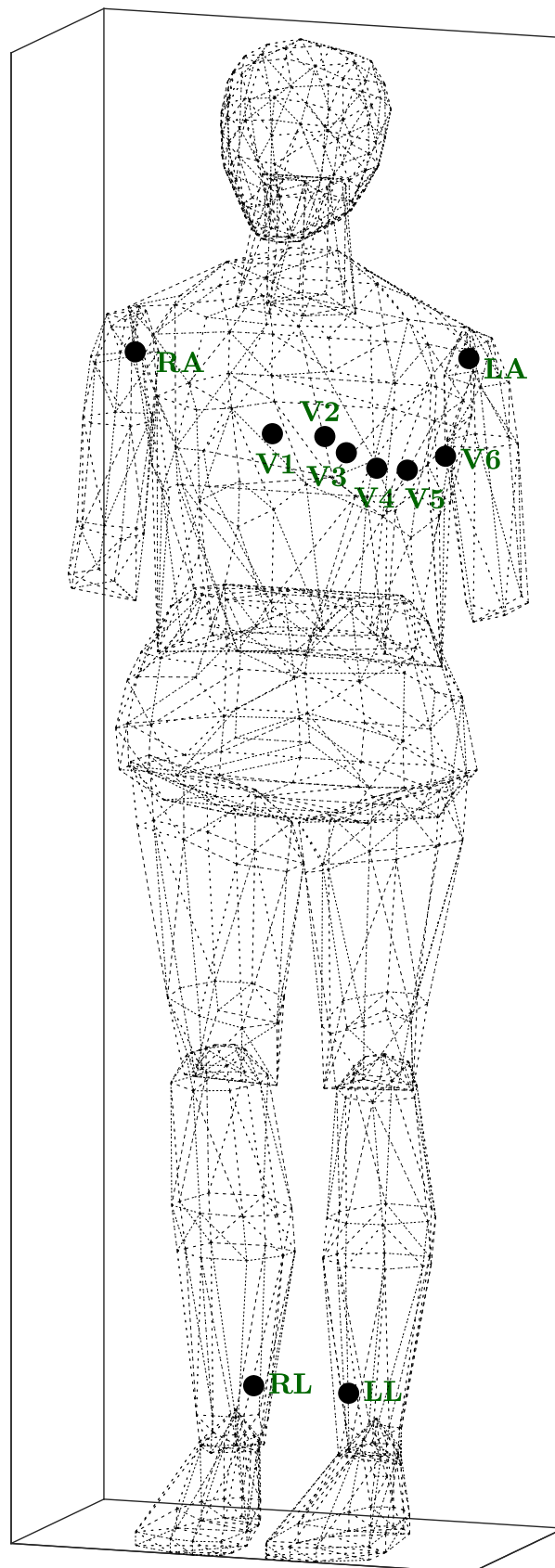
Figure 2.1. Standard ECG electrode placement.

VCG Configuration

The VCG is an alternative approach to evaluating cardiac function by which the ECG is considered as containing both magnitude and direction (Yang *et al.*, 2012; Hasan and Abbott, 2016). Historically, the preferred method for directly obtaining the three orthogonal leads relied on using the Frank VCG lead system. This non-standard ECG configuration contains seven electrodes in total. Five are located in the transverse plane with the two additional electrodes located on the back of the neck and the left foot, respectively (Frank, 1956). In this system, the three-dimensional representation of cardiac electrical activity can be obtained by measuring ECG in three directions; right-to-left (X-axis), head-to-feet (Y-axis), and front-to-back (Z-axis). Fig. 2.2 depicts the electrode configuration for such a system. The Frank lead configuration is no longer employed in clinical practice due to the non-standard setup of electrodes. Similar to the ECG, the physiological processes measured by the VCG yields a series of three-dimensional loops representing ventricular depolarisation and repolarisation, namely the: P-loop, QRS-loop and T-loop.

More recently, alternative methods have been proposed to obtain the VCG from the standard 12-lead ECG configuration; these are derived methods from the standard 12-Lead ECG. Such techniques are often based on mathematical transformations, optimization and parameter-fitting. Derived methods are not currently standardized and solely utilized in research activities. A well-known derived technique, the inverse Dower transform (IDT) (Edenbrandt and Pahlm, 1988), relies on the use of the pseudo-inverse matrix proposed earlier by Dower *et al.* (1980). Additionally, Kors *et al.* (1990) evaluated several models, namely through the use of: multivariate regression, a cardio-electrical activity model and quasi-orthogonal ECG leads. However, studies (Guillem *et al.*, 2009, 2008) have found the aforementioned methods to be lacking. Primarily, these techniques suffer from information loss or the introduction of unwanted information during reconstruction; thus, yielding a different result when compared to direct methods. Acar and Koymen (1999) proposed a singular value decomposition (SVD) based method for the reconstruction of orthogonal leads from ECG - although a well-equipped method, it similarly suffers from the notion that SVD is inherently sensitive to small disturbances in the signal. Thus, in this thesis we focus on the use of datasets employing the Frank Lead System.

PPG

PPG is an affordable optical method that measures blood volume changes in the microvascular bed of tissue with each heartbeat (Allen *et al.*, 2021). Devices measuring PPG contain
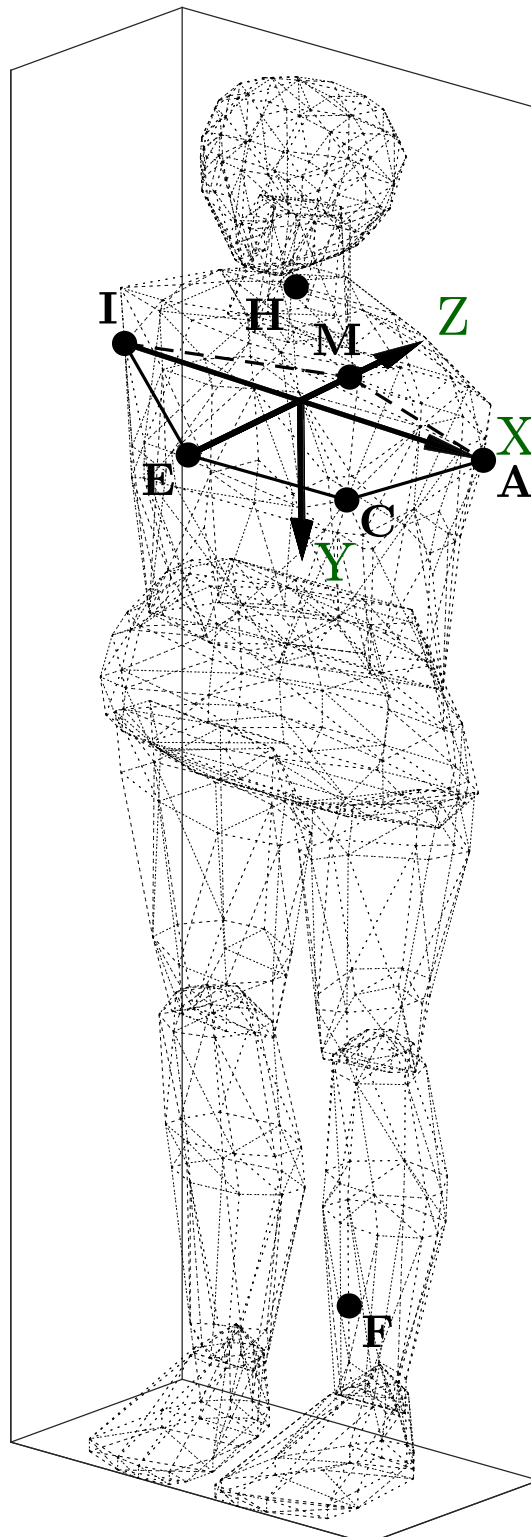
Figure 2.2. Standard configuration for a Frank Lead VCG System consisting of seven unipolar electrodes (A, C, E, I, M H and F). The signals are viewed in the three orthogonal directions (X, Y and Z). Adapted from Hasan and Abbott (2016).

a light source and a photodetector (Castaneda *et al.*, 2018). The detector is placed at one of two points: 1) along the light source or 2) on the opposite side of the tissue absorbing light radiation; the reflected light is proportional to variations in blood volume (Castaneda *et al.*, 2018). The portion of absorbed/reflected light correlates directly with changes in blood volume from which a continuous pulse wave signal can be obtained (Grote and Zou, 2017). Physiologically, the process which produces alternations in the detected light intensity pertains to the systolic and diastolic phase of the cardiac cycle. It is a cost-effective tool for monitoring and studying pulse rate and respiration. The study of physiology using PPG is beyond the scope of this thesis - instead, PPG is solely utilised for algorithm assessment.

2.1.3   ECG Evaluation

Since its inception, the ECG has been employed to study arrhythmia and heart disease. In the early twentieth century, Sir Thomas Lewis discovered an irregular heartbeat, atrial fibrillation (AF), via the use of ECG (Lewis, 1909). Subsequent research findings and medical establishment of cardiac conditions led to the similar use of ECG in the diagnosis of myocardial ischemia and myocardial infarction (Fye, 1994). Since then, the ECG has become a standard tool for studying all cardiac arrhythmia and disease. These conditions are qualitatively and quantitatively assessed by continued or sporadic changes in both temporal and morphological signal properties. In this section several important markers of cardiac lability are described, which are related to myocardial ischemia, myocardial infarction and nonischemic dilated cardiomyopathy.

ST Segment Changes

ST-segment changes are produced by the flow of injury currents (Wagner *et al.*, 2009). The currents are generated by voltage gradients across the boundary of ischemic and non-ischemic myocardium between the resting and plateau phase of the ventricular action potential, corresponding to the TQ and ST segments of the ECG, respectively (Kléber *et al.*, 1978). Common changes that occur in the course of myocardial ischemic (and infarction) episodes include: ST-segment depression and elevation, hyperacute T-wave changes, QRS complex variations and T-wave inversion (Wagner *et al.*, 2009). Currently, guidelines recommend a diagnosis of myocardial ischemia (or infarction) when two or more contiguous ECG leads exceed established threshold values (Alpert *et al.*, 2000; Thygesen *et al.*, 2007,

2012, 2018). Clinically, ST elevation, ST depression and T-wave changes are the most commonly utilised measures in acute myocardial ischemia for which the most recent universal guidelines (Thygesen *et al.*, 2018) require:

1. New ST-elevation at the J-point in 2 contiguous leads with the cut-point: $\geq$1 mm in all leads other than leads V_2-V_3 where the following cut-points apply: $\geq$0.2 mm in men $\geq$ 40 years; $\geq$2.5 mm in men $<$ 40 years, or $\geq$ 1.5 mm in women.
2. New horizontal or downsloping ST-depression $\geq$0.5 mm in 2 contiguous leads and/or T inversion $\geq$ 1 mm in 2 contiguous leads with prominent R wave or R/S ratio $>$ 1.

It is worth noting that AHA myocardial disease definitions are regularly updated as knowledge evolves (Alpert *et al.*, 2000; Thygesen *et al.*, 2007, 2012, 2018). As such, in the first universal definition (Alpert *et al.*, 2000), the requirements for myocardial ischemia stated:

Patients with ST segment elevation:

1. New or presumed new ST segment elevation at the J point in two or more contiguous leads with the cut-off points $\geq$0.2 mV in leads V1, V2, or V3 and $\geq$0.1 mV in other leads (contiguity in the frontal plane is defined by the lead sequence aVL, I, inverted aVR, II, aVF, III).

Patients without ST segment elevation:

(a) a. ST segment depression
(b) b. T wave abnormalities only

legend

New or presumed new ST segment depression or T wave abnormalities, or both, should be observed in two or more contiguous leads. Also, new or presumed new symmetric inversion of T waves $\geq$1 mm should be present in at least two contiguous leads.

Occasionally, myocardial ischemia may manifest ST segment changes to meet criteria in one lead but be marginally below the threshold for the contiguous lead (Thygesen *et al.*, 2012). Diagnostic values below guideline thresholds do not necessarily exclude the presence of an ischemic episode (or myocardial infarction) as a single static recording may miss the more complex beat-to-beat ECG changes that might be present in serial recordings (Thygesen *et al.*, 2012). The diagnostic significance of changes in the ST segment is well established, however, to improve accuracy, more sophisticated frameworks across serial recordings are necessary.

QTV

QTV is a beat-to-beat marker used to measure cardiac repolarisation and depolarisation lability in ECG. The simplest form, standard deviation of QT (SDQT), is defined as the beat-to-beat standard deviation of the QT-interval across a sequence of cardiac cycles:

$$SDQT = \sqrt{\frac{1}{N}\sum_{n=1}^{N}(QT_n - QT_{mean})^2}. \tag{2.1}$$

To enable performance comparison with previously proposed methods for measuring QTV (Schmidt *et al.*, 2014, 2018a; Porta *et al.*, 1998; Berger *et al.*, 1997), the primary focus of this thesis is on SDQT. The QT-interval pertains to the period that ventricular depolarisation and repolarisation occur. In ECG, to obtain the QT-interval, the detection of two temporal points are required, namely: the QRS-wave onset and the T-wave end (T_{end}) (Baumert *et al.*, 2016a). It is important to note that alternative measures of QT variability have been studied, however, they are all foundationally derived from the QT-interval. Standard alternative measures of QTV include: normalised QT interval variance, short-term QT interval variability and long-term QT interval variability. Another important measure of QTV, which incorporates heart rate information, is the QT variability index (QTV_i). Specifically, it is defined as the normalised QT interval variance (Baumert *et al.*, 2016a). In studies where the HRV may be non-negligible, this normalisation is important.

Under resting conditions, HRV is considered a significant physiological source of QTV (Cabasson *et al.*, 2012). This link between QTV and HRV stems from the cellular dependency of action potential duration on the cardiac cycle time (Zaza *et al.*, 1991). Although related, it has been demonstrated that a considerable QTV fraction is not correlated with heart rate (HR) - thus, a significant portion of QTV is not linearly caused by HRV and may contain important information (Almeida *et al.*, 2006). In addition to HRV, the relationship between QTV and T-wave amplitude has been studied. Hasan *et al.* (2013) found a significant difference in QTV between different leads and accredited the dissimilarity to varying T-wave amplitudes across the different leads. Additional research has suggested that leads with high SNR and tall T-waves tend to exhibit lower QTV (Avbelj *et al.*, 2003). The relationship between QTV and other ECG features highlights the need for techniques capable of accurately delineating the entire ECG when studying ventricular depolarisation and repolarisation.
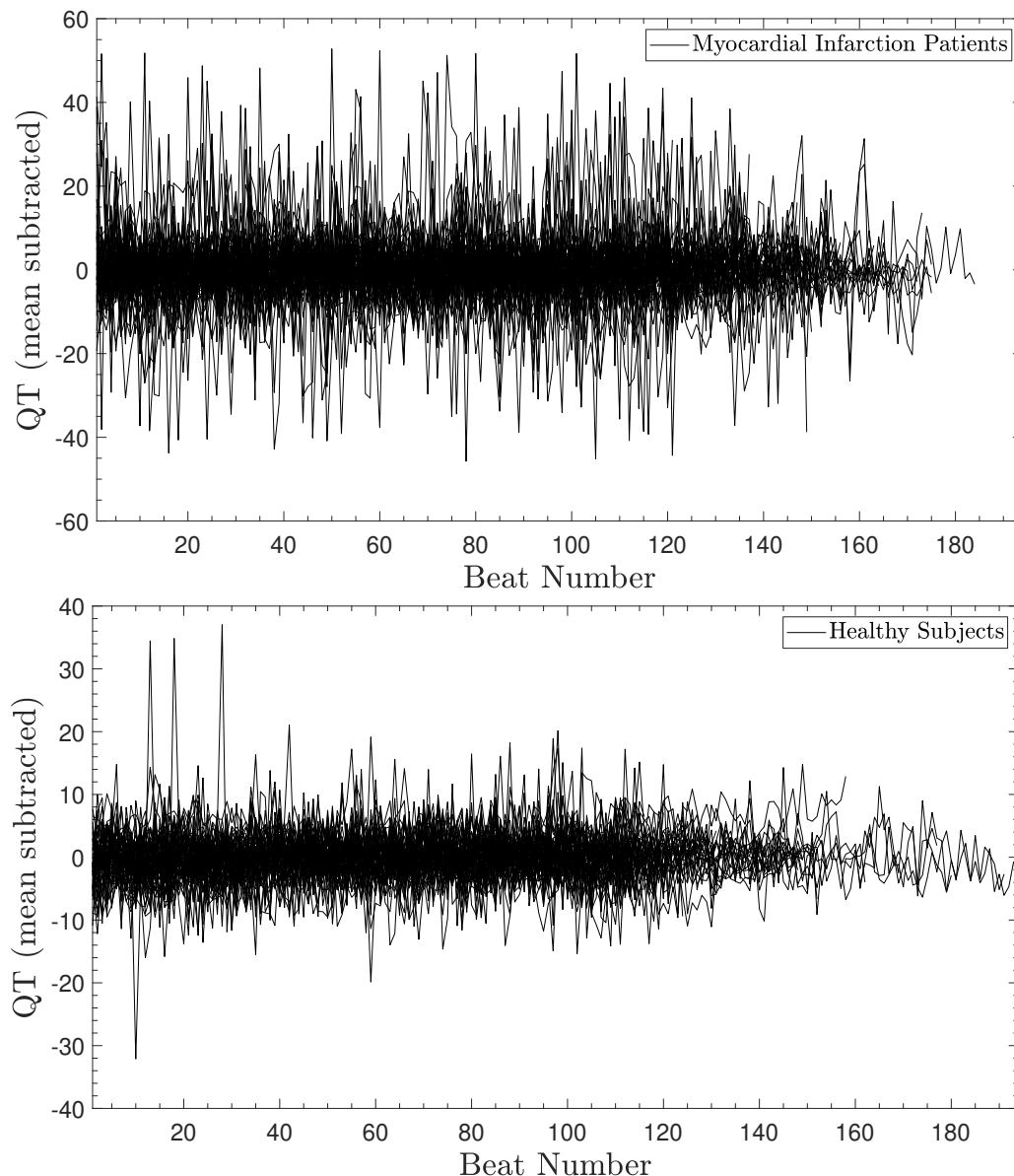
Figure 2.3. The QT interval measured across 148 subjects from the PTB database with each containing approximately two minute recordings. Increased variability can be observed in myocardial infarction patients (top) compared to healthy subjects (bottom).

QTV has been extensively studied across a broad range of cardiac diseases. It appears to be useful for the ECG screening of CAD, left ventricular (LV) hypertrophy and LV systolic dysfunction (Schlegel *et al.*, 2010). In CAD patients without prior myocardial infarction, SDQT was found to be significantly increased (Vrtovec *et al.*, 2000). Murabayashi *et al.* (2002) investigated the relationship between ischemic episodes in patients with known CAD. The investigation reported an association between acute ischemia and labile ventricular repolarisation, indicated by an enhanced QTV. The cause of this relationship is related to cellular changes, which accompany ischemic episodes, having a destabilising effect on ventricular repolarisation (Murabayashi *et al.*, 2002). Similarly, Hiromoto *et al.*

(2006) investigated the the relationship between QTV and LV function in patients with previous myocardial infarction. The authors reported a strong correlation between QTV, the infarcted site and LV function. In myocardial infarction patients, an elevated QTV has been reported (Hasan *et al.*, 2013). This phenomena can be observed in Fig. 2.3. Furthermore, the authors observed that optimal discrimination between myocardial infarction patients and healthy subjects could be observed by evaluating QTV across lead II. The interrelated relationship between CAD, myocardial ischemia and myocardial infarction may attribute to this recurrent observation in increased QTV. In hypertrophic cardiomyopathy (HCM) caused by beta-myosin heavy chain mutation, an increased QTV_i has been reported (Atiga *et al.*, 2000). Additionally, in HCM patients from ambulatory ECG, increased SDQT was observed (Cuomo *et al.*, 2004). In summary, the described works demonstrate the importance of assessing QTV when investigating cardiac defects.

QTV has similarly been investigated in non-cardiac diseases. Correlations between mental disorders and increased QTV have been observed. In panic disorder (PD) patients, an increased short-term QTV_i has been reported (Baumert *et al.*, 2016b; Pohl and K Yeragani, 2001; Yeragani and Kumar, 2000). Pohl and K Yeragani (2001) described a similar increase in QTV - rising with the ingestion of the sympathetic stimulation agent, isoproterenol. Additionally, 24-hour Holter ECG recordings have indicated higher QTV measures at night-time in patients with PD (Yeragani *et al.*, 2002). Short-term antidepressant treatment tended to increase QTV_i (Koschke *et al.*, 2009). Furthermore, in myocardial infarction patients, depression and QTV_i were correlated - suggesting an increased risk in SCD (Carney *et al.*, 2003). In sleep studies, elevated QTV has been observed in obstructive sleep apnoea (Baumert *et al.*, 2008). Similarly, an increased QT-corrected interval dispersion has been reported in obstructive sleep apnoea patients. Bonnet *et al.* (2005) observed that caffeine induced sympathetic activation resulted in increased QTV_i during rapid eye movement (REM) sleep. The authors concluded that the increase was most likely due to the sympathetic effects of caffeine. QTV has been evaluated in numerous other non-cardiac studies. In a spinal cord study (Ravensbergen *et al.*, 2012), increased QTV_i was reported for thoracic nerve injury (T5-T6); this level of spinal cord injury relates to the vertebrae located in the mid-back. Further studies have found a correlation between QTV and diabetes mellitus, autonomic neuropathy and renal failure (Baumert *et al.*, 2016a). The plethora of research on both cardiac and non-cardiac diseases suggests QTV may contain important information for improving the understanding of physiology and pathophysiology in these conditions. Additionally, evidence suggesting similar QTV changes across related diseases (e.g. - CAD, myocardial ischemia, myocardial infarction, CM and others) provides support

for continued research efforts. Application specific tools capable of capturing subtle beat-to-beat dynamics, both temporally and morphologically, are critical for the future study of QTV.

VCG Features

Increased beat-to-beat variability in the QT interval has been linked to heart disease and mortality. As such, a variety of VCG markers to assess ventricular repolarisation (QRS-loop) and depolarisation (T-loop) lability have been proposed. A common metric is total cosine R to T (TCRT), which is a measure of vector deviation between the QRS-loop and T-loop. It is obtained by calculating the cosine values between the dominant QRS-loop and T-loop vectors within the optimised decomposition space. The TCRT metric has been analysed in a series of studies (Acar *et al.*, 1999; Smetana *et al.*, 2004). The clinical utility of TCRT is unclear, showing predictive capabilities for cardiac mortality in some studies (Porthan *et al.*, 2009; Huang *et al.*, 2009), whilst not in others (Perkiömäki *et al.*, 2006; Lin *et al.*, 2007). The majority of previous studies utilised single beat analysis of the VCG. In Hasan *et al.* (2012a), beat-to-beat dynamics of TCRT were investigated by evaluating the mean and standard deviation across each recording. The authors observed no significant difference between myocardial infarction patients and healthy subjects. The aforementioned study (Hasan *et al.*, 2012a), is the most comprehensive analysis of beat-to-beat dynamics in myocardial infarction patients to date. Three distance variability (DV) features pertaining to dynamic ventricular depolarisation (T-loop) assessment presented in this study included: 1) standard deviation (SD) of mean loop length (MLL), 2) SD of DV_T and 3) mean of DV_T. Briefly, the MLL was obtained by the euclidean summation of consecutive points in the loop. The DV was obtained by taking the coefficient of variance of the shortest point-to-point distance between the T-loop and template T-loop; the shortest distance was determined by employing kNN between the two loops. Each of the three VCG features mentioned was reported to demonstrate a statistical difference between myocardial infarction patients and healthy subjects. Tereshchenko *et al.* (2010) investigated ventricular ventricular arrhythmias in implantable cardioverter-defibrillator (ICD) using beat-to-beat VCG metrics. The authors reported that large T-peak cloud volume (convex hull volume of T-peaks across a serial recording) is associated with increased risk of VT in patients with structural heart disease and systolic dysfunction. In a follow-up study, (Han and Tereshchenko, 2010) similarly

reported a correlation between elevated T-peak cloud volume, sustained VT and appropriate therapies. Additional investigations have reported predictive value between three-dimensional QRST integral sums and SCD (Sur *et al.*, 2013). The investigation of dynamic VCG features in cardiac diseases is promising and requires further study.

2.2 Registration and Machine Learning

In this section a brief overview of image registration and machine learning is provided. Registration and machine learning serve an important role in the original contributions of this thesis. Registration-inspired transformation and optimisation are employed in the study of ECG feature extraction. Machine learning is used to assess the discriminative abilities of given features in diagnosing heart disease.

2.2.1 Registration

Registration can be described as the process of aligning two sets of data by a spatial transformation. There are two primary fields of study in registration: image and point-set. The two are extremely intertwined and overlapping. Image registration relies on image intensities whereas point-set registration is applied across point clouds. In this thesis, they encompass the umbrella term - registration. Through registration, correspondences between data samples can be obtained. This is important in pseudo-periodic biomedical signals where subtle feature shifts manifest between cycles and in the presence of noise.

The general registration process consists of three distinct mathematical considerations: shape representation, transformation and registration criteria (Huang *et al.*, 2006). Shape representation pertains to the selection of data description, common choices include: clouds of points (Cartesian coordinates), Fourier descriptors and medial axes. Transformation corresponds to the mathematical model under which the data are transformed. Data can be transformed globally or locally. Global transformations homogeneously alter data and include the set of affine transformations: translation, rotation, skew (line parallelism preserving distortion) and scaling (Oliveira and Tavares, 2014). Local transformations correspond to inhomogeneous mathematical motions, common methods include: optical flow, free form deformations (FFD) and thin plate splines (TPS) (Huang *et al.*, 2006). Lastly, registration criteria relates to the process under which optimal transformation parameters are obtained. This can be achieved by an estimate of geometric correspondences which are then used

to estimate the transformation. Alternatively, energy functionals can be optimised using derivative/heuristic techniques. Registration and template adaptation draw many parallels. However, template adaptation methods typically neglect to treat temporal deviations as a two-dimensional process and with moving point-to-point correspondences.

2.2.2 Machine Learning

Classification describes the process in which a computer program is queried to specify which of k categories an input belongs to based on a feature vector (Goodfellow *et al.*, 2016). Where labelled data is provided (a priori knowledge), classification is considered supervised learning (Sathya and Abraham, 2013). Unsupervised learning describes a system where categorical labels are not provided. Instead, the classification algorithm infers category separation using techniques capable of determining which observations are related. Many classification algorithms exist, including but not limited to: linear discriminant analysis (LDA), adaptive boosting, naive Bayes, support vector machines, decision trees and logistic regression (Sarker, 2021). In this thesis, classification is performed by supervised learning methods, namely: kNN and LSTM. For brevity, a brief overview of machine learning techniques only related to the original contributions of this thesis are provided.
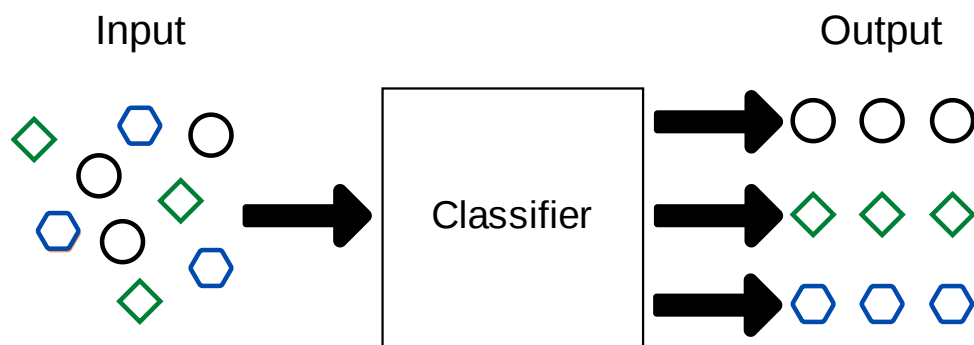
Figure 2.4. Flow diagram of an idealised supervised classifier trained to discriminate three categories (circle, hexagon and triangle).

Classification in supervised learning is defined by a series of processes. The first step requires the input of labelled observational data into the classification algorithm. For each observation, the probability it belongs to any given class is estimated using the cost function which the classifier was previously trained on. Common cost functions include distance metrics and statistical measures of similarity. The training step involves the optimised minimisation of the classification error between the input (labelled data) and the classified

output samples. Fig. 2.4 depicts the information flow for an arbitrary supervised learning classifier.

k-Nearest Neighbours

The kNN algorithm is a simple and interpretable method for classification requiring two design selections: 1) the distance function and 2) the value of k - which denotes the number of neighbours to evaluate the distance function against (Zhang, 2016). Classification is performed by a majority vote based on historical data stored in the framework (Sarker, 2021). For the case where k is selected to be an even number, the tie-break can be decided by evaluating the distance values to each of the k neighbouring samples, or at random. kNN is considered an instance-based learning method since it does not focus on constructing a general internal model, instead it stores all instances of the provided training data (Sarker, 2021).

Artificial Neural Networks

An artificial neural network (ANN) is a machine learning framework in which non-linear elements (neurons) are ordered in successive layers (Lek and Park, 2008). Information flow is unidirectional, flowing from the input layer to the output later, via a hidden layer or series of hidden layers. Nodes are connected between layers with no lateral connection between nodes or feedback in any given layer (Lek and Park, 2008). Each neuron contains a set of parameters, known as weights and biases, which through an iterative process (back-propagation) are updated to minimise the difference between predicted and target outputs. The predicted output is obtained by the forward-propagation process, in which the current weight and bias values are employed to produce an estimate (Goodfellow *et al.*, 2016).

Recurrent Neural Networks

Recurrent neural networks are a set of algorithms related to ANN with feedback links capable of incorporating current and past information. They are used in analysing and learning sequential data such as time series (Sarker, 2021). Generally, a recurrent neural network (RNN) contains a series of stacked neural networks that are capable of passing information across time steps. During back-propagation and forward-propagation, the state of the current time step is inferred from all previous time steps. The most commonly employed RNN is the LSTM. The LSTM was proposed to address long-term dependencies that occur

in muli-layer neural networks (Hochreiter and Schmidhuber, 1997). The authors introduced the use of memory cells, which are able to discern relevant information and control the information flow between stacked networks (Hochreiter and Schmidhuber, 1997).

2.2.3 Automated ECG Analysis Applications

A number of mathematical models have been employed in the ECG and VCG to measure cardiac repolarisation and depolarisation lability. Similarly, a series of classification frameworks have been used to assess their diagnostic and prognostic capabilities in assessing cardiac diseases. Here, a brief review is provided into: 1) automated (and semi-automated) QTV and VCG techniques and 2) myocardial infarction and myocardial ischemia classification methods.

QTV Methods

Automated ECG delineation is an area of research which has received much attention. ECG delineation is a difficult task due to the varying manifestation of conditions and diseases in waveform morphology. In QTV analysis, this task is further complicated by the subtle beat-to-beat changes and reduced signal amplitudes in the T-wave. Simulated data for the evaluation of the QT-interval has previously been generated (Baumert *et al.*, 2012), against which a series of algorithms have been evaluated (Schmidt *et al.*, 2014, 2018a). Similarly, annotated clinical data (QTDB) exists for the assessment of algorithmic measurement of the QT-interval and other waveforms.

Numerous methods have been proposed for measurement of the QT-interval. One of the most commonly employed is a derivative based technique (Baumert *et al.*, 2012). The derivative algorithm (Porta *et al.*, 1998) is dependent on a series of pre-processing steps, namely: QRS detection, parabolic fitting, identification of the isoelectric line, detection of the T-wave and signal differentiation. Subsequently, the T-wave end is located where the absolute value of the first derivative of the T-wave down slope is below a pre-determined threshold. The performance of this algorithm was reported to be sub-optimal in comparison to two early template based methods (Baumert *et al.*, 2012). Template based methods have evolved over time but follow the same underlying principle. A template of the entire beat or segment(s) of the beat is obtained by averaging across the sequence (Schmidt *et al.*, 2014, 2018a; Starc and Schlegel, 2006) or selecting a single representative beat (Berger *et al.*, 1997). Early template adaptation schemes were solely based on temporal adaptations. In

2.2.3 Automated ECG Analysis Applications

Berger *et al.* (1997), the focus is on manually defining a QT interval by annotating the beginning of the QRS complex and the T-wave offset for a single beat; the T-wave onset is similarly annotated. The ECG is resampled to 1 KHz and R-peak detections is performed via the automated Pan and Tompkins algorithm (Pan and Tompkins, 1985). For each beat, the T-wave template is then compressed or stretched based on a sum of squared differences error function with a progressive search performed to determine the optimal scaling factor (Berger *et al.*, 1997). Finally, the duration of this scaled T-wave combined with the constant time interval between the QRS onset and T-wave onset yields the estimated QT interval. In Starc and Schlegel (2006), a similar sub-segment adaptation approach is taken. However, the fundamental idea in this technique is to independently adapt template data for both the QRS complex and the T-wave in a fully-automated manner. Template generation is performed by averaging the respective waves across 60 beats, with a dissimilarity exclusion criteria included. Subsequently, the QRS-complex and T-wave are respectively shifted along the temporal axis to obtain the best-fit relative to the template. Baumert *et al.* (2012) reported that the two described template matching algorithms, particularly the time shifting algorithm (Starc and Schlegel, 2006), performed better in QT interval detection compared to conventional methods; the simulated data contained AWGN, BW and AM, respectively. Thus, the authors recommended the use of template adaptation techniques in future beat-to-beat analysis of QTV. More recently, Schmidt *et al.* (2014, 2018a) proposed two-dimensional signal warping across the duration of an entire beat. In their works, the authors stipulated that accurate QT interval measurement required adaptation across both time and signal amplitude. Briefly, two-dimensional signal warping is performed by obtaining a time-averaged template of the entire beat, with a rejection criteria. QT interval annotation can be obtained manually or automatically and R-peak detection is obtained by a previously proposed method (Afonso *et al.*, 1999) - in the absence of manual QRS annotations. The template is locally adapted by a geometrically defined grid of control points against each beat and optimised by minimising a sum of squared errors cost function. The resultant waveform yields a warped signal capable of capturing subtle morphological deviations in two-dimensions. The works of Schmidt *et al.* (2014, 2018a) yielded significantly improved results in QT interval measurement against the same simulated database and previously proposed template adaptation methods for QT interval detection (Berger *et al.*, 1997; Starc and Schlegel, 2006). Furthermore, statistical analysis of SDQT across the PTB database yielded a significantly increased QTV in comparison to the template stretch algorithm (Berger *et al.*, 1997).

The performance of two-dimensional signal warping has also been assessed against the QTDB. This database contains manual QT interval annotations and has been previously used by a series of a methods (Laguna *et al.*, 1994; Vullings *et al.*, 1998; Martinez *et al.*, 2004; Zifan *et al.*, 2005; Dubois *et al.*, 2007; Rincón *et al.*, 2011) to assess performance of ECG delineation with results reported for QRS onset and T-wave offset measurement. Early works (Laguna *et al.*, 1994), focused on delineation via the use of the differentiated ECG signal and information related to wave shape. The method utilised criteria to identify wave presence or absence in each lead according to the relative differentiated signal magnitude in the different waves. Subsequently, the wave boundaries were inferred using a threshold based analytical rule inferred from manual expert measurements. Later works by Vullings *et al.* (1998) proposed the use of dynamic time warping (DTW) across an annotated reference beat in three regions, namely the: P-region, QRS-region and T-region. DTW determines the optimal match between two time series by evaluating a cost path and imposing a series of restrictions; this method shares similarities with template adaptation. In Martinez *et al.* (2004), a wavelet based algorithm was proposed to delineate the ECG. At the time of publication (2004), the authors reported the lowest standard deviation error in the T-wave offset (18.1 ms) in supervised two lead evaluation. Zifan *et al.* (2005) proposed the automated delineation of ECG by using a piecewise derivative DTW; to date, this method has yielded the lowest standard deviation error in the measurement of the QRS onset (3.60 ms) across the QTDB. Consequent works, by Dubois *et al.* (2007), described an automatic ECG feature extraction technique using generalised orthogonal forward regression (GOFR) combined with a custom parameterised function - the Gaussian mesa function. GOFR segments the heartbeat signal into a series of Gaussian mesa functions where each wave is modelled by a single function; thus, producing an interpretable result. However, the authors did not report QRS onset results; additionally, the reported standard deviation error in T wave offset detection is the highest amongst the reviewed literature. Lastly, Rincón *et al.* (2011) proposed an additional wavelet-based ECG delineation algorithm with a multilead caveat to exploit the information available across multiple leads and improve accuracy, stability and resilience to artifacts compared to single-lead systems. At the time of publication (2011), the authors reported state-of-the-art performance in supervised two-lead evaluation - with their method yielding the minimum standard deviation error in the T wave offset (16.9 ms) and the second-lowest standard deviation error in the QRS onset (7.0 ms). However, the subsequent development of two-dimensional signal warping (Schmidt *et al.*, 2014) yielded both a lower standard deviation error in the T-wave offset

2.2.3 Automated ECG Analysis Applications

(12.8 ms) and QRS onset (6.1 ms) in supervised two lead evaluation. For detailed numeric results pertaining to the outlined algorithms refer to Table 4.3.

VCG Methods

Automated beat-to-beat QT interval feature extraction in VCG has received far less consideration than it's contemporary, the ECG. In large part, this is due to the relative sparsity of available VCG data and the difficulty in assessing VCG morphology relative to physiology. As such, a well-established metric akin to QTV in ECG has not been adopted for the assessment of ventricular depolarisation and repolarisation lability. Furthermore, no standard annotated database exists for the assessment of VCG loop feature accuracy. However, beat-to-beat methods have been assessed against simulated data (Astrom *et al.*, 2000) and in diagnostic or prognostic applications for several cardiac diseases (Hasan and Abbott, 2016).

Subtle beat-to-beat variation in QRS-loops of the VCG have been employed to study electrical instability of the heart. In such studies, the variability was quantified by the ensemble variance of successive time-aligned sinus beats (Ben-Haim *et al.*, 1991; Prasad and Gupta, 1979). Furthermore, these works considered an increased variance to be indicative of cardiac instability. However, these methods were inherently flawed as they employed inadequate means for respiratory compensation by neglecting loop alignment; thus, suffering from increased variability unrelated to cardiac defects. Loop alignment refers to the process of optimally positioning each beat to a reference beat. It can be considered a form of three-dimensional template adaptation where the loop(s) of each beat are adapted to a reference beat. To address this limitation, Sörnmo (1998) proposed a method for global alignment of VCG. The authors employed rotation, scaling and time synchronisation to achieve appropriate loop alignment. Parameter estimation was achieved using a maximum-likelihood estimator. The study reported that measurements on morphological variability were reduced by a factor of 0.53 after loop alignment. Further analysis by Astrom *et al.* (2000) assessed the breakdown noise level of the proposed loop alignment technique; concluding that the breakdown point is highly correlated to the loop morphology. Loop alignment analysis holds important implications for beat-to-beat assessment of trigonometric VCG features such as TCRT.

In Karsikas *et al.* (2009), the authors assessed differences in CAD patients versus healthy subjects using TCRT. The method employed a simple framework consisting of: digital filtering, an R-detector, removal of extrasystoles and heart-rate normalised segmentation

of the QRS-loop and T-loop. TCRT analysis has been further expanded to account for rate-dependence using regression fitting (Kentta *et al.*, 2010). In their investigation, the authors attempted to account for rate dependence by analysing a series of regression models, including: linear, hyperbolic, parabolic, logarithmic, shifted logarithmic, exponential and second-degree polynomial. Additional works, by Han and Tereshchenko (2010), proposed a method for the assessment of ventricular lability using convex hulls. The technique employed baseline wander correction using a zero-order polynomial fit between R-peaks and subtraction between the polynomial fit and the baseline. Severe noise was reduced with a low-pass filter and premature ventricular complex beats were manually rejected.

Ischemic Beat Classification

Myocardial ischemia detection methods have been explored using a variety of threshold-based and classification techniques. The literature in myocardial ischemia can be separated into two distinct areas - ischemic episode detection and ischemic beat detection. In this thesis the focus is on the beat specific aspect of ischemic detection. The database employed in this thesis, and existing ischemic beat classification research, is the EST-T database; which is publicly available with ischemic episode annotations on Physionet. To study ischemic beat detection, an external set of beat-specific annotations have been generated for this database. The key advantage in using this subset of updated annotations is that they do not assume that each beat in an ischemic episode may necessarily manifest as an ischemic beat. Techniques which assessed this same subset of ischemic beats are described below.

In Papaloukas *et al.* (2001), the authors used a knowledge-based technique (with thresholds for the J80 point and ST segment slope) in conjunction with pre-processing steps for ECG noise handling and feature extraction. Subsequent works (Papaloukas *et al.*, 2002b,a), employed the use of principal component analysis (PCA) and ANN for ischemic beat detection. Raw ECG information was fed into the classifier and PCA, a popular dimensionality reduction technique, was used to decrease the input feature size. Further investigations evaluated the use of multi-criteria decision analysis (Goletsis *et al.*, 2003, 2004) and mining-based association rule classification (Exarchos *et al.*, 2006). Additionally, fuzzy expert systems (Exarchos *et al.*, 2007; Tsipouras *et al.*, 2007) have been investigated in the development of ischemic beat classifiers. These systems employed the use of a crisp set of rules to deduce a series of fuzzy rules, thus, creating a fuzzy model.

2.2.3 Automated ECG Analysis Applications

Myocardial Infarction Classification

Myocardial infarction classification has been extensively studied in ECG. Researchers have used a variety of pre-processing methods, features and classifiers (Ansari *et al.*, 2017). Commonly employed pre-processing methods have included baseline wander removal, noise removal, beat averaging and ectopic beat removal (Ansari *et al.*, 2017). From a feature standpoint - morphological descriptors (e.g. ST-segment deviation), wavelet transforms and PCA have been widely employed to reduce dimensionality and improve robustness. Here, a broad overview of the primary classification techniques is described, with a specific focus on methods analysing the PTB database.

Classification techniques have greatly evolved with the advent of deep learning and improvements in computational resources. Earlier methods relied on less computationally demanding techniques such as DTW. In Huang and Kinsner (2002), the authors proposed a DTW system combined with thresholding to achieve frame classification - the study reported an 89.7% sensitivity and 84.6% specificity across a single recording from the MIT-BIH Arrhythmia database. Zhou *et al.* (2011) used a polynomial approximation combined with PCA and a support vector machine (SVM) to achieve classification - they reported an 98.7% sensitivity and 96.6% specificity across the PTB database. Arif *et al.* (2012) employed the use of a kNN scheme to achieve detection - obtaining a 99.6% sensitivity and 99.1% specificity across the PTB database. In Sharma *et al.* (2015), a multiscale energy and eigenspace approach was introduced for classification of myocardial infarction. The basis for the framework was that pathological information alters covariance structures of multiscale multivariate matrices; and that eignevalue analysis can capture these morphological deviations when combined with SVMs. The authors reported a 93% sensitivity and 99% specificity across the PTB database. More recently, numerous deep learning methods have been presented. Lui and Chow (2018) proposed a convolutional neural network (CNN) combined with a RNN to achieve classification. The study reported a 92.4% sensitivity and 97.7% specificity across the PTB database. Similar works by Acharya *et al.* (2017) reported a 95.5% sensitivity and 94.2% specificity by implementing a CNN against the same database. More advanced deep learning concepts such as, transfer learning, have also been presented in literature (Kachuee *et al.*, 2018). In this investigation, information learned from arrhythmia classification was utilised as a reference for training of the evaluated CNN classifiers. The authors reported a 95.2% precision and 95.1% recall rate across the PTB database, respectively. Image processing inspired techniques have also arisen in literature, where one-dimensional ECG data are transformed by the use of Gramian Angular Fields,

Recurrence Plots and Markov Transition Fields into an aggregated image (Ahmad *et al.*, 2021). CNN outputs of the images are then fed into an SVM to perform classification. The authors reported both a 98% statistical precision and recall rate across the PTB database.

Significantly lesser research efforts have been placed on VCG based myocardial infarction detection. This is in part due to a clinical preference toward analysing the ECG. However, some works have incorporated VCG data in their classification frameworks and reported promising results. In Yang (2011), the authors proposed a multiscale recurrence quantification analysis of VCG across multiple wavelet scales combined with three classification methods, namely: LDA, quadratic discriminant analysis and kNN. The overall classification accuracy of the LDA (accuracy-92.7%, sensitivity-96.5%, specificity-75%) was shown to outperform the scores of eight cardiologists (accuracy-87.2%, sensitivity-80.3%, specificity-97.1%) employed for the study by 5.5% across the PTB database. An additional analysis using DTW and self-organising maps across VCG was presented by the same group (Yang *et al.*, 2013) - they reported a 91.4% accuracy, 86.8% sensitivity and 92.5% specificity in distinguishing myocardial infarction patients from healthy subjects across the same database.

2.2.4   Limitations in Previous ECG Analysis Applications

Although great strides have been made, the presented literature on ECG and VCG evaluation methods still has several areas requiring further investigation. Firstly, for the analysis of ventricular depolarisation and repolarisation lability in VCG, no concerted effort has been made to capture subtle morphological changes, which carry important diagnostic and prognostic information. Current VCG literature focused on adaptation methods has solely explored global variations in loop morphology, namely: time synchronisation, translation, rotation and scaling. Nonetheless, previous investigations on loop morphology have presented important findings paving the way for further research. Furthermore, inhomogeneous template adaptation methods in ECG have been previously investigated and demonstrated state-of-the-art results in QTV measurement. Since the VCG consists of three orthogonal ECG leads, the state-of-the-art performance of template adaptation should theoretically extend in three-dimensions. Moreover, previously proposed methods in VCG analysis have primarily focused on trigonometric features such as TCRT. Important results have been demonstrated from the analysis of trigonometric variables, in turn, providing a basis for the analysis of geometric variables. The sparse analysis of geometric features has in part been due to the lack of an adequate VCG pre-processing framework. In summary, a tailored

2.2.4 Limitations in Previous ECG Analysis Applications

method has not been previously proposed to study complex VCG beat-to-beat variations in morphology.

Although template adaptation methods have previously demonstrated state-of-the-art results in ECG literature, further modes of improvement can be explored. Firstly, the majority of methods have focused on homogeneous template adaptation, in turn, neglecting to capture a significant amount of spatial information. For methods that have addressed template adaptation as a two-dimensional process, the correspondence problem between point-sets has not been treated as a moving and probabilistic process. Additionally, the performance of these methods has been been assessed across other quasi-periodic biomedical signals (e.g. - PPG). Hence, a general solution treating inhomogeneous template adaptation as a time-series registration process, ought to be explored using inhomogeneous template adaptation as a foundation.

In ischemic beat detection literature, little emphasis has been placed on utilising robust feature extraction methods such as template adaptation, which have recently demonstrated improved performance relative to previously proposed methods. Additionally, current literature studying ischemic beat detection has neglected to utilise appropriate cross-validation techniques, thus reporting results which are not necessarily representative of true performance across unseen data. This is the case as previous works have permitted data leakage between training and validation sets in the classification process. A hold-out or k-fold cross validation scheme has not been employed in these works. Thus, the evaluation of systems with adequate feature extraction and cross-validation should be explored to build on previous works.

In myocardial infarction applications, little research effort has been placed on utilising VCG for classification. Furthermore, the use of LSTMs has been neglected. LSTMs should theoretically be able to capture subtle and complex morphological relations pertaining to variability across temporal sequences - by exploiting past information. Furthermore, pre-processing involving the use of template adaptation techniques has received little attention. Such methods have been shown, in this thesis and previous works, to exhibit improved capabilities in capturing subtle beat-to-beat morphological variations. Hence, pre-processing and classification are both areas which can be further investigated in myocardial infarction detection.

Although promising research has been conducted on VRV in non-ischemic CM patients, the potential for risk stratification remains unclear. In particular, beat-to-beat variability metrics

have received little attention outside of HRV and QTV_i. Beat-to-beat variability has been observed across a variety of cardiac conditions and diseases. Thus, further study of ECG and VCG metrics assessing risk stratification in non-ischemic CM patients should be pursued to provide additional insights.

2.3 Contributions

The key contributions that this thesis provides are separated into two parts: algorithm development and respective applications. In the algorithm development chapters, gaps in current VCG and ECG algorithmic literature are addressed. Subsequently, in the applications chapters, the developed algorithmic frameworks from the first section are employed in the analysis of several cardiac diseases, including: myocardial ischemia, myocardial infarction and non-ischemic CM.

2.3.1 Algorithmic Development

Firstly, VCG analysis was addressed as an inhomogeneous template adaptation process. This study introduced a method capable of capturing subtle beat-to-beat morphological deviations in three-dimensional data. Previous literature has solely addressed this as a homogeneous process; focusing on global changes in morphology. Furthermore, geometric features of T-loop variability were adapted from previous works and applied to study myocardial infarction. The method utilised parametric fitting drawn from computer vision studies in the form of - FFD, combined with kernel ridge regression to capture localised deviations in signal morphology. State-of-the-art pre-processing was performed utilising two-dimensional signal warping, for the purpose of T-loop extraction.

Subsequently, a novel two-dimensional template adaptation method was formulated as a modified registration process. Similarly to the first method, the technique employed FFD parametrisation, however, in two-dimensions. In this work, the FFD control point grid was resolved as an incremental process via gradient based optimisation. This produced an interpretable physical result pertaining to the control point locations. Furthermore, a constrained correspondence matrix was employed which permitted for non-binary probabilistic correlations between samples of the template and target data, thus, allowing for temporal interpolation. The method was assessed against state-of-the art ECG algorithms using previous benchmarks, and additionally against simulated PPG data. The latter demonstrated the generalisation capabilities of the algorithm in other quasi-periodic biomedical signals.

2.3.2   Algorithmic Applications

A novel technique for ischemic beat detection was proposed using the correspondence based two-dimensional template adaptation algorithm. The framework employed a semi-automated and fully-interpretable model for the detection of ischemic beats by combining template adaptation with a kNN classifier. The interpretability aspect is significant as many previous works in ischemic detection have neglected to employ methods which can readily be understood by medical practitioners, thus, limiting clinical potential. Furthermore, in ischemic beat detection, previous works have neglected to undertake appropriate cross validation of their systems. In these works, data leakage has been permitted between training and testing data, thus providing a biased assessment of performance. In this thesis, algorithmic assessment is performed using a hold-out strategy to yield more representative statistical measures of performance on unseen data.

Lastly, three-dimensional VCG template adaptation was applied across two smaller studies for the purpose of myocardial infarction detection and VRV analysis in non-ischemic CM. In the myocardial infarction study, two limitations of previous works were addressed - the lack of appropriate pre-processing for VCG and the lack of a classifier capable of capturing historical data (i.e. - LSTM). The second study is a novel investigation into VRV and risk stratification in patients with non-ischemic CM; an area of research that is still unclear. In this investigation, all-cause mortality was assessed against dynamic VCG features and $cQTV_i$ - where patients with a high $cQTV_i$ were found to have a higher all-cause mortality in univariate survival analysis.

Inhomogeneous Template Adaptation of Temporal Quasi-Periodic Three-Dimensional Signals

The content of this chapter is a modified version of the publication:

Karisik, F. and Baumert, M. (2019), 'Inhomogeneous Template Adaptation of Temporal Quasi-Periodic Three-Dimensional Signals', *IEEE Transactions on Signal Processing* **67**, pp. 6067–6077.

Abstract

We propose a novel framework for performing inhomogeneous template adaptation on temporal three-dimensional data. Templates of interest are first globally translated and rotated using statistical methods in the form of Procrustes analysis. In this globally adapted form, the data is parameterized to a minimum bounding rectangular prism using a parameterization method known as free-form deformation. The parameterized model is then reduced to a linear least squares problem, which subsequently allows for a robust local template adaptation scheme utilizing a non-parametric formulation. To account for complex noise behaviour encountered in quasi-periodic signals, we ensue to complete the framework with an adaptive noise model. We demonstrate the power of the proposed framework using three applications: firstly, we quantify the ability of the proposed framework to track geometric features of heart disease on a synthetic dataset containing three-dimensional electrocardiogram signals. Next we track these features on a publicly available real dataset (PTB database) to demonstrate its potential in heart disease diagnostics. Lastly, we apply the proposed framework to map three-dimensional velocity profiles using the publicly available Complex Upper-Limb Movements database.

3.1   Introduction

In signal processing, template adaptation is a technique utilized to match two patterns. Template adaptation accounts for morphological changes by allowing certain variations in the template signal, for which a minimization technique is utilized to obtain the optimal transformation.

Template adaptation techniques are particularly paramount in quasi-periodic signal processing applications (Schmidt *et al.*, 2014; Starc and Schlegel, 2006; Berger *et al.*, 1997; Andreotti *et al.*, 2013). Traditionally, three-dimensional template adaptation techniques in signal processing have focused on a global scale (Astrom *et al.*, 2000). Global adaptation refers to obtaining an optimal homogeneous rotation, translation, scaling and reflection. Conversely, local adaptation refers to obtaining an inhomogeneous data transformation reflecting localized morphological changes. In this paper, we introduce a novel

framework for applying an inhomogeneous template adaptation for temporal quasi-periodic three-dimensional signals using a global-to-local approach.

We relate template adaptation to the registration problem commonly encountered in computer vision. Registration refers to the problem of obtaining a mapping function between two finite point sets in order to minimize a mutual distance metric (Maiseli *et al.*, 2017). Similar to template adaptation, rigid (global) registration refers to homogeneous transformations and non-rigid (local) registration refers to inhomogeneous transformations. Extensive research has been undertaken in non-rigid registration with many applications in shape and image recognition (Vemuri *et al.*, 1998; Huang *et al.*, 2006; Oliveira and Tavares, 2014). The registration problem is an ill-posed problem and has thus received much attention in literature (Besl and McKay, 1992; Pomerleau *et al.*, 2015; Pluim *et al.*, 2003; Crum *et al.*, 2004; Hill *et al.*, 2001). Broadly speaking, non-rigid registration methods differ in three main aspects: representation, transformation and registration criterion (Huang *et al.*, 2006). In this work, we focus on the transformation aspect of registration techniques.

The iterative closest point (ICP) algorithm is perhaps the most notable registration method due to its simplicity and efficacy. Although many variants exist, the generalized ICP approach obtains an optimal translation and rotation by minimizing some error metric iteratively (Besl and McKay, 1992). From a transformation model perspective, the ICP algorithm iteratively performs an optimal rotation and translation. This transformation model is considered to be the simplest and one of the most commonly used registration methods; however the registration method is highly susceptible to outliers in its fundamental form.

Another class of non-rigid registration methods is based on computer graphics parameterization, where a reference shape is embedded into a user defined shape described by its control points. Many such parameterizations exist, including but not limited to: free-form deformation (FFD) (Sederberg and Parry, 1986), barycentric coordinates (Floater *et al.*, 2005) and thin-plate splines (Bookstein, 1989). From the aforementioned, FFD is the most commonly implemented technique in registration problems. In this work, we focus on a probabilistic idea of shape formed by a prior based on FFD with a noise adaptive regularization term; in the process avoiding expensive iterative transformations. Sederbeg and Parry introduced FFD in 1984 as a computer graphics deformation technique. In three dimensions, FFD models embed data into a parallelepiped lattice of control points, where subsequent shifting of control points results in smooth localized deformations. Due to its low computational cost and relative ease of implementation, FFD is the dominant parameterization model in registration techniques. Various models for shifting the control points have

been proposed. Rueckert *et al.* (2001) suggested the use of a mutual information based criterion to solve FFD embedded magnetic resonance image registration problems. Many similar methods have been proposed in the field of image registration (Pluim *et al.*, 2003), however these methods are known to be computationally expensive. In this work, we introduce an adaptive non-parametric least squares minimization to achieve a computationally cost-effective transformation.

In signal processing, where temporal quasi-periodic signals are commonly of interest a prior one-to-one correspondence can be obtained by re-sampling or interpolating the target shape to match the length of the reference shape; assuming quasi-periodicity. Thus, with a correspondence in place, we treat quasi-periodic signals as the transformation aspect of a registration problem, with a focus on obtaining a mapping function between a template and noisy target signal. This is the first such formulation in three-dimensional signal processing.

We aim to illustrate the potential of the forthcoming algorithm by quantifying its ability to robustly measure the variation of three-dimensional physiological signals. Additionally, we aim to illustrate its potential for three-dimensional tracking of hand movement. The electrocardiogram (ECG) is one of the most extensively studied physiological signals (Almeida *et al.*, 2006; García *et al.*, 2003; Sameni *et al.*, 2007). It describes the temporal changes in summed electric potential created by heart muscle cells (Clark and Kruse, 1990). A significant segment of the ECG is denoted as the QT interval. It represents the period of the ventricular depolarization and repolarization process during a cardiac cycle. These processes vary non-linearly from beat-to-beat and elevated QT interval variability has indicated to be a robust predictor of cardiac diseases as well as mortality (Baumert *et al.*, 2016a; Hasan *et al.*, 2012a). Quantifying these subtle changes is technically challenging and and sophisticated template matching algorithms have shown to produce state-of-the-art performance (Baumert *et al.*, 2012; Starc and Schlegel, 2006). Relatedly, vectorcardiography (VCG) is the method of recording the electrical field vector magnitude and direction of activity in the heart (Chou, 1986). VCG produces a method to represent cardiac electrical activity in three orthogonal directions. Recently, beat-to-beat variability in several VCG features has indicated the ability to provide potential diagnostic information for myocardial infarction patients (Hasan *et al.*, 2012a). However, existing signal processing methods utilized to study morphology solely focus on a global template adaptation, neglecting inhomogeneous morphological changes.

3.2 Methodology

In this section, we describe in detail the template adaptation framework. We first explain Procrustes analysis as a statistical tool to achieve global adaptation. Next, we describe the parameterization technique applied on the template. Thereafter, we introduce the notion of ridge regression and formulate our problem as a kernel ridge regression (KRR). We expand on the KRR by briefly describing the kernel used in this work. Next, we present a method for dealing with observations of varying noise level through a simple noise estimation technique. To conclude the section, we describe a subtlety in our implementation boosting performance time and provide a pseudo-code implementation of the proposed framework.

3.2.1 Procrustes Analysis

Procrustes analysis is a statistical shape analysis technique most commonly used to globally align shapes by any combination of optimal translation, rotation, scaling and reflection (Rohlf and Slice, 1990). In our proposed framework, we employ Procrustes analysis for global translation, scaling and rotation of the template. The template and target data are treated as ordered three-dimensional signals. The problem of optimal translation, scaling and rotation can be expressed as an optimization problem to obtain the translation component (T), scaling factor (s_0) and the rotation component (R) in the ensuing equation:

$$Y_g = s_0 R(Y_o) + T,$$

(3.1)

where where Y_g denotes an $N \times 3$ matrix containing the globally adapted template and Y_o denotes an $N \times 3$ matrix containing the original template signal. Procrustes analysis commonly employs a least squares formulation and singular value decomposition (SVD) to obtain the optimal values. The optimal rotation can be obtained using the centroids of the template and target data combined with a SVD. Firstly, we obtain the centroids in the following manner:

$$\bar{Y}_o = \frac{1}{N} \sum_{a=1}^{N} Y_o^a,$$

(3.2)

$$\bar{Y}_t = \frac{1}{N} \sum_{a=1}^{N} Y_t^a,$$

(3.3)

3.2.1 Procrustes Analysis

where Y_t an $N \times 3$ matrix containing the target signal, $\bar{Y}_o$ a three-dimensional vector and $\bar{Y}_t$ a three-dimensional vector. SVD factorizes a matrix into the product of three matrices; (5), where the columns of U and V are orthonormal and the diagonal matrix D contains positive real entries (Strang, 2016). Using the obtained centroid values and SVD the optimal rotation matrix can be obtained in the following manner:

$$H = \sum_{a=1}^{N}(Y_o^a - \bar{Y}_o) \times (Y_t^a - \bar{Y}_t)^T, \tag{3.4}$$

where the SVD of H is given by:

$$H = UDV^T, \tag{3.5}$$

leading to the optimal rotation matrix:

$$R = VU^T. \tag{3.6}$$

Figure 3.1. Example of a three-dimensional global adaptation (red) of template (green) to noisy target (black). The top row (a) shows the result of the adapted three-dimensional signal. Rows two (b), three (c) and four (d) depict the amplitude of each adapted orthogonal channel X, Y and Z against time.

Using the result of the optimal rotation matrix, the optimal global scaling factor and transla-tion matrix can be obtained. The global scaling factor is defined by the normalized trace of

the diagonal matrix D. The translation is the sum of two elements; the rotated centroid of the template and the centroid of the target data. Mathematically, this can be expressed as:

$$T = -R(Y_o) + Y_t. \tag{3.7}$$

The result of the globally adapted template using Procrustes analysis can be observed in Fig. 3.1. Although the global adaptation serves as a useful first step in adapting the template, it is unable to adapt the template to capture subtle inhomogeneous morphological changes.

3.2.2 FFD Parameterization

Free-form deformation is a computer graphics technique for deforming geometric data in a free-form manner (Sederberg and Parry, 1986). Data are embedded into a three-dimensional parallelepiped, defined by lattice of control points, where each embedded data point is parameterized to the lattice of control points. By applying a FFD parameterization onto geometric data, a linear relationship between the control points and data can be obtained. We exploit the linear relationship to formulate a non-parametric statistical template adaptation method.

Mathematically, FFD is defined in terms of a tensor product tri-variate Bernstein polynomial. Free-form deformation imposes a local coordinate system on a parallelepiped region (Sederberg and Parry, 1986; Procházková, 2017). In this work, a constant lattice of $2 \times 2 \times 2$ (eight control points) was used for all experiments. Fig. 3.2 illustrates a three-dimensional signal enclosed by the minimum-bounding rectangular prism containing the globally adapted template and the target signal as denoted in the caption. Any point, Y_g^a, in the globally adapted template signal, Y_g, has (s, t, u) coordinates in a FFD system expressed as:

$$Y_g^a = X_o + sS + tT + uU. \tag{3.8}$$

The (s, t, u) coordinates of Y_g^a can be obtained in the following manner:

$$s = \frac{T \times U(Y_g^a - X_o)}{T \times U \times S}, \tag{3.9}$$

3.2.2 FFD Parameterization

$$t = \frac{S \times U(Y_g^a - X_o)}{S \times U \times T}, \tag{3.10}$$

$$u = \frac{S \times T(Y_g^a - X_o)}{S \times T \times U}, \tag{3.11}$$

where X_o denotes the origin of the parallelepiped and $\{S, T, U\}$ the embedding lengths of the parallelepiped from the origin. In this coordinate system, the control points can be expressed as:

$$P_{ijk} = X_o + \frac{i}{l}S + \frac{j}{m}T + \frac{k}{n}U, \tag{3.12}$$

where l, m, n denote the number of control points in each of the three directions (i.e. $l, m, n = 1$) of the lattice and i, j, k the index (i.e. $i, j, k = \{0, 1\}$) of each control point in the respective direction. To obtain a linear relationship between any sample point, a of Y_g^a, and an FFD lattice control point, P_{ijk}, requires evaluation of the following equation:

$$
\begin{aligned}
x_{ijk}^a = \sum_{i=0}^{l} \binom{l}{i}(1-s)^{l-i}s^i \times \\
\sum_{j=0}^{m} \binom{m}{j}(1-t)^{m-j}t^j \times \\
\sum_{k=0}^{n} \binom{n}{k}(1-u)^{n-k}u^k
\end{aligned}
\tag{3.13}
$$

where s, t and u denotes the embedding rectangular prism localized coordinate system. Thus, by applying an FFD parameterization for each point in the template signal, Y_g, we can obtain the following linear relationship:

$$Y_g = XV, \tag{3.14}$$

where X denotes the $N \times 8$ matrix containing the FFD weights and V the 8×3 matrix containing the control point spatial coordinates.

To obtain a linear least squares adaptation of the template signal to a target signal, Y_t, that is, obtain the optimal location of the control points using (14), we formulate the location of the control points in the following manner:

$$V_l = (X^T X)^{-1} X^T Y_t, \tag{3.15}$$

such that,

$$Y_l = XV_l, \tag{3.16}$$

where V_l denotes the optimal location of the lattice control points and Y_l the locally adapted template. Although elegant, this parametric template adaptation formulation is unable to robustly adapt the template signal to a target signal due to a finite dimensional relationship between the parameterization and data. To address this issue, we introduce a novel non-parametric method with adaptive hyper-parameter estimation in the following section. We formulate the linear least squares regression as a kernel ridge regression problem. We no longer attempt to adapt the template by spatially shifting the control points in three-dimensions, but instead we utilize the parameterized coordinates as input weights into the non-parametric method; in the process conceding the smoothness properties of FFD, and instead inheriting the smoothness properties of the nonparametric model described in the next section. The parameterization of the template data to a minimum-bounding rectangular prism is performed for each new target signal. In addition, the Procrustes analysis transformation produces a set of more robust FFD weights compared to a direct parameterization on the original template. This is achieved by embedding the globally adapted template to a lattice closer resembling the target signal.
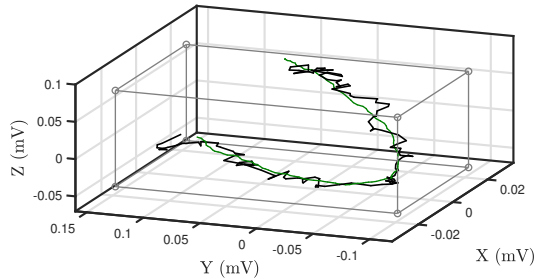
Figure 3.2. Example of globally adapted template (green) parameterization to a minimum-bounding rectangular prism (grey) containing the three-dimensional template and current target beat (black).

3.2.3   Kernel Ridge Regression

Kernel ridge regression can be considered the kernel extension of ridge regression (Schölkopf *et al.*, 2013). Ridge regression is a formulation of linear least squares which adds a regularization term to the standard formulation (Marquardt and Snee, 1975). The role of regularization in the proposed framework is to penalize overfitting the template to noisy observations. Regularization can also serve as a method to produce a unique solution in regression problems (Neumaier, 1998). Formulating the inhomogeneous template adaptation process in

the form of a KRR, we obtain:

$$f^*(Y_t, \Lambda, l, c_1) = K(K + c_1\Lambda)^{-1}Y_t, \tag{3.17}$$

where Λ denotes the adaptive diagonal regularization matrix, l the adaptive kernel length, c_1 an adaptive scalar multiplying factor and K the kernelized form of the FFD weights matrix X. We estimate c_1 on a target-to-target shape basis using a heuristic method described in the forthcoming section. Using this formulation, the parameterization matrix is embedded by a kernel function that translates the finite-dimensional parametric model into a non-parametric model. In this work, we employ a smoothing Gaussian kernel function (Hofmann *et al.*, 2008). Mathematically, this kernel function can be expressed in the following form:

$$k(x, x') = exp(-\frac{|x - x^2|}{2l^2}), \tag{3.18}$$

where l denotes the kernel width (Duvenaud, 2014). The kernel width dictates the length of the wiggles in the adaptation function. For all experiments in this work, we used a variation of a common mean estimation for the kernel width (Hofmann *et al.*, 2008) as described in Algorithm 1; we added a standard deviation factor to account for variations in scale. The Gaussian kernel function was selected for its smoothing properties which are inherent to the bell-shaped Gaussian distribution. The result of the local adaptation can be observed in Fig. 3.3.

3.2.4 Adaptive Noise Estimation

To account for the dynamic nature of noise levels that may be encountered in quasi-periodic signals, we employed an adaptive data-driven diagonal regularization matrix, which differs from traditional regularization models that employ an identity matrix. We propose the use of a normalised stationary noise estimation model, where each entry of the diagonal matrix λ is estimated as the difference between observations. For an $N \times N$ diagonal matrix, Y_{target}, the ath diagonal entry can be mathematically expressed as:

$$\Lambda_a = \frac{Y_t^a - Y_t^{a-1}}{max(\Lambda)}. \tag{3.19}$$

The intuition behind using a simple differentiation noise model stems from attempting to penalize large deviations between points; thus simultaneously penalizing adaptations not
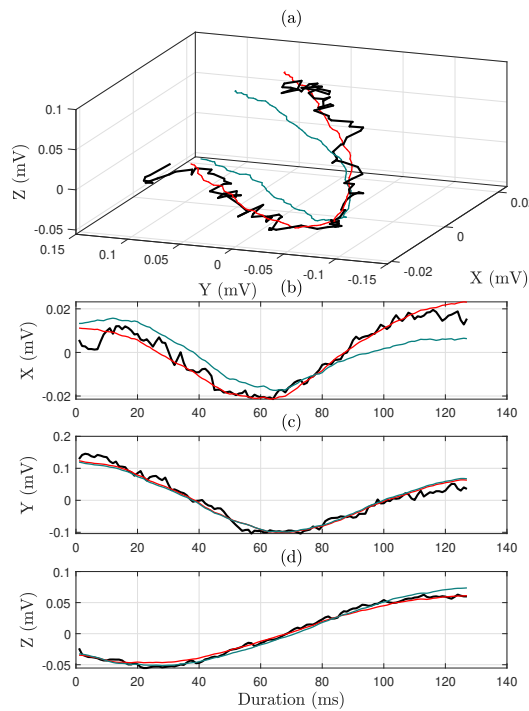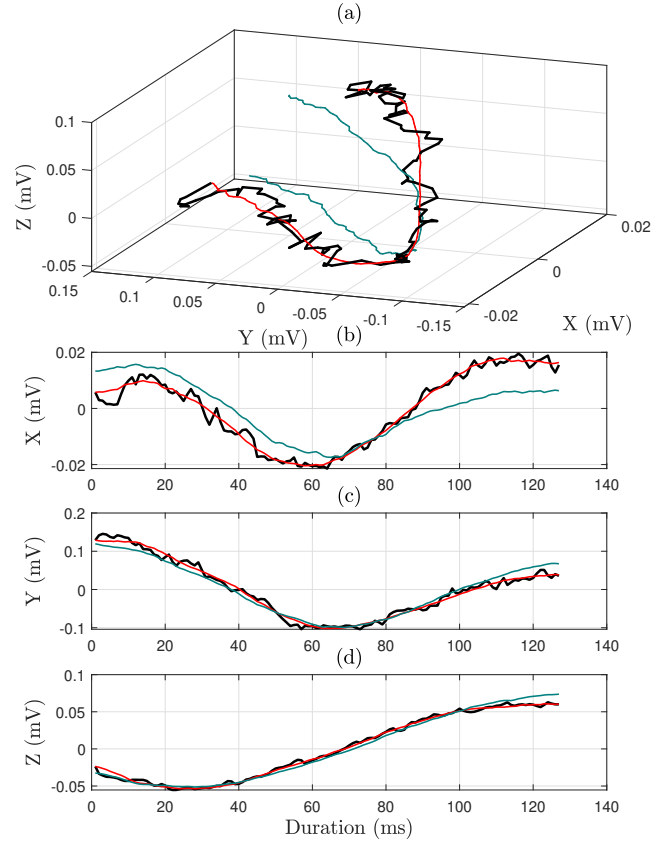
Figure 3.3. Example of a three-dimensional global-to-local adaptation (red) of template (green) to noisy target (black). The top row (a) shows the result of the adapted three-dimensional signal. Rows two (b), three (c) and four (d) depict the amplitude of each adapted orthogonal channel X, Y and Z against time.

abiding to a quasi-periodic behavior and large deviations generated by a low SNR. Furthermore, we introduce an entirely novel adaptive heuristic for estimating the ridge regularization factor, c_1. The heuristic employs an activation function utilizing an inter-related ratio of channel variance, r_v, from the target signal. The ratio is defined as the minimum channel variance divided by the sum of the three channel variances; the domain of r_v is: $[0, \frac{1}{3}]$. We introduce the following piecewise activation function:

$$
f(r_v) = \begin{cases} -r_v log_{1.5}(r_v^{r_v}) & 0 < h \le \frac{1}{3}, \\ 0 & \text{otherwise.} \end{cases}
\tag{3.20}
$$

The range of the activation function across the aforementioned domain is: $[0, -\frac{1}{3}log_{1.5}(\frac{1}{3}^{\frac{1}{3}})]$. The introduced activation function logarithmically reduces the estimate of c_1 in relation to r_v, a novel feature related to the planarity of the target signal; an increase in planarity requires a reduction in regularization.

The entirety of the concepts proposed in this work can be readily implemented. However, it should be noted that in our implementation of the FFD parameterization, we used a vectorized solution to obtain the FFD weights, this implementation was found to perform considerably faster than a conditional statement based implementation ($\sim$7 times faster).

Algorithm 1 Algorithm for global-to-local template adaptation.

Input: Y_o, Y_t

Output: $f^*(Y_t, \Lambda, l, c_1)$

1: Interpolate target signal, Y_t, to length of template signal, Y_o.

2: Compute globally adapted template, Y_g, using Procrustes analysis.

3: Generate minimum-bounding rectangular prism (MBRP) control points containing the globally adapted template and the current Y_t.

4: **for** $a = 1$ to N **do**

5:     Parametrize into X matrix each data point of Y_g to MBRP using FFD.

6:     Obtain differential noise estimate:
   $\Lambda_a = \frac{Y_t^a - Y_t^{a-1}}{max(\Lambda)}$.

7: **end for**

8: Hyper-parameter estimation:

   Obtain pairwise distance, $pdist$ of X, such that:

   $l = mean(pdist) + 2std(pdist)$.

   Obtain variance of each Y_t channel (Var_{XYZ}), such that:

   $r_v = \frac{min(Var_{XYZ})}{\sum Var_{XYZ}}$.

   Apply non-linear activation function, yielding, c_1.

9: Perform kernel ridge regression to obtain locally adapted template:

   $f^*(Y_t, \Lambda, l, c_1) = K(K + c_1 \Lambda)^{-1}(Y_t)$.

3.3   Applications

In this section we perform a quantitative analysis of the proposed framework; in addition to tracking three-dimensional features on synthetic signals, we demonstrate the potential for tracking features on real data, a simple classifier and mapping upper-limb movements.

3.3.1   Synthetic VCG Feature Tracking

Morphological changes in the ST segment of an ECG are an established diagnostic indicator of myocardial injury or infarction (Nikus *et al.*, 2014; Morris and Brady, 2002; Hasan *et al.*,

Table 3.1. Sum of squared errors (mV) across the three analysed methods and varying SNR.

T-wave Inversion	Proposed Method				Procrustes Analysis				Butterworth Filter			
SNR	10dB	15dB	20dB	25dB	10dB	15dB	20dB	25dB	10dB	15dB	20dB	25dB
$-0.1A_T$	1432	839	520	359	2234	2079	2051	2053	10554	11398	11887	12165
$-0.2A_T$	1439	853	540	417	2107	1921	1879	2168	10553	11190	11562	13113
$-0.3A_T$	1468	881	577	462	2146	1938	1887	2047	10732	11438	11852	12934
$-0.4A_T$	1654	997	643	467	2476	2248	2194	2055	12391	13148	13592	13317
$-0.5A_T$	1880	1130	731	466	2774	2499	2433	1965	14039	14864	15351	13252
$-0.6A_T$	1688	1010	653	434	2436	2128	2040	1731	12896	13491	13855	12504
$-0.7A_T$	1672	997	641	427	2504	2174	2070	1851	13135	13690	14034	12932
$-0.8A_T$	1866	1108	705	464	2763	2379	2255	1886	14721	15183	15481	14321
$-0.9A_T$	1872	1111	702	501	2784	2358	2207	2172	15229	15575	15819	15791
$-A_T$	1749	1024	634	452	2516	2106	1954	1873	13860	14062	14220	14511

2013). In vectorcardiography, the three-dimensional extension of the ECG across orthogonal channels, several spatial features of the T-loop have been proposed as potential indicators of myocardial injury or infarction. In this work, we use several variations of two features suggested by Hasan *et al.* (2013): 1 - the mean-loop-length (MLL), defined as the summation of the distance between consecutive points in a VCG, and 2 - the distance variability (DV), defined as the vector containing the Euclidean distances between corresponding points of a template three-dimensional signal and an adapted three-dimensional signal.

We evaluated the ability of our proposed framework to robustly capture VCG features in three-dimensional signals corrupted by various noise sources and signal-to-noise ratios (SNR). In the process, we simulated common high-amplitude noises that cannot be removed by standard signal processing methods such as: baseline wander, muscle artefact and electrode movement (Sameni *et al.*, 2007); combined with additive white Gaussian noise for which techniques exist. The simulated analysis includes a noise model consisting of an equally weighted combination of the four aforementioned noise sources. By using a synthetic multi-channel ECG generator (Sameni *et al.*, 2007), we simulated morphological changes across the T-wave. The VCG was obtained from eight standard ECG leads using the Frank lead transformation. Fig. 3.4 illustrates eight synthetic ECG leads (a) converted to three orthogonal leads via a Frank lead matrix transformation (b), for which the QRS-loop (segment between ('o') annotations in (b)) and T-loop (segment between (*) annotations in (b)) are plotted within a human torso (Mayol, 2019).

To map complex morphologies, the T-wave was varied by lowering the signal amplitude, A_T, of the wave in leads V1-V3 of the synthetic ECG in steps of $-0.1A_T$ between $-0.1A_T$: $-A_T$. The aim of this experimental setup was to simulate T-wave inversion, an indicator of myocardial infarction (Pollehn, 2002). Our experimental setup for testing the described

3.3.1 Synthetic VCG Feature Tracking
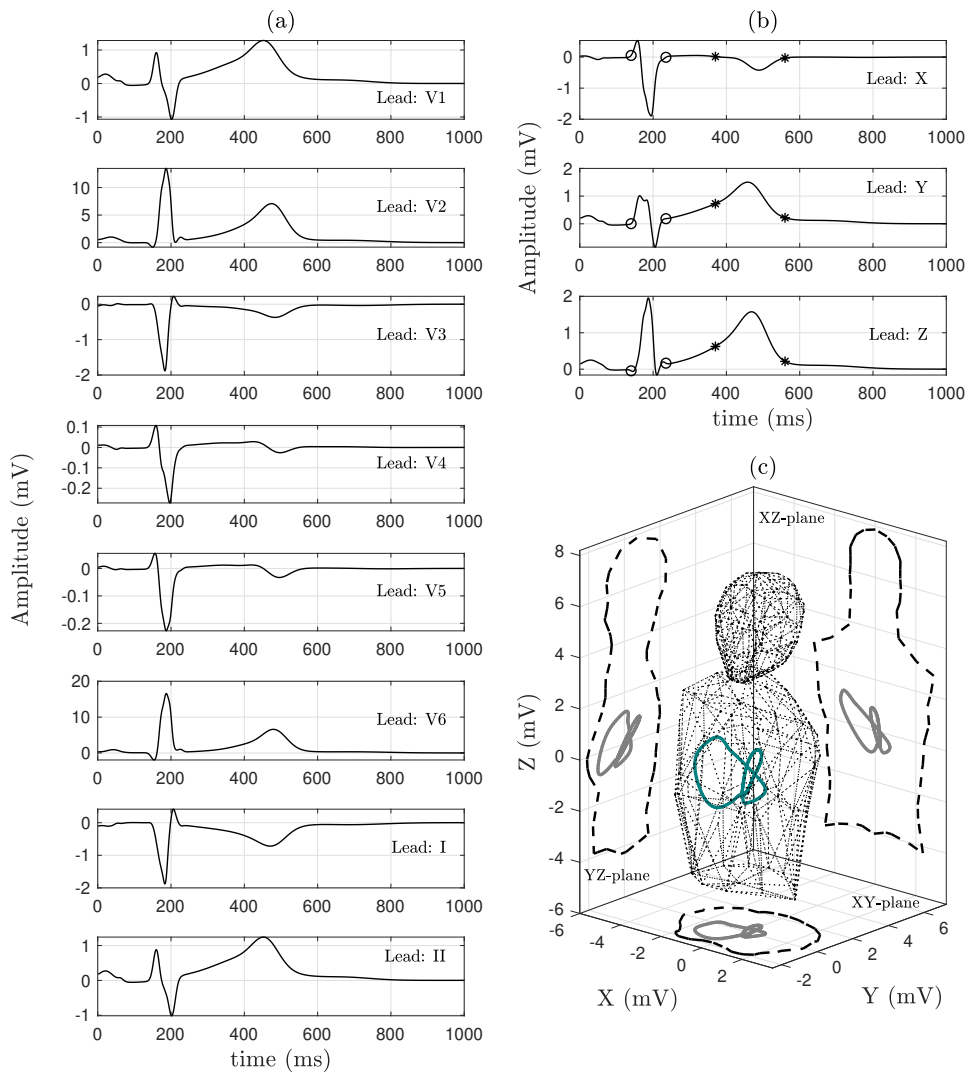
Figure 3.4. Example of synthetic multi-lead ECG (a) across one beat. Three-orthogonal leads (b) are obtained by performing a Frank lead matrix transformation onto the eight ECG leads (a). The QRS-loop (segment between 'o' markers in (b)) and T-loop (segment between '*' markers in (b)) from Leads X, Y and Z can be observed in (c); with projections onto the three orthogonal planes.

framework was motivated by similar morphological modelling in the ECG by Porta *et al.* (1998). In addition, a non-linear random (seeded) T-wave morphological change was applied at the T-wave onset and offset, respectively. The random deviation was drawn from a set of 20 possible deviations at each the T-wave onset and offset. At each step of A_T 30 seconds of noisy synthetic data was produced; this can be observed in Fig. 3.5 for $-0.5A_T$. Thus across each noise level (10dB, 15dB, 20dB and 25dB), 300 seconds of simulated multichannel ECG data was generated for each SNR level. To provide a comparative narrative we analysed the beat-to-beat performance of two additional methods across the dataset: Procrustes analysis and Butterworth bandpass filtering (bandpass range: 0.05-40Hz, according to American Heart Association recommendations (Bailey *et al.*, 1990)).

In Table 3.1, we observe the sum of square errors performance of the proposed method compared to the two other methods; the proposed method outperforms the other methods in all instances. In Fig. 3.6 we provide a comparative performance of the proposed framework with the two other methods in tracking the beat-to-beat T-wave features across different steps of the negated A_T and noise levels. Comparing the T-loop feature errors across different amplitudes and SNR levels in Fig. 3.6, it is evident that the proposed method outperforms both Procrustes analysis and Butterworth bandpass filtering in each instance.
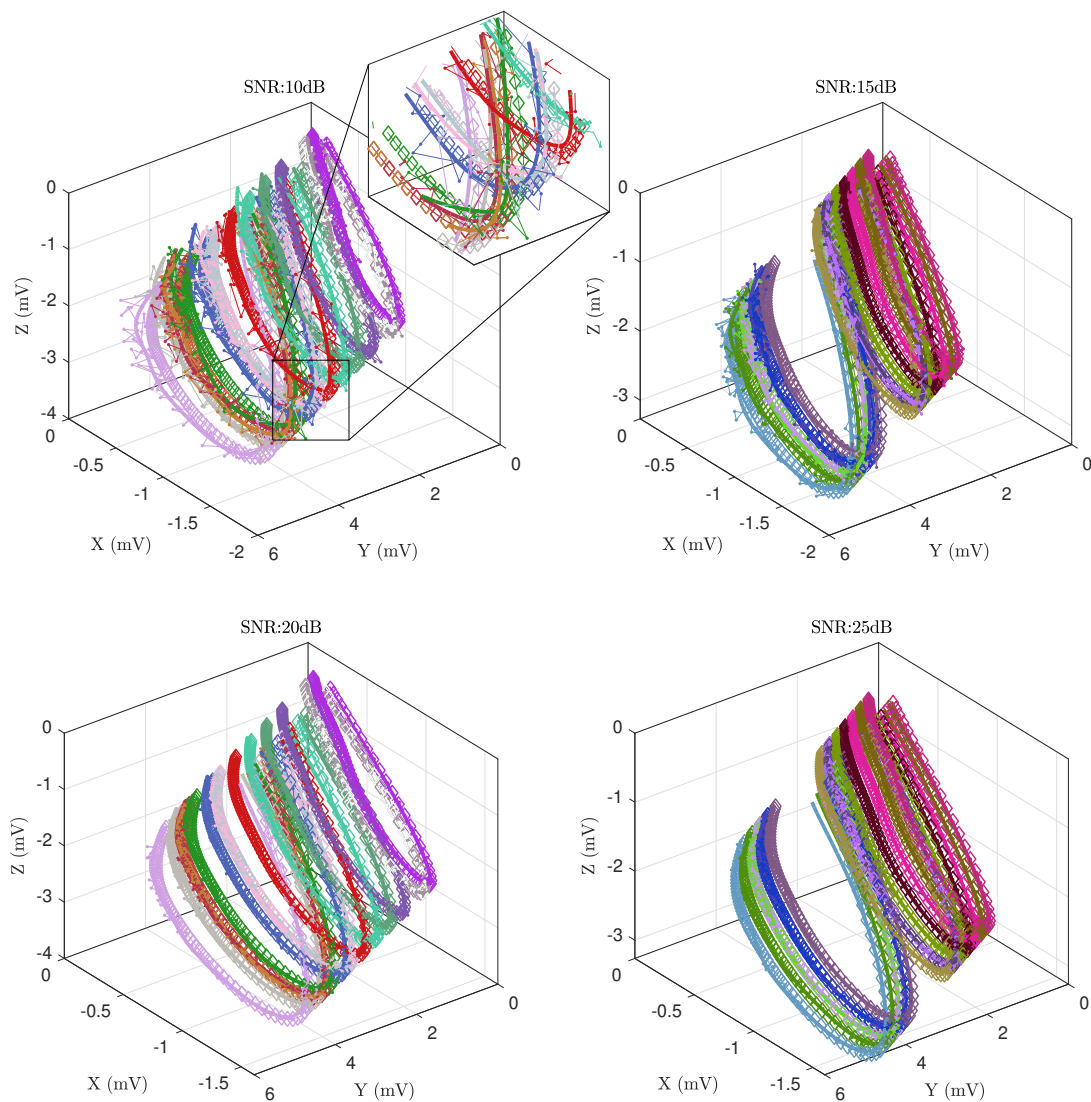
Figure 3.5. Comparison of adaptation results across various SNR (10dB to 25dB) for 30 seconds of simulated vectorcardiogram T-loop data. Examples show an identical simulated target truth (diamond marked trace) across each of the plots, the accumulated sampled noisy data across the 30 seconds (circle marked line) and the adapted result for each beat (unmarked line). Each colour is associated to a single beat.

Figure 3.6. Results of VCG feature tracking on the synthetic data using the proposed method, Procrustes analysis and Butterworth bandpass filtering. The cumulative error percentage of MLL_T (left), $IQR\ of\ DV_T$ (center) and the $Median\ of\ DV_T$ (right) features is depicted across varying noise levels (10-25dB) and T-wave inversions, where an x-axis value of -1 indicates a waveform multiplied by -1 across the synthetic dataset (note: the y-axis is logarithmic).

3.3.2   PTB Database Myocardial Infarction Feature Tracking

Tracking of beat-to-beat features is a critical element in the diagnosis and monitoring of cardiac conditions and events. To exemplify the usefulness of our proposed framework, we applied our algorithm across the PTB database containing the ECG of 79 patients with acute myocardial infarction (22 female, mean age 63 $\pm$ 12 years; 57 male, mean age 57 $\pm$ 10 years) and 69 control subjects (17 female, 42 $\pm$ 18 years; 52 male, 40 $\pm$ 13 years). We extracted approximately two minutes of ECG recording for each patient. The database is publicly available (Goldberger *et al.*, 2000; Bousseljot *et al.*, 1995).

To extract the relevant segments of the ECG waveform pertaining to the T-loop, we applied the 2DSW algorithm (Schmidt *et al.*, 2014). The algorithm utilizes an inhomogeneous template matching scheme in two-dimensions to track interval changes across the ECG. In our application, we were only interested in tracking the onset and offset of the T-loop.
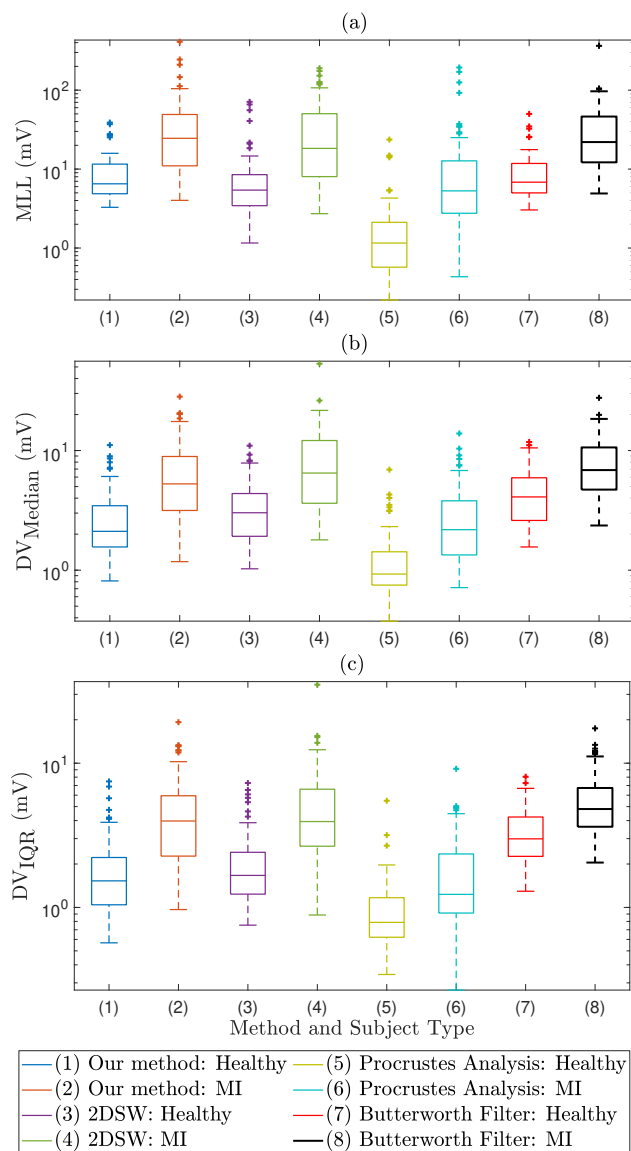
Figure 3.7. Box plots comparing T-wave beat-to-beat features of healthy subjects and MI patients across the four methods analysed.

We generated the T-loop VCG template using the ensemble average across the entire recording for each patient. In the template generation process and the subsequent adaptation process, each T-loop beat was interpolated to match the length of the respective template. Additionally, we normalized each T-loop using the loop vector-norm of the singular values. Template adaptation was then performed utilizing the proposed framework.

3.3.3 PTB Database Classification

To further elaborate on the comparative narrative, we studied the feature tracking ability of 2DSW, Procrustes analysis and Butterworth bandpass filtering (0.05-40Hz).

We tracked the features studied in the previous section: MLL and DV. The beat-to-beat variability was calculated as the standard deviation of each feature. Fig. 3.7. illustrates the box plot representation of the beat-to-beat feature statistics for normal subjects and MI patients across the database; this has been illustrated for each of the four methods analysed. The features were considered statistically significant if $p-$ value < 0.05, using the unpaired Student t-test. Statistical significance was achieved for each feature across all methods; thus providing limited intuition in terms of the practical advantages of our proposed method. Consequently, we proceeded to develop a simple classifier for the four methods utilising the three studied T-wave features.

3.3.3 PTB Database Classification

To evaluate the capabilities of the proposed method in potential diagnostic applications for MI we implemented a reciprocal regressor. The reciprocal regressor was utilized in consideration with the rightward skew that is prevalent across the feature distributions for each method (note: the Fig. 3.7 y-axis is logarithmic). The scores of the reciprocal regressor for each method were respectively analysed using the receiver operating characteristic (ROC) curve. Fig. 3.8 illustrates the ROC and area under the curve (AUC) result for each method. It is evident that template adaptation techniques yield superior results compared to the frequency domain filtering method. Furthermore, the AUC of the template adaptation methods increases with complexity. At the lower end of the AUC-value spectrum is Procrustes analysis, which only considers global translation, rotation and scaling. Furthermore, in comparison to 2DSW, the proposed technique produces a slightly higher AUC value.
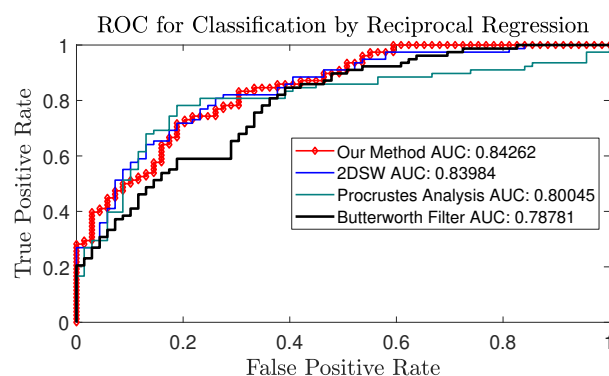
Figure 3.8. The ROC curves for the regressor output scores and the associated AUC value for each method.

3.3.4   Complex Upper-Limb Movement Tracking

In point-to-point hand movements, hand trajectory motion has indicated a bell-shaped velocity profile (Abend *et al.*, 1982). Analysis of hand movements is important in studying the correlation between brain activity and muscle motion. The data analyzed in this work was recorded using a three-dimensional camera-based motion capture system (VICON, Oxford UK).
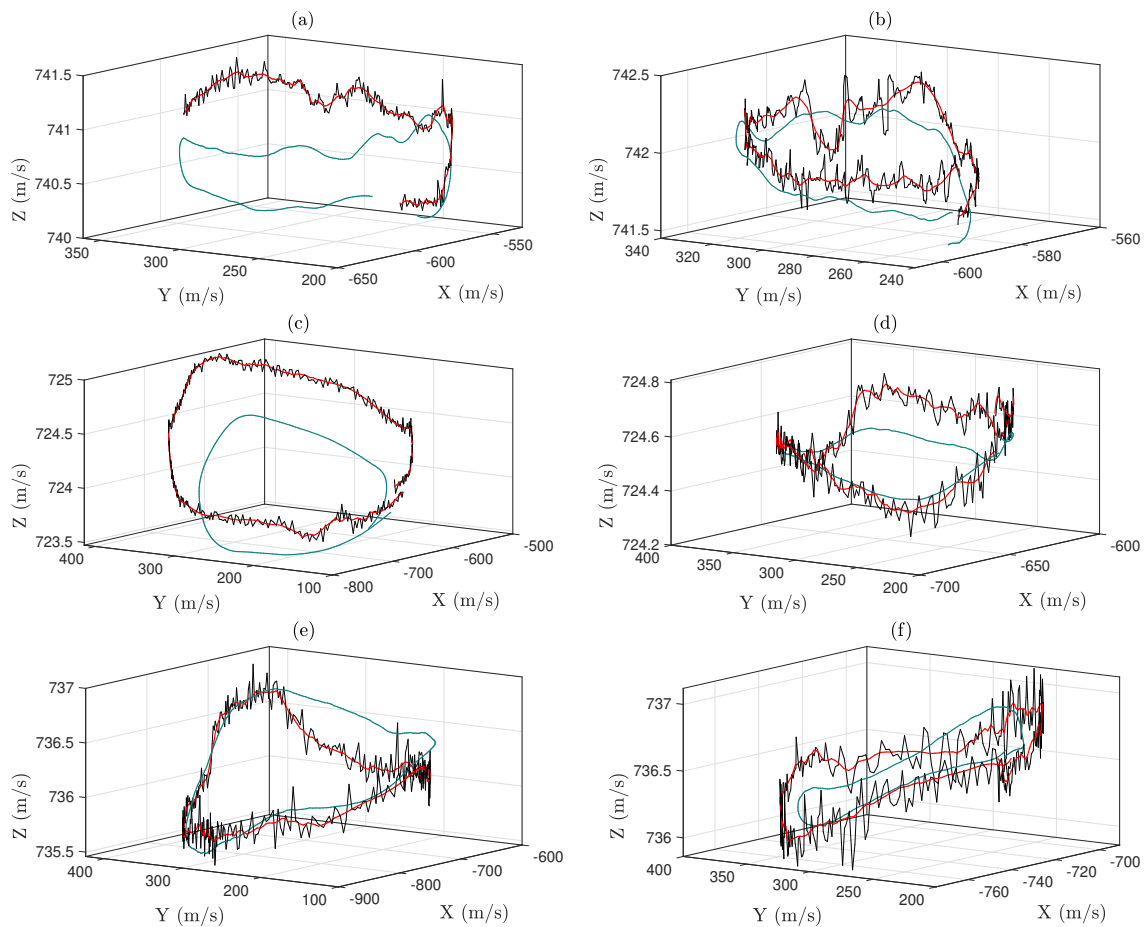
Figure 3.9. Results of using the proposed framework on the Complex Upper-Limb Movements database. Velocity profile template adaptations (red) to noisy target velocity profiles (black) using the templates (green). The triangle (left column: (a), (c), (e)) and ellipse (right column: (b), (d), (f) and) velocity profiles of three people (rows).

More recently, Miranda *et al.* (2018) found a broad set of complex upper-limb movements can similarly be modelled as a combination of motor primitives with a bell-shaped velocity profile. For a particular hand trajectory, a template trajectory motion can be obtained by averaging across the dataset. By obtaining a three-dimensional template velocity profile, the

suggested framework can be used to track subtle variations between consecutive quasi-periodic upper limb movements. As an example, we show several three-dimensional trajectories from the Complex Upper-Limb Movements database which contains hand trajectory obtained from ten subjects as they were performing various prescribed upper-limb motor tasks. The database is publicly available on the PhysioNet site (Goldberger *et al.*, 2000). For three people, we show the result of an adapted template for the three-dimensional velocity profile of a triangle and ellipse. Using the limited data, in which patients may only have repeated the same action several times, we used a Savitzky-Golay filter to obtain a smoothed peak-retaining (Schafer, 2011) template. The Savitzky-Golay filter utilized a third order polynomial with a frame length of thirteen. Visual results can be observed in 3.8. The first column presents the results of the template adaptation scheme across three peoples' velocity profiles as they attempted to draw a triangle. Similarly, for each person, the second column indicates the velocity profiles of an ellipse (see 3.9).

3.4   Discussion

In this contribution we proposed a novel template adaptation scheme for tracking three-dimensional signals. To the best of our knowledge, this is the first framework for adapting three-dimensional signals, where the channels are spatially correlated. The proposed framework presents a technique to treat noisy quasi-periodic temporal three-dimensional signals. By employing an appropriate parameterization technique and then formulating a non-parametric solution, the proposed work is able to detect subtle inhomogeneous variations in temporal shapes. In comparison to transformation algorithms traditionally found in literature, the proposed framework does not require an expensive optimization problem to obtain the optimal location of the FFD control points. Instead, by forfeiting the traditionally exploited smoothness properties of free-form deformations, it exploits a computationally cheaper alternative in the form of a least squares non-parametric method. Our proposed framework is capable of producing smooth template adaptations capturing non-linear changes by adaptively selecting the kernel width. Furthermore, by employing such a kernel function, our algorithm doesn't abandon the notion of smoothness but relies on the smoothness properties associated with Gaussian kernels instead. The inexpensive nature of the proposed framework is significant for the purpose of real-time applications such as biomedical diagnostic devices.

In addition to computational efficiency, accuracy signifies another important aspect of the proposed framework. The proposed framework was capable of tracking cardiac disease

features amongst various noise levels using simulated data. The algorithm produced relatively small errors amongst 10dB noise levels, and improved with an increasing SNR. The proposed method achieved superior results to Procrustes analysis and frequency based filtering. Furthermore, this conclusion was supported by the results obtained from analyzing the PTB database, where the algorithm detected statistically significant differences in VCG features between myocardial infarction patients and normal subjects; and in addition produced the highest AUC value compared to three other methods employing reciprocal regression scores. This demonstrates the applicability of the proposed framework in tracking quasi-periodic signal morphology. However, it should be noted that the orthogonality of the analysed VCG data is only assumed, thus there is a potential limitation in the analysed features arising from this fact. Orthogonal statistical transformations such as SVD distort the anatomic-orientation information observable in raw VCG data.

Furthermore, by applying the proposed framework to the Complex Upper-Limb Movements database, another potential application to a three-dimensional signal processing problem was illustrated. The ability of the proposed method to translate to an independent and differently distributed database illustrates the prowess of the heuristic hyper-parameter estimations; particularly for the regularization term.

3.5   Conclusion

We have proposed a framework for locally adapting variously shaped noisy quasi-periodic three-dimensional signals. We quantified the performance across a synthetic dataset and demonstrated superior results to a global adaptation method and bandpass filtering. Using real vectorcardiograms, the proposed template adaptation algorithm proved to be effective in detecting subtle beat-to-beat morphological changes in patients with myocardial infarction; demonstrated by the classification analysis. Additionally, we illustrated the ability of the proposed work to adapt a template across various quasi-periodic velocity profiles, with varying morphology and noise levels. Importantly, it should be noted that the proposed work proposes an entirely adaptive framework. Thus, the framework may be beneficial in applications where quasi-periodic motion tracking is of importance.

Template Adaptation of 2D Quasi-Periodic Data Using a Soft-Assign Localized Correspondence Matrix

The content of this chapter is a modified version of the publication:

4

Abstract

In this work we propose a framework for the adaptation of arbitrary quasi-periodic time series. We parameterize and adapt data using traditional free form deformations. The method follows an alternating approach, inspired by the robust point matching algorithm, under which a correspondence matrix is updated and the subsequent deformation is obtained; thus, the template data are adapted to the target data. We demonstrate the performance of the algorithm across several ECG and PPG databases and compare it to previous works.

4.1 Introduction

In signal processing, template adaptation is a technique employed to match two patterns. Template adaptation aims to deform a parameterized template signal to a target signal by optimizing a cost function. Global adaptation aims to retrieve a universal transformation matching the template data to the target data. Such adaptations have been proposed in three-dimensional applications (Astrom *et al.*, 2000; Karisik and Baumert, 2019). Local adaptation, on the other hand, seeks to obtain deformations capturing subtle variations unique to subsets of the data (Karisik and Baumert, 2019; Schmidt *et al.*, 2014, 2018a).

Most previous research addressed the problem of template adaptation by pre-aligning an established and prominent feature of the quasi-periodic pattern. By imposing an initial alignment on the template, prior works have been limited by assuming a correspondence between the remaining samples of the template and target signals with respect to the reference feature. Whilst this approximation is robust when a singular quasi-periodic feature is of concern, it is of limited value for quasi-periodic signals. For instance, where physiological signals are of concern, in excess of five features may manifest for any given cycle. Our work seeks to overcome this significant limitation. Two fields of literature are particularly relevant to our problem, signal warping and registration techniques.

Signal warping is a well established audio processing technique inspired by the necessity to overcome temporal contractions and expansions in word pronunciations. In dynamic time warping (DTW) (Vintsyuk, 1968), perhaps the most commonly employed warping algorithm, data are compared sample to sample between a reference and target sequence. A rectangular matrix map is generated by analysing a Euclidean distance cost function.

The algorithm is then tasked with the dynamic programming problem of obtaining the least cost path. Many variations and constraints have been applied to DTW, with the Sakoe-Chiba band being amongst the most popular. The Sakoe-Chiba band limits the permissible warping path across the rectangular matrix. Further inspired variants include: correlation optimized warping (Tomasi *et al.*, 2004), derivative DTW (Keogh and Pazzani, 2001) and *FastDTW* (Salvador and Chan, 2007). Although differences beyond the scope of this work exist in the frameworks of DTW algorithms, they are linked by a common target: to capture one-dimensional shifts between time-series. Warping algorithms have been employed in time series analysis (Vullings *et al.*, 1998; Huang and Kinsner, 2002; Ramírez *et al.*, 2017), however, they are incapable of capturing features in two dimensions and are therefore of limited use in quasi-periodic time series. Due to the limitations of signal warping in template adaptation we ensue to relate our problem to the registration process.

Registration is the process of aligning two sets of data in two-dimensional and three-dimensional applications. In point set registration and image registration (where a prior correspondence may exist, but is increasingly distorted) a broad field of research exists. Our work primarily draws inspiration from point set registration techniques due to their general reliance on Cartesian coordinates; image registration methods hold a preference toward image intensities. Specifically, the registration problem seeks to establish a bijective or strictly injective (not bijective) mapping between two sets of data, permitting sample rejection. In time series data, focusing on injective mappings would be a theoretically flawed approach, that is, permitting the rejection of samples would undermine the sampling process. Similarly, focusing on bijective mappings, that is, a one to one correspondence between samples, may yield insufficient adaptations due to inhomogeneous temporal variations. Consequently, insufficient samples would exist in local regions to amply match features between the template and target signals. Thus the problem of template adaptation in time series data needs to permit for data interpolation (non-binary correspondences). As such, our work seeks to combine assumptions specific to the adaptation of time series data with the foundations of traditional registration techniques. We ensue to describe related registration techniques and their relevant features.

Based on global deformations, the iterative closest point (ICP) algorithm is amongst the simplest and earliest point set registration methods proposed (Besl and McKay, 1992). In ICP the model dataset is iteratively rotated and translated to match the target dataset; the process involves the evolving estimation of a correspondence variable and universal transformations. ICP is commonly employed in the registration domain due to it's ease of

implementation and performance on simple problems. Many variants of ICP have been proposed to improve robustness (Pomerleau *et al.*, 2015). However, even amongst these variants the subpar performance of ICP in the presence of noise limits its applicability in time series analysis. Although ICP is inadequate for the problem of time series adaptation due to its reliance on global adaptation and sensitivity to noise, our method draws motivation from the iterative nature of the process.

To address the need for inhomogeneous adaptations we explore a family of algorithms for the local parameterization of data. In point set registration, one such popular parameterization technique is thin-plate splines (TPS) (Bookstein, 1989). TPS and related methods require explicitly determining two sets of corresponding points to retrieve the deformations pertaining to the rest of the shape. TPS has an inherent analogy to the physical bending energy of a thin metal plate whilst providing smooth deformations. The most popular TPS based registration method is that of Chui and Rangarajan (2003), based on earlier works (Rangarajan *et al.*, 1996; Gold *et al.*, 1998). The technique jointly estimates the correspondence matrix and thin plate spline parameters by an alternating and iterative process. Optimization is performed by deterministic annealing and demonstrates strong performance in the presence of few outliers. Although TPS registration methods are not appropriate for time series adaptations due to their underlying bijective mapping assumption, we draw inspiration from the deterministic annealing optimization inherent to the process.

Another family of registrations pertaining to local parametrizations are free form deformations (FFD) (Sederberg and Parry, 1986; Huang *et al.*, 2006). Under FFD, data are embedded by a lattice of control points where consequent shifting of a control point results in locally weighted deformations. Free form deformations similiarly provide smoothness guarantees. Traditional FFD offers global support across control points, meaning the entire lattice can be shifted. Contemporary FFD techniques provide local support which is sufficient for minute variations in shape, but cumbersome for a unitary lattice offset. In contrast to TPS, FFD parameterizations provide no capacity guarantee to retrieve the exact target shape by deformation of the source shape under noisy conditions. In signal processing, where signal to noise components are often indeterminate, exact shape retrieval would be akin to overfitting. Thus, a deformation model with a strong mapping prior, such as cubic or Bernstein polynomial based methods, are suitable in meeting this balance between obtaining a correspondence matrix (with probabilities which aren't necessarily binary) and shape fitting. As such, our framework employs FFD to achieve non-binary probabilities.

Specifically, in the proposed work we formulate a template adaptation technique for quasi-periodic time series data inspired by the aforementioned techniques. We aim to demonstrate that the algorithm can capture subtle variations in quasi-periodic signals. Our focus is on biomedical data, namely, electrocardiogram (ECG) and photoplethysmogram (PPG). The ECG and PPG are amongst the most extensively studied physiological signals (Sörnmo and Laguna, 2006; Laguna *et al.*, 2016; García *et al.*, 2000b; Gil *et al.*, 2010); the ECG represents variations in the summed electrical potential generated by heart muscle, whilst the PPG describes volumetric changes of blood circulation using a photodetector at the surface of the skin. An important ECG feature is the QT interval, which represents the period of ventricular depolarization and repolarization of a cardiac cycle. QT interval variability (QTV) is a non-linear process observed from beat-to-beat and is algorithmically difficult to quantify. Robust tracking of the QT interval is of utmost importance as elevated QT variability has been found to be a predictor of heart disease and mortality (Hasan *et al.*, 2012a; Baumert *et al.*, 2016a). Additionally, elevated QTV has been observed in sleep apnea (Baumert *et al.*, 2008; Schmidt *et al.*, 2018b), demonstrating the broader importance of this feature. Similarly, robust tracking of the dicrotic notch in PPG is of importance to assess properties of the arterial vascular system (Middleton *et al.*, 2011).

Although our work draws intuition from the registration field, we propose a novel algorithm with assumptions suited to time series deformations. First and foremost, this is motivated by our efforts to propose a solution to the incomplete correspondence assumption observed in template adaptation literature. Furthermore, we address the problem utilizing a well-defined geometric parameterization to achieve guaranteed mathematical smoothness and a continuous cost function. The intent of these secondary contributions is to address further limitations observed in signal processing literature related to template adaptation. Lastly, and perhaps most importantly, our technique aims to illustrate its potential as a general framework for the adaptation of arbitrarily shaped quasi-periodic data by extending the analysis to the application of PPG. Although our method is not exclusive to the biomedical domain, we focus on such applications due to the prevalence of quasi-periodic data in the field.

4.2   Methodology

4.2.1   Normalization

In the proposed method data are first mapped into a unity box by min-max normalization. This is performed to generalize parameter selection across the model. Consider Y to be the

length N template signal and Q to be the length N target signal. We denote the normalized template data, $\widetilde{Y}$, where $\widetilde{Y_a^x}$ and $\widetilde{Y_a^y}$ denotes the ath sample value across the x (temporal) and y (amplitude) axes, respectively. Similarly, we denote the normalized target data, $\widetilde{Q}$, where $\widetilde{Q_b^x}$ and $\widetilde{Q_b^y}$ denotes the bth sample value across the x (temporal) and y (amplitude) axes, respectively.

4.2.2 Deformation Representation

Our technique employs traditional free form deformations (Sederberg and Parry, 1986) to place a prior on the method such that adaptations yield constrained results modelled by a product of Bernstein polynomials; in turn reducing the effects of noise. Under this process the template sequence is embedded to a lattice of control points. Subsequent shifting of control points results in locally weighted deformations of the data. In FFD, a local coordinate system is first imposed on the data:

$$\widetilde{Y}_a = X_o + s_a S + t_a T, \tag{4.1}$$

where X_o denotes the origin of an $l \times m$ lattice of control points, P^0, and $\{S, T\}$ the embedding lengths of the lattice along the x-axis and y-axis, respectively. The (s, t) coordinates of sample point $\widetilde{Y}_a$ can be obtained in the following manner:

$$s_a = \frac{\widetilde{Y_a^x} - P_{min}^x}{P_{max}^x - P_{min}^x}, \tag{4.2}$$

$$t_a = \frac{\widetilde{Y_a^y} - P_{min}^y}{P_{max}^y - P_{min}^y}, \tag{4.3}$$

where $\{P_{min}^x, P_{max}^x, P_{min}^y, P_{max}^y\}$ denotes the set containing the minimum and maximum control point values along the x-axis and y-axis, respectively. In this coordinate system, the resultant deformation of shifting P^0 to P^1 is defined by the tensor product of Bernstein polynomials:

$$\widetilde{f}(\widetilde{Y}) = \sum_{i=0}^{l} \sum_{j=0}^{m} \beta_i(s_a)\beta_j(t_a)P_{ij}^1, \tag{4.4}$$

where $\beta_i(s_a) = \binom{l}{i}(1 - s_a)^{l-i}s_a^i$ and $\beta_i(t_a) = \binom{m}{j}(1 - t_a)^{m-j}t_a^j$. Given Eq. 4, FFD can be reformulated as an incremental process, i.e. $P^1 = P^0 + \delta P$, where $\delta P = \Theta = \{\delta P_{i,j}^x, \delta P_{i,j}^y\}$

and $(i, j) \in [1, l] \times [1, m]$. Thus, the deformation process can be re-written as:

$$\widetilde{f}(\Theta; \widetilde{Y}) = \sum_{i=0}^{l} \sum_{j=0}^{m} \beta_i(s_a) \beta_j(t_a) (P_{ij}^0 + \delta P_{ij})$$

$$= \sum_{i=0}^{l} \sum_{j=0}^{m} \beta_i(s_a) \beta_j(t_a) (P_{ij}^0) + \tag{4.5}$$

$$\sum_{i=0}^{l} \sum_{j=0}^{m} \beta_i(s_a) \beta_j(t_a) (\delta P_{ij}).$$

Under this formulation the first term of the deformation process, P_{ij}^0, returns the initial parameterized template, $\widetilde{Y}$, based on the linear precision of Bernstein polynomials. The second term, δP_{ij}, corresponds to a shift of the control points and the resultant shape deformations they produce. Thus, we can reformulate Eq. 5 to:

$$\widetilde{f}(\Theta; \widetilde{Y}) = \widetilde{Y} + \delta \widetilde{f}(\Theta; \widetilde{Y}), \tag{4.6}$$

Fig. 4.1 illustrates an ECG parameterized to a 6×6 FFD lattice. This concludes the description of the transformation model pertaining to our proposed technique. In the subsequent section, we formulate the adaptation cost function and demonstrated how to estimate Θ.
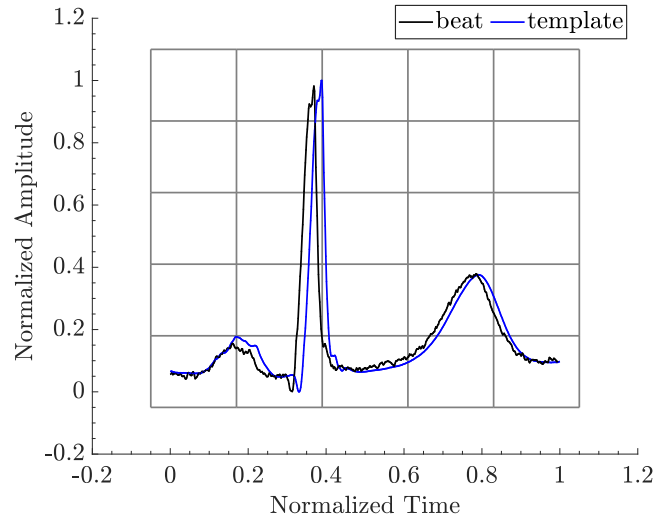
Figure 4.1. Example of an ECG template (blue) and beat (black) parameterized to an FFD lattice of 6×6 control points.

4.2.3 Correspondence Weighting & Deformation

To account for localized temporal shifts in quasi periodic data, we introduce a correspondence matrix. We relax the traditional restrictions placed on the correspondence matrix

4.2.3 Correspondence Weighting & Deformation

where the assignment problem seeks to obtain a strictly injective (not bijective) or bijective mapping; instead we permit the solution to interpolate temporal and amplitude values by allowing for a non-binary correspondence between template and target data. Furthermore, we abstain from incorporating an outlier slack variable. In point set registration problems, outliers related to injective mappings manifest when inappropriate samples have been drawn in the preprocessing feature extraction step. In signal processing, each time step corresponds to a deterministic interval, thus proposing an algorithm permitting for injective mappings where certain time stamps can be discarded would be a naive approach under which the removal of information would be permitted.

Our correspondence matrix formulation is inspired by the work of Rangarajan *et al.* (1996) and adapted to the signal processing domain. In addition to removing the binary constraint between template and target samples, we introduce a band matrix to minimize the permissible search space by the optimization algorithm. The reduced search space aims to prevent the minimization process returning a solution corresponding to an undesirable deformation. The energy function we seek to minimize in this work has the form:

$$E(M, \widetilde{f}) = \sum_{a=1}^{N} \sum_{b=1}^{N} z_{a,b} m_{a,b} \| \widetilde{Q_b} - \widetilde{f}(\Theta; \widetilde{Y_a}) \|^2 +$$

$$\lambda \| \widetilde{f}(\Theta; \widetilde{Y_a}) \|^2 + \tau \sum_{a=1}^{N} \sum_{b=1}^{N} m_{a,b} \log m_{a,b} \tag{4.7}$$

$$- \log \xi \sum_{a=1}^{N} \sum_{b=1}^{N} m_{a,b},$$

where $m_{a,b}$ fulfils $\sum_{a=1}^{N} m_{a,b} = 1$ and $\sum_{b=1}^{N} m_{a,b} = 1$ for $a, b \in \{1, ..., N\}$, $m_{a,b} \in [0, 1]$, $z_{a,b} \in \{0, 1\}$ and $M = [m_{a,b}]$. M holds the correspondence values between each template and target sample. The first term corresponds to the least squares error measure between all samples of the template and the target with a band matrix incorporated. In the below example of a tridiagonal band matrix, z has the form:

$$z_{a,b} = \begin{pmatrix} z_{1,1} & z_{1,2} & 0 & \cdots & & \cdots & 0 \\ z_{2,1} & z_{2,2} & z_{2,3} & & & & \vdots \\ 0 & \ddots & \ddots & \ddots & & & \vdots \\ \vdots & & \ddots & \ddots & & \ddots & 0 \\ \vdots & & & z_{N-1,N-2} & z_{N-1,N-1} & z_{N-1,N} \\ 0 & \cdots & \cdots & & \cdots & z_{N-1,N} & z_{N,N} \end{pmatrix},$$

where the notion of a band matrix similarly extends to a matrix with a bandwidth greater than one (greater than the tridiagonal case). The matrix, $z_{a,b}$, serves as a binary matrix where the bandwidth determines the range of template samples evaluated against the target samples. This helps to reduce the solution space. In our work the bandwidth is set as a percentage of the signal length. The second term is the standard L2 ridge regularization term observed in statistical modelling and is incorporated to reduce overfitting. The third term is an entropy barrier function serving to constrain the values of $m_{a,b}$ in the range: $[0, 1]$. The multiplier, τ, enforced onto the barrier function is employed to permit for the process of annealing in the optimization step of the algorithm. Annealing, specifically simulated annealing (SA), is a commonly employed optimization technique that treats the objective function as a system energy and is analogous to the annealing process of solids. SA searches for the function minimum by decreasing the system temperature; the search is more stochastic at higher temperatures and gradually becomes more deterministic as the temperature parameter is lowered. Deterministic annealing (DA) is a closely related derivative of simulated annealing under which the minimization of the objective function is treated as the minimization of the free energy of the system. DA considers the minimum energy at each temperature and in turn deterministically optimizes the objective function (Peyvandi, 2017). Annealing is incorporated into the network to ensure that through an iterative process an improved local suboptimal solution can be obtained. An in-depth discussion relating to the motivation for annealing based optimization is provided by Rangarajan *et al.* (1996). The fourth term is incorporated to prevent zero matches in the correspondence matrix; the value is set close zero in order to satisfy the Sinkhorn-Knopp algorithm condition, $m_{a,b} > 0$. The Sinkhorn-Knopp method is utilized to meet the doubly stochastic constraints imposed on the cost function in Eq. 7 and is justified in (Rangarajan *et al.*, 1996); it operates by alternating between row and column normalizations until a guaranteed convergence transpires (Knight, 2008).

Similar to the work of Chui and Rangarajan (2003) the proposed technique operates on the principle of alternating estimations between the correspondence matrix and transformation (control point shifts); this is performed repeatedly and in conjunction with deterministic annealing. In the first step of the alternating technique we take the derivative of Eq. 7 with respect to $m_{a,b}$ and equate it to zero, from this we can obtain the following analytic result:

$$m_{a,b} = e^{-z_{a,b} \frac{\|\tilde{Q}_b - \tilde{f}(\Theta; \tilde{Y}_a)\|^2}{\tau}} + \zeta. \tag{4.8}$$

The value of ζ is set using a heuristic under which we take the minimum value obtained in

(a) Iteration: 1

(b) Iteration: 2
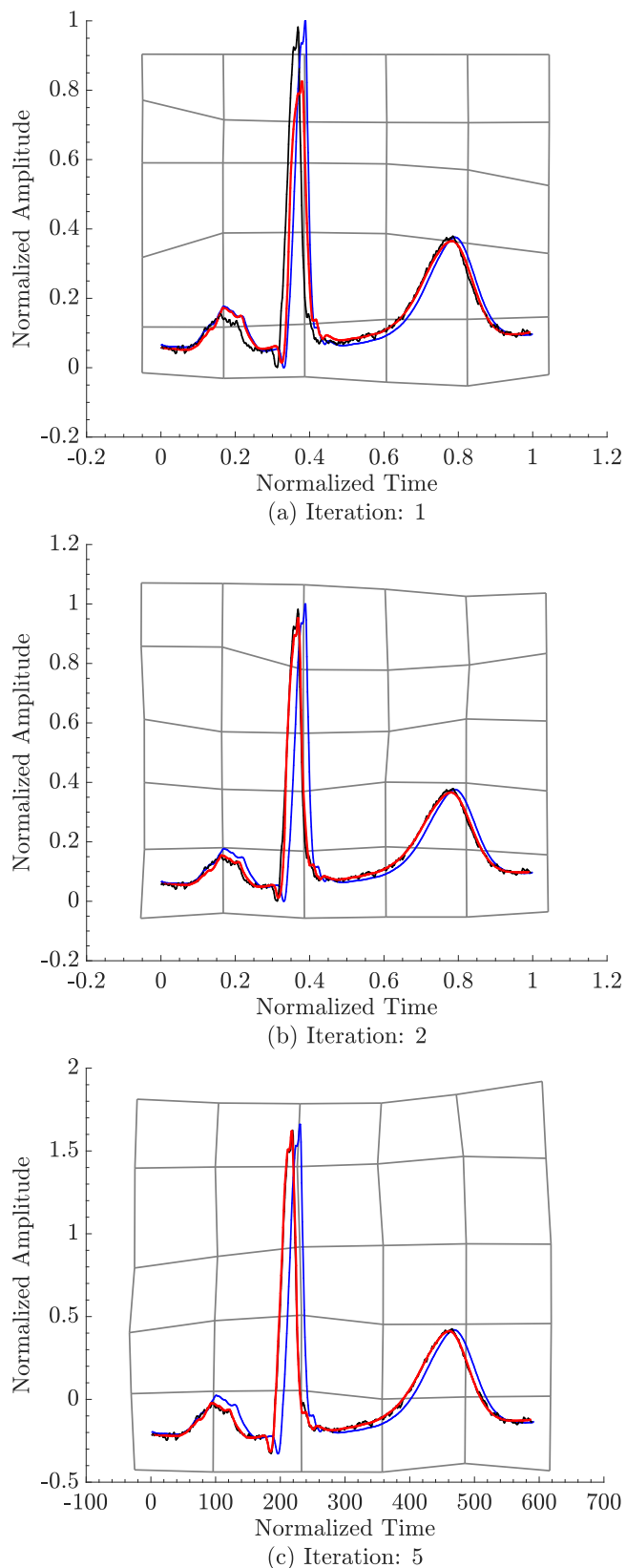
(c) Iteration: 5

Figure 4.2. Example of an ECG template (blue) adapted (red) to a noisy beat (black) on the first (a), second (b) and fifth (c) iteration. The first two iterations are illustrated under the data being normalized whilst the final iteration (c) demonstrates the data scaled back to pre-normalization values.

Eq. 8 with ξ excluded. The intuition behind assigning this specific positive non-zero value is that it represents the minimum observable correspondence between the template and target; thus, serving as the lowest data-driven (observable) value which could be employed. We set the value in this fashion to ensure numerical stability and prevent the overestimation of this constant incorrectly influencing the Sinkhorn-Knopp normalization. To obtain the optimal control point shift estimation, we differentiate Eq. 7 with respect to Θ, that is:

$$\frac{\partial E(M,\widetilde{f})}{\partial \Theta_{i,j}} = -2\sum_{a=1}^{N}\sum_{b=1}^{N} z_{a,b} m_{a,b}(\widetilde{Q}_b - \widetilde{f}(\Theta; \widetilde{Y}_a))$$

$$(\nabla \widetilde{f}(\Theta; \widetilde{Y}_a).\frac{\partial \delta \widetilde{f}(\Theta; \widetilde{Y}_a)}{\partial \Theta_{i,j}} + 2\lambda \widetilde{f}(\Theta; \widetilde{Y}_a).$$

(4.9)

Eq. 9 is solved utilizing an adaptive gradient descent method due to the substantially varying magnitude of gradient sizes between different control points and directional derivatives. This technique is employed to obtain the transformation estimate in a timely manner and to discourage the parameter solution settling at a saddle point for extended iterations. We utilize the RMSprop adaptive gradient descent method to achieve faster convergence compared to traditional gradient descent (Hinton *et al.*, 2012). For parameter, $\Theta_{i,j}$, the related partial derivative (i.e. - left-hand side of Eq. 9) at iteration, $step$, of the gradient descent is:

$$g_{i,j_{step}} = \frac{\partial E(M,\widetilde{f})}{\partial \Theta_{i,j}}\Bigg|_{step}.$$

(4.10)

Therefore, the gradient update for any given parameter $\Theta_{i,j}$ can be obtained by the following memory based two step process:

$$v_{i,j_{step}} = \alpha v_{i,j_{step-1}} + (1-\alpha)(g_{i,j_{step}})^2,$$

(4.11)

where α denotes the momentum value and $v_{i,j_{step}}$ the exponentially decaying average of the previous squared gradients. Thus the $(i,j)^{th}$ parameter is updated by:

$$\Theta_{i,j_{step+1}} = \Theta_{i,j_{step}} - \frac{\eta}{\sqrt{v_{i,j_{step}}} + \epsilon} g_{i,j_{step}},$$

(4.12)

where η denotes the general learning rate and ϵ a small constant to prevent division by zero. The update rule accumulates the previous gradient in some proportion which prevents rapid growth in v_t and encourages the optimizer to continue converging.

4.2.4 De-normalization

To obtain the adapted template in the original scale we perform the inverse of the normalization function described in *Subsection A* across the x-axis and y-axis, respectively:

$$f_a^x(\Theta; \widetilde{Y}_a) = \frac{\widetilde{f}_a^x(\Theta; \widetilde{Y}_a) - Y_{min}^x}{Y_{max}^x - Y_{min}^x},$$

$$f_a^y(\Theta; \widetilde{Y}_a) = \frac{\widetilde{f}_a^y(\Theta; \widetilde{Y}_a) - Y_{min}^y}{Y_{max}^y - Y_{min}^y}.$$

(4.13)
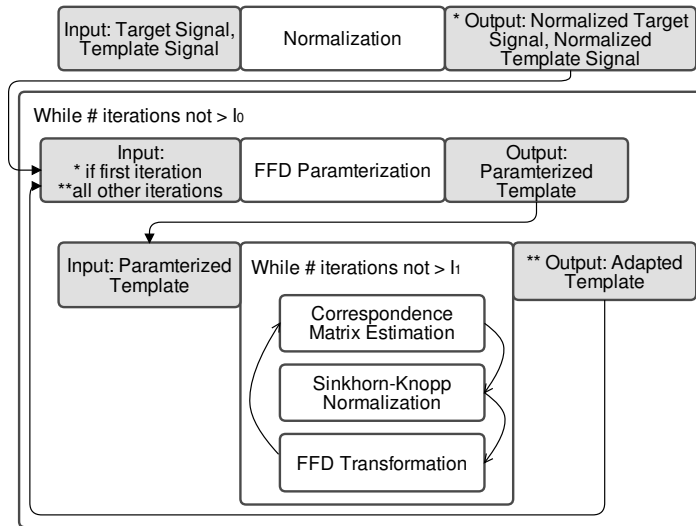
Figure 4.3. The proposed adaptation framework given a target signal and template signal.

In the current work we determined values to suffice for a coarse optimization utilizing deterministic annealing and RMSprop across an external ECG database. In doing so we set, $I_0 = 3$, $I_1 = 5$ and $I_2 = 20$. These values were selected under the condition that no gradient magnitude was larger than 0.001 normalized units across a subset of the external ECG database. M was initialized by solving Eq. 8 under the starting pose of the data being matched and the incremental control point shifts, δ, being initialized to zero. Annealing followed a schedule of an approximately tenfold reduction in the magnitude of τ at each update. This was determined to be an amply low (yet coarse) reduction rate through trial and error. The band matrix was initialized with a bandwidth of 0.75% of the template length and updated at the same rate upon each iteration of I_0, as observed in line 11 of Algorithm 1. The intent of widening the matrix bandwidth in this manner was to permit for the incremental adaptation of the template signal. The penalty factor λ was set to 0.05. To tune the λ

Algorithm 2 Pseudo code for template adaptation.

Input: Υ, Q
Output: $f(\Theta; \widetilde{Y})$

1: Initialize parameters τ, M, δ and bandwidth.
2: Normalize Y and Q to $\widetilde{Y}$ and $\widetilde{Q}$, respectively.
3: **while** # of iterations $\leq I_0$ (deterministic annealing step) **do**
4:     Parametrize $f(\Theta; \widetilde{\widetilde{Y}})$ to $l \times m$ FFD lattice using (1)-(6).
5:     **while** # of iterations $\leq I_1$ (alternating update step) **do**
6:         Update M using (8) and Sinkhorn's method.
7:         **while** # of iterations $\leq I_2$ maximum steps **do**
8:             Update Θ using (9)-(12).
9:         **end while**
10:    **end while**
11:    Update τ and band matrix bandwidth.
12: **end while**
13: De-normalize $\widetilde{f}(\Theta; \widetilde{Y_a})$ to $f(\Theta; \widetilde{Y_a})$ using (13).

---

and bandwidth hyperparameters, we used a grid-search method to minimize the error of the cost function across a subset of the external database. Following standard optimization values η, α and ϵ were respectively set to 0.001, 0.9 and 1×10^{-7} (Team, 2020). Additionally, the template and target signals were normalized to the maximum temporal length and amplitude, respectively, to permit for generalized hyper-parameter estimation. Fig. 4.2 demonstrates an example ECG adaptation from the first to the fifth iteration. Algorithm 1 depicts pseudo code describing the adaptation framework given a template and target signal. Fig. 4.3 complements Algorithm 1 by illustrating the iterative process of the framework.

4.3 Applications

In this section we undertake a qualitative study of the proposed technique and compare it to previously published algorithms. We also provide a graphic gallery of adaptations. It should be noted, for each instance that a feature is evaluated (Q-onset, T-end and dicrotic notch), the template is manually annotated. The subsequent temporal location of the annotated index/indices denotes the adapted template location for the given feature. In addition, template generation is performed via detection of the signal signature peaks and a predefined number of selected samples on either side of these apexes.

4.3.1 Simulated ECG Data

To determine the performance of our proposed technique with respect to common ECG artefacts known to corrupt the QT interval (Baumert *et al.*, 2016a), we employed data previously described by Porta *et al.* (1998) and evaluated in several related studies. In summary,

4.3.1   Simulated ECG Data

a single ECG beat of a healthy 26 year old subject was extracted from lead II at a sample rate of 1000 Hz and 12-bit amplitude resolution. Subsequently, the T-wave amplitude, W_T, of the reference beat was lowered from W_T to $0.1W_T$ in decrements of $0.1W_T$. The ten cardiac beats were replicated 500 times, forming ten synthetic recordings consisting of 500 beats each. Thus, each recording was characterized by varying T-wave amplitude and maintaining a QTV of zero. Additive white Gaussian noise (AWGN), baseline wander (BW) or sinusoidal amplitude modulation (AM) were introduced to model further distortions; in turn producing 30 recordings overall. The synthetic ECG data is characterized by a constant QT interval, therefore an ideal detection system would yield zero QTV.

Table 4.1 and Fig. 4.4 illustrate the QTV results across the synthetic ECG dataset for the proposed algorithm and five other methods. Observing Table 4.1, it is evident that the two most simplistic algorithms, Conventional (Porta *et al.*, 1998) and Template Stretch (Berger *et al.*, 1997), yield a significantly higher QTV in contrast to their counterparts. The Conventional method is a threshold derivative based technique whilst Template Stretch is a technique where temporal contractions and expansions are applied across the entirety of a template (manually annotated) cardiac cycle. The two algorithms present rather porous results across the baseline wander test, indicated by the high standard deviation in Table 4.1. Furthermore, in the presence of Gaussian noise or baseline wander the performance of the two algorithms is dependent on the T-wave amplitude. This is illustrated by the decreasing QTV as the amplitude acquisition range increases in sub-plots (a) and (b) of Fig. 4.4.

In the second tier of performance are the 2DSW and Template Shift (Starc and Schlegel, 2006) algorithms, respectively. 2DSW is a technique under which inhomogeneous template (manually annotated) adaptations are performed whilst the Template Shift algorithm is a technique under which separate QRS and T-wave templates (automatically annotated) are generated and independently shifted in time. Observing Table 4.1, both algorithms obtained a QTV above 1 ms with a comparatively lower standard deviation to the aforementioned algorithms. The results of Fig. 4.4 suggest a weakly inverse relationship between the T amplitude acquisition range and QTV pertaining to these two algorithms.

Producing state-of-the-art performance are i2DSW (Schmidt *et al.*, 2018a) and the proposed method. i2DSW (manually annotated) is a weighted variant of 2DSW. Observing Table 4.1, i2DSW yields a 0.84 ± 0.51 QTV across the synthetic data. The superior performance of i2DSW, relative to previous works, is superseded by the proposed method for

Table 4.1. Summary of the QTV across the proposed algorithm and five others.

QTV	Algorithm					
	2DSW	Conventional	Template Shift	Template Stretch	i2DSW	Proposed Method
Gaussian Noise (ms)	0.68	3.36	0.91	1.58	0.24	0.37
Baseline Wander (ms)	2.05	6.38	1.48	9.66	0.97	0.22
Amplitude Modulation (ms)	0.67	1.09	2.02	0.93	1.32	0.32
Mean ± SD (ms)	1.13 ± 1.04	3.61 ± 3.76	1.47 ± 1.17	4.06 ± 4.29	0.84 ± 0.51	0.30 ± 0.07

which we obtained a 0.3 ± 0.07 QTV across the dataset. Furthermore, Fig. 4.4 demonstrates that both algorithms are agnostic to the the T-wave amplitude, presenting a near constant QTV across various amplitudes.
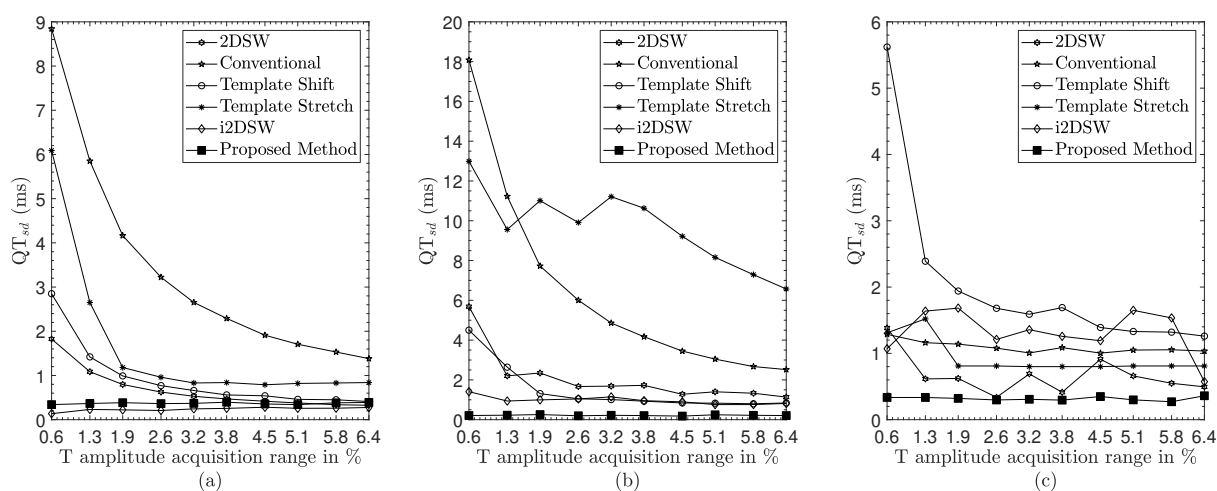
Figure 4.4. Results across the zero QTV simulated ECG data using the proposed method and five other published techniques. High accuracy performance is indicated by algorithms with QTV closer to zero. QTV across Gaussian noise (a), baseline wander (b) and amplitude modulation (c) is illustrated.

4.3.2 PTB Database QT Variability Tracking

Tracking of beat-to-beat variability is essential for the robust study of cardiac control, abnormalities and diseases (Porta *et al.*, 2015; Baumert *et al.*, 2011a, 2008). It is of utmost importance for QT interval measurement techniques to robustly capture pathophysiological variations. As such, we evaluate the sensitivity of the proposed technique against that of several existing methods. We utilize the readily available PTB Diagnostic ECG Database (Bousseljot *et al.*, 1995) containing 79 patients with acute myocardial infarction (22 female, mean age 63 ± 12 years; 57 male, mean age 57 ± 10 years) and 69 control subjects (17-female, 42 ± 18 years; 52 male, 40 ± 13 years). Approximately two minutes of sampled

data were extracted for each subject. Previous efforts have examined the PTB database to determine if myocardial infarction patients possess statistically different QT variability when compared to healthy controls (Hasan *et al.*, 2013). Furthermore, Hasan *et al.* (2013) also concluded that ECG Lead II distinguished the two groups most effectively. We utilized Lead II in this work.

The data were pre-processed to meet the requirements of the proposed algorithm. For each subject we extracted the beats using QRS annotations and beat rejection criteria from Schmidt *et al.* (2014). A beat was excluded if the normalized Manhattan distance exceeded $1\mu V/sample$ across the 2DSW algorithm. This criterion was imposed to ensure identical beats across subjects were evaluated between the proposed method and previous methods. Next, the mean beat length was obtained. For each recording all beats were linearly interpolated to the respective template length via shrinking or stretching. The template length was obtained by taking the average beat length across the recording. Template QT annotations were manually marked.
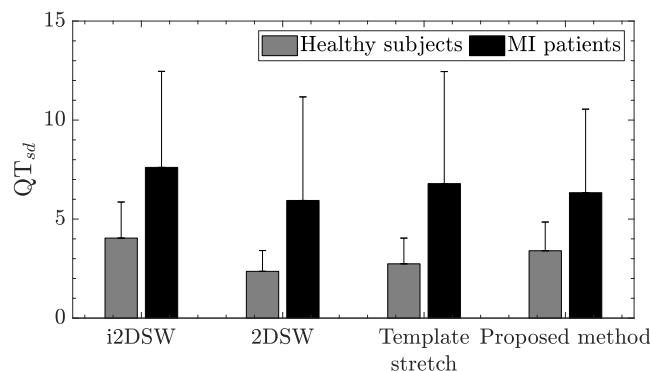
Figure 4.5. QTV results obtained across the PTB database using the proposed method and three others. The results are summarized across healthy subjects (grey) and MI patients (black) in the form of the mean (bar) plus standard deviation (line segment).

Fig. 4.5 illustrates the mean and standard deviation obtained by applying the proposed technique and several other popular algorithms. Each algorithm showed a statistically significant difference in QTV (p - value < 0.05 using the unpaired student t-test) between control subjects and MI patients. Observing Table 4.2, it is evident that the proposed algorithm marginally yields the lowest coefficient of variation across healthy subjects in the PTB database. Furthermore, our framework and i2DSW produced a notably lower coefficient of variation across MI patients compared to the template stretch and 2DSW algorithms. This is further evidence supportive of the decreased dispersion obtained across the synthetic dataset and, hence, superior performance achieved by the proposed method.

Table 4.2. Summary of the coefficient of variation for the proposed method and other methods.

Algorithm	Healthy Subjects	MI Patients
i2DSW	0.45	0.64
2DSW	0.44	0.88
Template Stretch	0.47	0.83
Proposed Method	0.43	0.67

4.3.3   QTDB

To study the performance of our algorithm in tracking beat-to-beat QTV, compared to manual annotations, we utilized the QT Database (QTDB) (Laguna *et al.*, 1997). This database contains 105 subject recordings with manual annotations pertaining to clinically important ECG features (onset, peak and end markers for P, QRS, T and where present U waves). Each recording contains at least 30 annotated cardiac cycles. The QTDB contains a variety of ECG morphologies and thus presents for a robust analysis of QT detection. The template for each recording was obtained by averaging the entirety of the equi-length cardiac cycles for each subject. Furthermore, beat rejection was employed via the use of the Hausdorff Distance, a commonly employed metric to measure how far two metric subsets are from one another. The cut-off criteria for the Hausdorff distance was obtained by selecting the value of the 95th percentile of the supervised two lead Hausdorff distance values (i.e. rejection of bottom 5%); for comparative purposes, the 5% rejection value was selected to closely match the minimum rejection rate of 94.7% of 2DSW, as observed in Table 4.3.

To account for the two commonly employed strategies for evaluating the QTDB we have analysed the performance of our algorithm based on a single lead and two leads. This is important to note as the associated manual annotations are based on two leads. In single lead analysis, each lead is independently delineated and the resultant features are compared to the reference annotations (single lead evaluation). Alternatively, in two lead analysis, each lead is independently delineated and the reference annotation is utilized to determine the algorithmic annotation that most closely matches the reference value for each beat.

Table 4.3 illustrates the QRS-onset and T-end results of the proposed method and several other methods across the QTDB. For each algorithm, we present the mean and standard deviation across the database. Since we are evaluating beat-to-beat variations (QTV) the standard deviation is of primary interest whilst the mean presents little value. Observing the single lead evaluation, we see that our algorithm yields comparable performance to the state-of-the-art algorithms. Furthermore, the supervised two lead evaluation results demonstrate that our algorithm yields the lowest standard deviation across the T-onset compared

Table 4.3. Summary of the QTV across the QTDB of the proposed algorithm and seven others.

Algorithm (lead used)	Q-onset			T-end		
	Se (%)*	mean	std	Se (%)	mean	std
single lead evaluation (all results in ms)						
(Zifan *et al.*, 2005) (2)	74.8	-5.22	3.60	63.4	6.72	33.5
(Vullings *et al.*, 1998) (1)	81.5	-0.8	10.6	79.4	9.4	49.0
(Dubois *et al.*, 2007) (1)	n.a.	n.a.	n.a.	82.1	45.0	38.6
(Dubois *et al.*, 2007) (2)	n.a.	n.a.	n.a.	81.6	42.8	40.3
(Rincón *et al.*, 2011) (1)	99.6	5.4	8.4	99.3	-5.3	22.7
(Rincón *et al.*, 2011) (2)	99.7	8.6	12.6	99.2	-4.6	27.2
(Schmidt *et al.*, 2014) (1)	88.3	-4.1	7.1	90.3	-5.6	15.1
(Schmidt *et al.*, 2014) (2)	88.6	-6.0	7.9	90.7	-6.8	16.5
Proposed Method (1)	92.0	0.6	8.4	92.0	1.32	17.7
Proposed Method (2)	89.6	0.6	8.4	89.6	1.32	17.4
supervised two lead evaluation (all results in ms)						
(Martinez *et al.*, 2004)	100	4.6	7.7	99.8	-1.6	18.1
(Martinez *et al.*, 2004) **	99.9	-3.6	8.6	99.0	13.5	27.0
(Dubois *et al.*, 2007)	n.a.	n.a.	n.a.	93.6	34.8	30.3
(Rincón *et al.*, 2011)	100	3.4	7.0	100	-2.4	16.9
(Schmidt *et al.*, 2014)	92.6	-3.0	6.1	94.7	-3.7	12.8
Proposed Method	95.0	5.3	5.8	95.0	11.4	12.5

* SE denotes the sensitivity, i.e. the percentage of evaluated beats.
**(Martinez *et al.*, 2004) evaluated (Laguna *et al.*, 1994)
and reported the results.

to all algorithms. Similarly, we can observe that the Q-onset standard deviation holds the second lowest standard deviation value.

4.3.4 Simulated PPG Data

In order to demonstrate the potential of the proposed method in PPG applications, we evaluated the performance of the algorithm in tracking the dicrotic notch across simulated data containing common factors known to affect PPG feature measurements. Some previous works have utilized this physiological feature to improve systolic blood pressure estimation (Gu *et al.*, 2008) and to study athletic differences via PPG pulse shape (Wang *et al.*, 2015). To the best of our knowledge there are no expertly (manually) annotated databases to evaluate the performance of dicrotic notch detection algorithms. To overcome this limitation in literature, we have used a synthetic PPG generation tool (Charlton *et al.*, 2019). Briefly, a set of PPG beats were replicated to generate simulated signals consisting of trains of PPG beats, each of 210 seconds duration sampled at 500 Hz. Consequently, distortions in the form of amplitude modulation or baseline wander were introduced, leading to two

Table 4.4. Summary of the dicrotic notch variability across the proposed algorithm versus Li et al.

Algorithm	dicrotic notch					
	AWGN		AM		BW	
	mean	std	mean	std	mean	std
all results in ms						
(Li *et al.*, 2010)	53.40	50.50	2.19	0.58	2.98	3.81
Proposed Method	-0.57	5.31	0.31	1.11	0.26	1.91

distorted recordings. The distortions were repeated for a range of 29 physiologically plausible RR intervals, resulting in 58 recordings overall. Additionally, for the undistorted 210 seconds recording, additive white Gaussian noise was introduced and the distortion was repeated 29 times from 20 dB to 10 dB. Thus, the database contained 87 recordings in total. Since the RR interval is constant across the recordings, the dicrotic notch variability is zero. Therefore, algorithm performance is evaluated based on the obtained dicrotic notch variability and its proximity to zero. We have attached the modified simulated database in the supplementary material.

Furthermore, we evaluated the performance across the only open-source dicrotic notch detection algorithm, proposed by Li *et al.* (2010). The results are summarised in Table 4.4. Similar to the QT interval, we are interested in the beat-to-beat tracking ability of the algorithm and therefore focus on the standard deviation. In the instance of AWGN and BW our algorithm outperforms the other evaluated method. Regarding AM distortion, our technique produced comparatively competitive results.

4.3.5   BIDMC PPG Adaptations

To further illustrate potential applications of the proposed algorithm, we have included a visual gallery of adaptations on PPG data. The publicly available BIDMC PPG and Respiration Dataset (Pimentel *et al.*, 2017; Goldberger *et al.*, 2012) contains 53 eight minute recordings of PPG sampled at 125 Hz; the data were previously utilized to benchmark algorithms for estimating the respiratory rate from the PPG. For a particular subject, a template PPG was obtained by averaging the data across a thirty second interval; where the signal apex (systolic peak) was taken as the reference point to delineate each beat. In this work, we extracted template PPG for seven subjects across the BIMDC database and subsequently plotted five adaptations for each subject. Fig. 4.6 depicts the effectiveness of template adaptation achieved by the proposed algorithm.
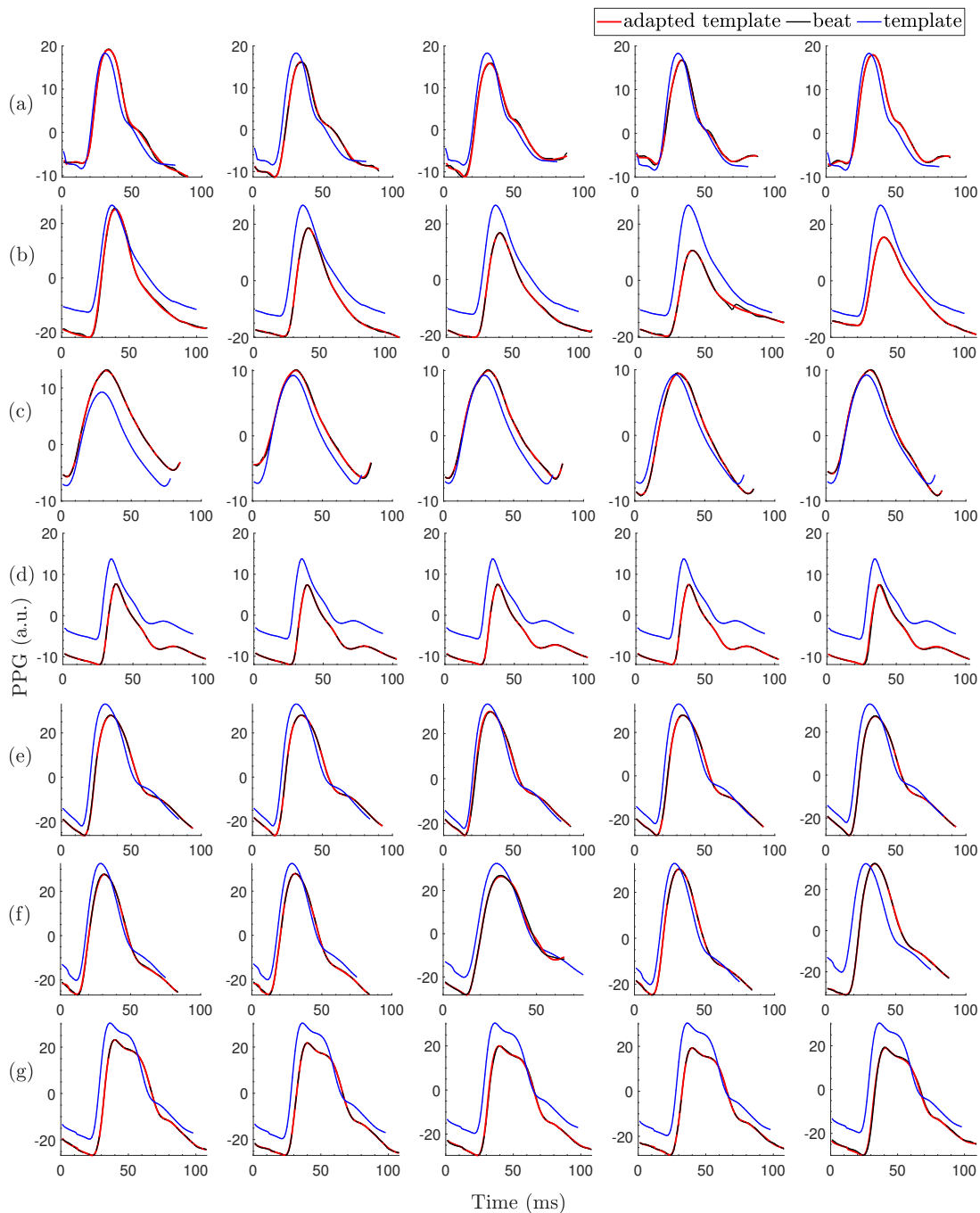
Figure 4.6. Example of seven subjects (a) - (g) across the BIMDC database. For each subject five beats were considered from left to right. In each instance the template (blue) is adapted to the beat (black) producing the resultant deformation (red).

4.4   Discussion

The proposed method is a general framework for 2D template adaptations. In comparison to previously proposed template adaptation algorithms in signal processing literature our method is based on a robust mathematical foundation. By using free form deformations

and a quadratic cost function we obtain mathematically smooth and continuously differentiable adaptations. Furthermore, we introduce a doubly stochastic correspondence matrix, which provides correspondence probabilities between two sets of signals. Under the proposed model, binary correspondences were persistent for pronounced features such as the R-peak of the ECG. For less evident features, the algorithm obtained non-binary probabilities which acted as temporal interpolation points. The advantage of permitting non-binary correspondences in the doubly stochastic matrix stems from the fact that contraction and expansion of localized regions in quasi-periodic data may not match up with the number of relevant samples in the given region. Non-binary correspondences are permissible by virtue of the fact that a spline interpolation method is being utilized under which there is no guarantee that the deformation model can retrieve an exact adaptation to the target data; that is, the model provides no guarantee that template data can perfectly match noisy samples. This is a desirable property as the proposed algorithm is restricted from overfitting. Furthermore, the use of deterministic annealing reduces the need to estimate an appropriate Lagrangian multiplier for the entropy term in Eq. 7, as multiple solutions are iterated over to yield a final adaptation. Similarly, the band matrix is gradually increased to reduce the need for the approximation of a valid domain and to permit gradual deformations.

We have demonstrated the ability of the algorithm to perform on several databases. Compared to previously proposed QTV algorithms our method illustrated superior results across the baseline wander and amplitude modulation synthetic ECG tests. Furthermore, it achieved comparable results to the best performing algorithm across the white Gaussian noise test. The high level of performance on QTV analysis is further supported by the results obtained on the PTB database. Our algorithm detected statistically significant differences in QTV between myocardial infarction patients and normal subjects, which is in alignment with the comparative studies observed in 4.5. Furthermore, our algorithm yielded a similarly low coefficient of variation to i2DSW for MI patients across the PTB database; thus, further illustrating its ability to robustly estimate QTV. Regarding the QTDB, our method produced competitive single lead results compared to the state-of-the-art and yielded superior results under supervised two-lead analysis. This suggests that the proposed method may produce state-of-the-art QTV tracking under appropriate channel selection. By applying our proposed method to the BIDMC database we provided a visually intuitive representation of the algorithms prowess and applicability to PPG data. Importantly, we performed the adaptations utilizing the same hyperparameters used across the two ECG datasets, in turn demonstrating the generalisation ability of our framework. The results were further backed by a beat-to-beat analysis into the dicrotic notch of the PPG. Our algorithm demonstrated

superior results to a state-of-the-art arterial blood pressure delineator. However, it is important to note that the difference in performance may not be as prevalent if a dedicated PPG dicrotic notch delineator were available for comparison.

4.5   Conclusion

We have proposed a 2D template adaptation framework with a robust theoretical foundation. Our method is able to detect subtle features in noisy quasi-periodic time series. It is of interest to note that the hyperparameters were kept constant across experiments. Thus, suggesting the described method may be an important tool in various applications where 2D quasi-periodic time series are of interest.

4.6   Control Point Partial Derivatives

The derivatives from Eq. 9 with respect to the FFD control point parameters can be easily obtained. For an $l \times m$ grid of control points, each parameter is denoted by:

$$\delta P_{i,j} = (\delta P_{i,j}^x, \delta P_{i,j}^y),$$

where $i = 1, \cdots, l$ and $j = 1, \cdots, m$. Under this notation, consistent with the methodology section, for the $(i,j)^{th}$ control point, the following holds:

$$\frac{\partial \delta \widetilde{f}(\Theta; \widetilde{Y})}{\partial \delta P_{i,j}^x} = \begin{bmatrix} \beta_i(s_a)\beta_j(t_a) \\ 0 \end{bmatrix},$$

$$\frac{\partial \delta \widetilde{f}(\Theta; \widetilde{Y})}{\partial \delta P_{i,j}^y} = \begin{bmatrix} 0 \\ \beta_i(s_a)\beta_j(t_a) \end{bmatrix}.$$

Interpretable Classification of Cardiac Ischemic Beats Using Correspondence Based Template Adaptation

The content of this chapter is a modified version of a text under review in IEEE Transactions on Biomedical Engineering.

5

Abstract

The classification of ischemic beats in ECG is a critical component in the detection of myocardial ischemic episodes. Importantly, interpretable techniques are necessary for widespread adoption of automated beat classification methods in the clinical setting. As such, in this work we propose a novel and interpretable ischemic beat classification framework. The method utilizes a recently developed feature extraction algorithm employing correspondence based template adaptation to retrieve morphological features from the ECG. Template adaptation permits for the manual annotation of morphological features, thus allowing the inclusion of expert knowledge. We pair the feature extraction technique with an interpretable classification method - k-nearest neighbours. Combined, the two components yield an intuitive and robust model. We demonstrate the performance of the proposed framework by evaluating the method across a task-specific database utilizing ECG data from the European ST-T Database and comparing the results against a set of previously proposed models. To provide a more robust measure of performance on unseen data by the proposed work we employ subject-wise validation alongside the conventionally used beat-wise validation.

5.1   Introduction

Myocardial ischemia occurs when blood flow to the heart is reduced due to a partial or complete obstruction of a coronary artery. According to World Health Organisation (WHO) estimations, ischemic heart disease accounted for upwards of 9 million deaths in 2016 (Nowbar *et al.*, 2019). The presence of myocardial ischemia is important in the prognosis of ischemic heart disease and is diagnosed by several methods including the electrocardiogram (ECG) (Shimokawa and Yasuda, 2008). Due to the high mortality rates of ischemic heart disease and prognostic abilities of ECG, robust and pragmatic diagnostic tools are of utmost importance.

The ECG represents variations in the total electrical potential produced by heart muscle. ECG recordings have been extensively used in signal processing and machine learning literature for the purpose of: beat classification (Lyon *et al.*, 2018), physiological marker

analysis (Baumert *et al.*, 2016a; Porta *et al.*, 2007; Martínez *et al.*, 2006), and wearables (Bayoumy *et al.*, 2021). In the ECG, ischemic episodes manifest in the ST interval (Channer and Morris, 2002), representing the period between the ventricular depolarisation offset and the ventricular repolarisation offset of the cardiac cycle (Shimokawa and Yasuda, 2008). Such episodes are observable by slow morphological changes in the ST segment and/or T-wave. ECG monitoring is a well-established and non-invasive procedure for detecting such morphological changes. However, visual ECG monitoring is time-consuming, expensive and error-prone. Thus, robust and interpretable automated techniques for ischemic detection can assist physicians towards more objective and efficient diagnosis.

Robust classification of ischemic beats is of paramount importance in accurately detecting ischemic episodes. Conventionally, a moving-window of classified beats is evaluated to determine ischemic episodes. In this work, we exclusively focus on the problem of ischemic beat classification. We discuss several studies which evaluate ischemic episode detection but only for the purpose of describing their ischemic beat classification methodology.

Numerous efforts have been made to classify ischemic beats using ECG including both interpretable and black-box models. Exarchos *et al.* (2006) employed an automated methodology based on association rule mining for the detection of ischemic beats. Association rule mining is a data mining technique commonly employed in pattern discovery of unsupervised learning problems. In Goletsis *et al.* (2004), a combined genetic algorithm and multiciriteria decision analysis based method was used to detect ischemic beats. In Papaloukas *et al.* (2001, 2002c), the authors utilized a knowledge-based technique with previously studied threshold levels of various morphological features in the ST-T interval.   Exarchos *et al.* (2007) employed a methodology for the automatic creation of fuzzy expert systems from an initial training dataset is proposed. The framework consists of a three-step process: (a) extraction of a set of rules from a decision tree derived from the training dataset, (b) transformation of the set of rules into a fuzzy model and (c) the optimization of the fuzzy model's parameters using a global optimizer. Similarly, Presedo et al.   Presedo *et al.* (1996) focused on a fuzzy based implementation using expert knowledge. A related fuzzy based model was proposed in Tsipouras *et al.* (2007). Orrego *et al.* (2012) presented a dimensionality reduction study based on fuzzy rough sets. Their work described a novel framework based on entropy, neighbourhood techniques and a modified feature selection algorithm across a large feature space. In García *et al.* (2000a), a detection algorithm is applied to the filtered root mean square series of differences between the beat segment

and an average pattern to detect anomalous segments. Ranjith *et al.* (2003) used a rule-based method consisting of ST-segment deviation and T-wave amplitude measurements for the detection of ischemic episodes in a cardiac cycle. Comparison of ST segment changes from a reference ST segment level is a well established technique (Jager *et al.*, 1998). In Correa *et al.* (2014) the authors utilized vectorcardiogram parameters for the purpose of ischemic characterization; this approach requires three orthogonal leads or a transformed 12-lead system. Tseng *et al.* (2016) proposed and evaluated the performance of a support-vector machine and spare representation using a modified rule-based method. Limitations of previous works have included: a) not using beat-by-beat ischemic annotations; b) subpar statistical measures (sensitivity/specificity) when evaluated against test data.

Similar to other biomedical engineering applications, neural networks have been extensively employed in ischemic beat classification. In Stamkopoulos *et al.* (1998); Maglaveras *et al.* (1998a) a dimensionality reduction (non-linear principal component analysis) based feature extraction method combined with a neural network was employed to achieve beat classification. Similarly, Maglaveras *et al.* (1998b) proposed a bidirectional associative memory neural network for the classification of ischemic beats. In Papadimitriou *et al.* (2001), the authors describe a supervising network self-organizing map model. This type of model employs unsupervised learning for simple to resolve regions of beats in the learning process and supervised learning for difficult ones in a two stage training procedure. Furthermore, Pelaez *et al.* (2014) used a multi-layer perceptron neural network combined with wavelet transforms for the purpose of ischemia classification. Neural network and other black-box based methods have produced state-of-the-art results but are inherently plagued by a lack of interpretability. This characteristic limits their clinical adoption, hence more transparent techniques with similar performance are needed. More recently, several other works (Park *et al.*, 2012; Kumar and Singh, 2016) have claimed state-of-the-art performance across ischemic beat detection, however, they do not seem to have used the same set of updated (beat-by-beat) annotations as reported in earlier related works (see Table 5.6).

Here, we proposed a fully interpretable and robust ischemic beat classification system. The framework includes a recently proposed feature extraction technique which has yielded state-of-the-art performance in ECG feature extraction across several databases. Furthermore, the technique permits for the prior/expert knowledge inclusion by means of manual annotation. We elected to employ a k-nearest neighbour (kNN) classifier to provide a simplistic and interpretable model which may pave an easier path toward future research

and/or clinical adoption. Furthermore, contrary to earlier works we tune and evaluate our algorithm in a more robust manner by undertaking a subject-wise training/validation and testing process. The method was developed and evaluated on an updated set of ischemic beat annotations for the European ST-T Database. The original and publicly available annotations provide descriptions for ischemic episodes. Thus, a task-specific set of annotations was utilized which provides a description for each beat as noisy, ischemic or normal. In this work, we only quantitatively compare our results against methods that have been evaluated against beat-by-beat ischemic annotations. The proposed work is aimed at ischemic beat classification and therefore ought to only be evaluated against methods with the same objective that have utilized task-appropriate annotations.

5.2   Methodology and Materials

In this section we describe the proposed classification framework in detail. Firstly, we explain the feature extraction process using a recently proposed template adaptation technique. The process is based on a non-rigid registration algorithm which is able to account for deviations in magnitude and amplitude via non-binary correspondences between template and target data samples. Next, we describe the interpretable kNN classifier. We conclude by providing a detailed description of the dataset alongside the training, validation and testing process. The framework was implemented in MATLAB 2019b using GPU capabilities and the algorithm evaluation was performed using high-performance computing resources available at The University of Adelaide.

5.2.1   Feature Extraction

Correspondence based template adaptation (Karisik and Baumert, 2021) is a technique which fits a template time series to a target time series. By annotating morphological features on the original template data the corresponding features can readily be identified upon adaptation. In this work fiducial points were manually annotated across the template by the authors. The method is underpinned by two fundamental processes: parameterisation and energy minimisation. We commence by describing the parameterisation process as it is a fundamental prerequisite for defining the energy minimisation formula and subsequent optimisation.

As in Karisik and Baumert (2021), a min-max normalization is first performed on both the template (deforming - D) and target data (fixed - F). We denote the normalized template by

5.2.1 Feature Extraction

$\widetilde{D}$ which encapsulates a 2D array containing the time and amplitude dimensions, respectively; i.e. for a given sample, a, $\widetilde{D_a} = [\widetilde{D_a^x}, \widetilde{D_a^y}]$. Similarly, we denote the target data by $\widetilde{F_a}$, i.e. for a given sample, b, $\widetilde{F_b} = [\widetilde{F_b^x}, \widetilde{F_b^y}]$.

The deformation technique utilized in Karisik and Baumert (2021) is based on free-form deformations (FFD) which enforce smooth adaptations and are defined by a localised coordinate system, that is:

$$\widetilde{D_a} = X_o + s_a S + t_a T. \tag{5.1}$$

In (1), the origin of an $l \times r$ control point lattice, P^0, is denoted by X_o and the embedding lengths of the lattice are represented by S (x-axis) and T (y-axis).

In FFD, the (s, t) coordinate for a given sample, $\widetilde{D_a}$, can be obtained by:

$$s_a = \frac{\widetilde{D_a^x} - P_{min}^x}{P_{max}^x - P_{min}^x}, \tag{5.2}$$

$$t_a = \frac{\widetilde{D_a^y} - P_{min}^y}{P_{max}^y - P_{min}^y}, \tag{5.3}$$

where P_{min}^x, P_{max}^x, P_{min}^y and P_{max}^y are the four control points corresponding to the minimum and maximum spatial coordinates of the lattice.

Once parameterised to an FFD grid, a deformation from the control point lattice P_0 to the control point lattice P_1 is obtained by the Bernstein polynomial tensor product:

$$\widetilde{g}(\widetilde{D}) = \sum_{i=0}^{l} \sum_{j=0}^{r} \beta_i(s_a) \beta_j(t_a) P_{ij}^1. \tag{5.4}$$

In (4), $\beta_i(s_a) = \binom{l}{i}(1 - s_a)^{l-i} s_a^i$ and $\beta_i(t_a) = \binom{m}{j}(1 - t_a)^{m-j} t_a^j$. By the linear precision of FFDs, we can express (4) as an additive process: $P^1 = P^0 + \delta P$, i.e.

$$\widetilde{g}(\Theta; \widetilde{D}) = \sum_{i=0}^{l} \sum_{j=0}^{r} \beta_i(s_a) \beta_j(t_a) (P_{ij}^0 + \delta P_{ij})$$

$$= \sum_{i=0}^{l} \sum_{j=0}^{r} \beta_i(s_a) \beta_j(t_a) (P_{ij}^0) + \tag{5.5}$$

$$\sum_{i=0}^{l} \sum_{j=0}^{r} \beta_i(s_a) \beta_j(t_a) (\delta P_{ij}).$$

Here, $\delta P = \Theta$ and (i, j) denotes the indices of the $l \times r$ control point lattice. In (5), the first term represents the initial template and the second term the contribution of the incremental control point shifts. Therefore, (5) can be expressed as:

$$\widetilde{g}(\Theta; \widetilde{D}) = \widetilde{D} + \delta\widetilde{g}(\Theta; \widetilde{D}). \tag{5.6}$$

Utilizing the relationship obtained in (6), we ensue to formulate the adaptation cost function and the means by which Θ is estimated. In Karisik and Baumert (2021) the correspondence based template adaptation can be described by minimising the following cost function iteratively:

$$E(M, \widetilde{g}) = \sum_{a=1}^{N} \sum_{b=1}^{N} z_{a,b} m_{a,b} \|\widetilde{F}_b - \widetilde{g}(\Theta; \widetilde{D_a})\|^2 +$$

$$\lambda\|\widetilde{g}(\Theta; \widetilde{D_a})\|^2 + \tau \sum_{a=1}^{N} \sum_{b=1}^{N} m_{a,b} \log m_{a,b} \tag{5.7}$$

$$- \log \xi \sum_{a=1}^{N} \sum_{b=1}^{N} m_{a,b}.$$

In (7), $m_{a,b}$ is constrained (via the Sinkhorn-Knopp method (Knight, 2008)) by $\sum_{a=1}^{N} m_{a,b} = 1$, $\sum_{b=1}^{N} m_{a,b} = 1$ ($m_{a,b} \in [0,1]$); m contains the correspondence probabilities between the two input datasets. The first term represents the error measure (least squares). A band matrix constraint is imposed on the system by the introduction of the binary (0 or 1) variable z. This constraint is introduced to limit the range of permissible comparisons between the template and target sets. As an example, in the tridiagonal case z can be represented by:

$$z = \begin{pmatrix} z_{1,1} & z_{1,2} & 0 & \cdots & & \cdots & 0 \\ z_{2,1} & z_{2,2} & z_{2,3} & & & & \vdots \\ 0 & \ddots & \ddots & \ddots & & & \vdots \\ \vdots & & \ddots & \ddots & & \ddots & 0 \\ \vdots & & & z_{N-1,N-2} & z_{N-1,N-1} & z_{N-1,N} \\ 0 & \cdots & \cdots & \cdots & & z_{N-1,N} & z_{N,N} \end{pmatrix}.$$

The bandwidth of the band matrix in the present work is set as a portion of the template length (see (Karisik and Baumert, 2021)). The second term is employed to regularize the system. The third term (entropy barrier function) is utilized to restrict the values of $m_{a,b}$ to a number between 0 and 1 (inclusive). Relatedly, τ is used to allow for annealing during optimisation. The fourth term bars zero values in the correspondence matrix to satisfy

the constraints of the Sinkhorn-Knopp algorithm. In the current framework, due to the low sampling rate (250 Hz) and significant morphological changes caused by ST-segment and T-wave changes, a grid size of 2×10 was used. The dimensions were obtained by undertaking a restricted parameter sweep across various grid sizes from a small training data batch and obtaining a minimised mean squared error.

Optimisation of the described template adaptation method is based on an alternating estimation approach between m and the morphological deformation Θ. This is systematically performed in an iterative approach whilst incorporating annealing. To estimate $m_{a,b}$ in the first iteration, (7) can be differentiated w.r.t $m_{a,b}$ and equated to 0. This produces the analytic solution:

$$m_{a,b} = e^{-z_{a,b} \frac{\|\widetilde{F}_b - \widetilde{g}(\Theta;\widetilde{D}_a)\|^2}{\tau}} + \zeta. \tag{5.8}$$

To computationally avoid near-zero matches a heuristic is employed to define ζ (see (Karisik and Baumert, 2021)). The estimated (optimal) control point shifts and subsequent transformation are then obtained by differentiating (7) w.r.t Θ:

$$\frac{\partial E(M,\widetilde{g})}{\partial \Theta_{i,j}} = -2 \sum_{a=1}^{N} \sum_{b=1}^{N} z_{a,b} m_{a,b} (\widetilde{F}_b - \widetilde{g}(\Theta; \widetilde{D}_a))$$

$$(\nabla \widetilde{g}(\Theta; \widetilde{D}_a) . \frac{\partial \delta \widetilde{g}(\Theta;\widetilde{D}_a)}{\partial \Theta_{i,j}} + 2\lambda \widetilde{g}(\Theta; \widetilde{D}_a). \tag{5.9}$$

The method used to solve (9) is based on gradient descent (adaptive), namely RMSprop (Hinton *et al.*, 2012). The intent of using such an approach is to address the diverse range of gradients across control points. Furthermore, adaptive methods assist in reducing the time to reach a minima and discourage saddle points.

The adapted template is de-normalized in an inverse manner to the initial normalization to recover the original time and amplitude scales. This concludes the feature extraction methodology. We ensue to describe the selected features, classifier and database.

5.2.2 Features

In the proposed framework the following set of features are fed into the classifier:

1. the QT interval;
2. the T-wave amplitude;
3. the ST area;

4. the ST deviation;

5. the ST slope;

6. age (patient data);

7. the JT-peak interval;

8. and the ST interval.
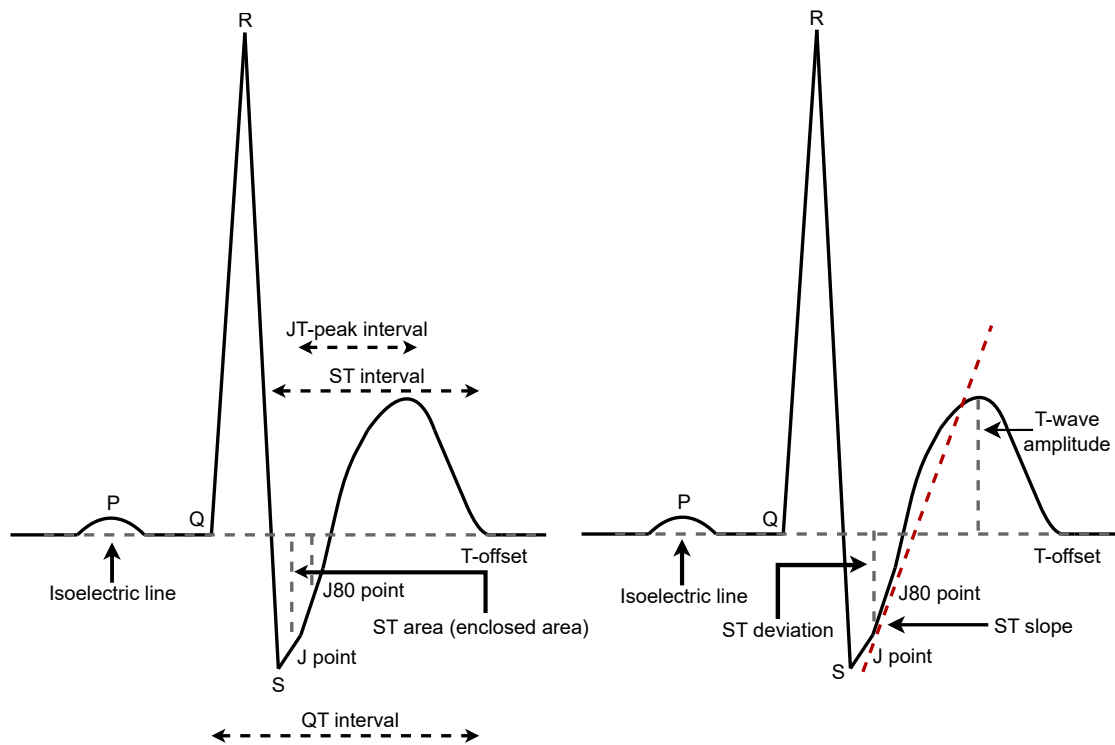
Figure 5.1. The set of morphological features which are extracted via the use of correspondence based template adaptation. This set of features serves as the classifier input.

The feature set primarily consists of morphological features (see Fig. 5.1) which have been extracted via correspondence based template adaptation. The original template data were manually annotated due to the complex morphology of the ECG. Briefly, the QT interval represents the period pertaining to the ventricular depolarization and repolarization process during a cardiac cycle and is defined by the temporal length from the QRS-onset to the T-wave offset. The T-wave amplitude represents the amplitude deviation of the T-wave peak from the isoelectric line. The ST area represents the area between the ECG, isoelectric line, J point and J80 point. The ST deviation is defined as the distance between the J80 point and the isoelectric line (the same feature between the J point and the isoelectric line is also utilized). The intent of this feature is to capture the amplitude deviation of the ST segment. The ST slope is the gradient of the line connecting the J and J80 points. The

JT-peak interval represents the temporal length of the J point to the T-peak. Lastly, the ST interval denotes the interval between the S point and the T-wave offset.

5.2.3 Classification

In the proposed work a k-nearest neighbour (kNN) approach is employed to differentiate between normal and ischemic beats. The kNN classification algorithm is amongst the most popular and interpretable techniques in statistical learning literature. The primary principle behind the method is that if the majority of the k (pre-specified) nearest neighbours of an instance under classification belong to a particular class, then the instance is labelled as belonging to the majority class (see Fig. 5.2). The nearest neighbour evaluation is performed in the feature space where a distance function is employed to enable comparison. For the binary classification problem consider an unknown instance, C_u, and consider a known instance, C_{t1}, belonging to the training set; each instance contains a nine element vector containing the described morphological features. A distance measure, in this case the correlation coefficient, is employed to then generate a set of distances against all training samples, which for the given case is obtained by:

$$Distance_{correlation} = \frac{\sum_{f=1}^{N_f} C_{u,f} C_{t1,f}}{\sum_{f=1}^{N_f} C_{u,f} \sum_{f=1}^{N_f} C_{t1,f}}. \tag{5.10}$$

The voting method is then employed on the nine features ($N_f = 9$) across the 30-nearest neighbours and hence classification is achieved. The kNN algorithm contains only a single hyperparameter, k.
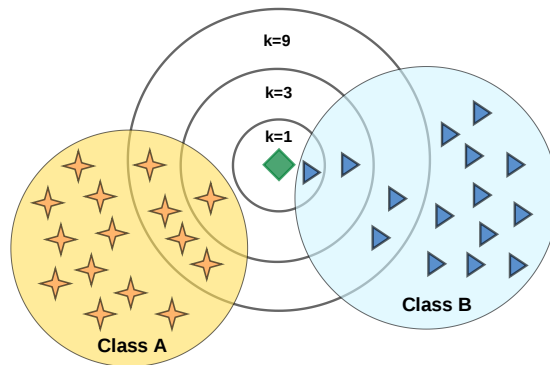
Figure 5.2. An example of a binary kNN classifier for k=1,3 and 9. The diamond (green) denotes the query point, the stars (yellow) denote Class A members and the triangles (blue) denote Class B members.

5.2.4 Database

We used the European ST-T Database (Taddei *et al.*, 1992), which is publicly available on PhysioNet (Goldberger *et al.*, 2012). The ECG measurements were obtained by thirteen research groups from eight countries. The goal of the study was to prototype an ECG database for the assessment of ambulatory ECG monitoring systems. The database comes with annotations pertaining to ST-segment and T-wave changes which contain further descriptions denoting the nature of the events (ischemic/non-ischemic). For the purpose and evaluation of the described classification framework, a task-specific database was employed utilizing the ECG measurements from the original European ST-T database combined with updated beat-by-beat annotations. The annotations were independently labelled by three clinicians as ischemic, noisy or normal. Any discrepancies in annotations were amended after a mutual evaluation by the three clinicians. The European ST-T database contains 90 continuous two-channel recordings, each two hours in length, taken from 79 ambulatory ECGs. The subjects were 70 men (aged 30-84) and 9 women (aged 55-71). The data were sampled at 250 samples per second with a 12-bit resolution over a 20 mV input range. A myocardial ischemia diagnosis was present or suspected in each subject. The task-specific ECG database was formed by extracting eleven hours of continuous two-channel data from 10 representative files of the original database as observable in Table 5.1 (this subset of data was selected and annotated by earlier works - see Table 5.6). Across the eleven hour excerpt, 20 ischemic ST-segment episodes and 20 ischemic T-wave episodes were present. The accumulated data resulted in 86 384 cardiac beats of which 6 754 were discarded on account of improper QRS detection and/or artifacts. From the remaining 76 989 beats, 37 663 (48.92%) were labelled as ischemic and the rest as normal.

For algorithm evaluation, we employed two strategies. Firstly, we used a inter-subject training/validation/testing split. The validation step was used to tune the k value of the classification framework. Fig. 5.3 demonstrates the accuracy of the system against varying values of k. Steady performance is illustrated across varying values of k, with the optimal value occurring at $k = 30$. This value was selected and employed across all the remaining algorithm evaluation in the ensuing sections. Furthermore, the broad range of k values with a comparably high accuracy demonstrate the robustness of the selected feature set. A less robust set may be highly dependent on the value of k; this is because a high variance across the features would yield vastly different performance. Upon attaining a set of suitable values and performance metrics the framework was employed across the testing data. Table 5.2 demonstrates the split across the training, validation and testing data. In
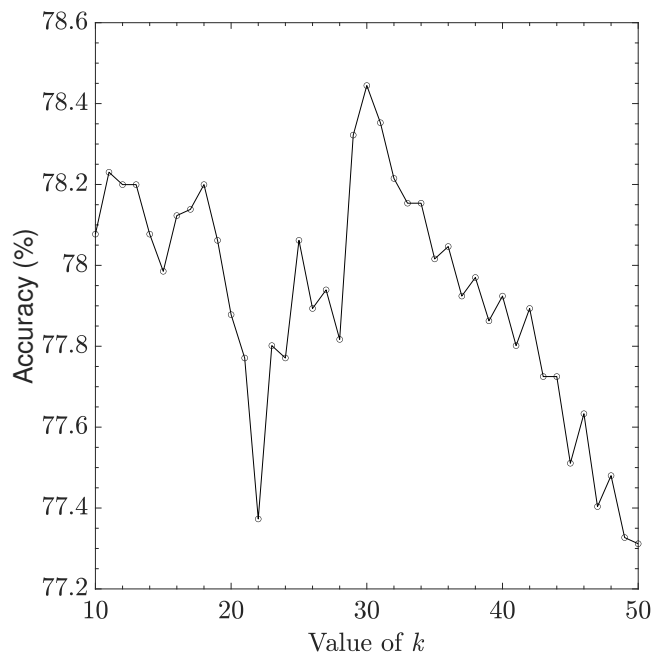
Figure 5.3. Accuracy of the different k values from 10 to 50 nearest neighbours against the validation set (see Table 5.2); accuracy is defined as the percentage of correctly classified beats.

summary, fourteen out of twenty recordings (70%) were used for the training purposes, two out of twenty recordings (10%) were used for validation and the remaining four out of twenty recordings (20%) were used for testing purposes; each set was constructed to very nearly form a balanced split between ischemic and normal beats. A more robust measure of cross-validation such as leave-one-out (LOO) was not employed in a subject-wise manner due to the difficulty of generating a balanced distribution of ischemic and non-ishemic beats across the limited data available.

Secondly, we used an intra-subject training and testing split similar to Goletsis *et al.* (2004) and in line with previous works observable in Table 5.6. This type of training and testing split was utilized to be able to fairly compare results against previous efforts made across the task-specific database. The validation data consisted of 26936 beats and the testing data was comprised of 50 053 beats. A K-fold (100) cross-validation (see 5.3) was employed on this subset of the data and observed in parallel to the subject-wise validation. No further hyper-parameter tuning was performed when evaluating the algorithm in a beat-wise manner to avoid over-fitting.

Table 5.1. Summary of subject recordings and respective durations utilized from the European ST-T Database (subset containing beat-by-beat annotations).

Subject	Hour(s)
e0103	1
e0104	2
e0105	1
e0108	1
e0113	1
e0114	1
e0147	1
e0159	1
e0162	1
e0206	1

Table 5.2. The training/validation/testing splits across the two-lead ECG for each subject.

Subject	Channel 1	Channel 2
e0103	Training	Testing
e0104	Training	Training
e0105	Validation	Training
e0108	Validation	Training
e0113	Training	Training
e0114	Training	Training
e0147	Training	Training
e0159	Training	Testing
e0162	Testing	Training
e0206	Testing	Training

Table 5.3. Performance against the training and validation data for k-fold validation (beat-wise) and the hold-out strategy (subject-wise).

Validation Method	Sensitivity (%)	Specificity (%)
K-fold (beat-wise)	93	94
Hold-out (subject-wise training)	93	94
Hold-out (subject-wise validation)	88	70

5.3   Results

In this section we evaluate the proposed framework and compare it to the sensitivity/specificity benchmarks set by previously published methods. We perform model assessment and evaluate the classifier performance across both a beat-wise and subject-wise validation. Table 5.3 shows the test/validation results for the K-fold (beat-wise) and the hold-out (subject-wise) approaches, respectively. An average sensitivity of 93% and average specificity of 94% is observed across the 100-fold evaluation of the framework. Furthermore, a 93% sensitivity and 94% specificity is observed against the training set of the hold-out method - whilst an 88% sensitivity and 70% specificity is seen across the validation set of the hold-out method.

Table 5.4 summarises the raw false positive and false negative results across the subject-wise test data. Similarly, Table 5.5 summarises the raw false positive and false negative results across the beat-wise test set. Table 5.6 demonstrates that the proposed framework yields a 93% sensitivity and 94% specificity across the beat-wise validation and a 98% sensitivity and 70% specificity across the subject-wise validation. It should be noted that

Table 5.4. Test results against the subject-wise validation. Ischemic beats are denoted by I and normal beats are denoted by N.

Table 5.5. Test results against the beat-wise validation. Ischemic beats are denoted by I and normal beats are denoted by N.

Predicted Class

	I	N	total
I	7890 (50.7%)	167 (1.1%)	8057
N	2274 (14.6%)	5336 (34.3%)	7610
total	10164	5503	15667

True Class

Predicted Class

	I	N	total
I	22916 (45.8%)	1570 (3.1%)	24486
N	1804 (3.6%)	23763 (47.4%)	25567
total	24720	25333	50053

True Class

Table 5.6. Performance comparison of ischemic beat detection across similar techniques and against the ESC ST-T Database (equivalent subset).

Algorithm	Sensitivity (%)	Specificity (%)
Rule-based (Papaloukas *et al.*, 2001)	70	63
ANN and PCA (Papaloukas *et al.*, 2002b)	90	90
ANN & parametric modelling (Papaloukas *et al.*, 2002a)	81	84
Multicriteria decision analysis (Goletsis *et al.*, 2003)	90	89
Genetic algorithms & multicriteria decision analysis (Goletsis *et al.*, 2004)	91	91
Association rule mining-based (Exarchos *et al.*, 2006)	87	93
Automated creation of fuzzy expert system (Exarchos *et al.*, 2007)	91	92
A framework for fuzzy expert system creation (Tsipouras *et al.*, 2007)	81	73
Current work (beat-wise)	93	94
Current work (subject-wise)	98	70

other methods have been proposed, however, they have employed alternative evaluation measures or test sets, thus making direct comparison unattainable.

Lastly, Fig. 5.4 illustrates the receiver-operating-characteristic (ROC) curves when the binary classifier is evaluated in a beat-wise and subject-wise manner. The area under the curve (AUC) value for the beat-wise and subject-wise approach is 0.9781 and 0.8044, respectively.
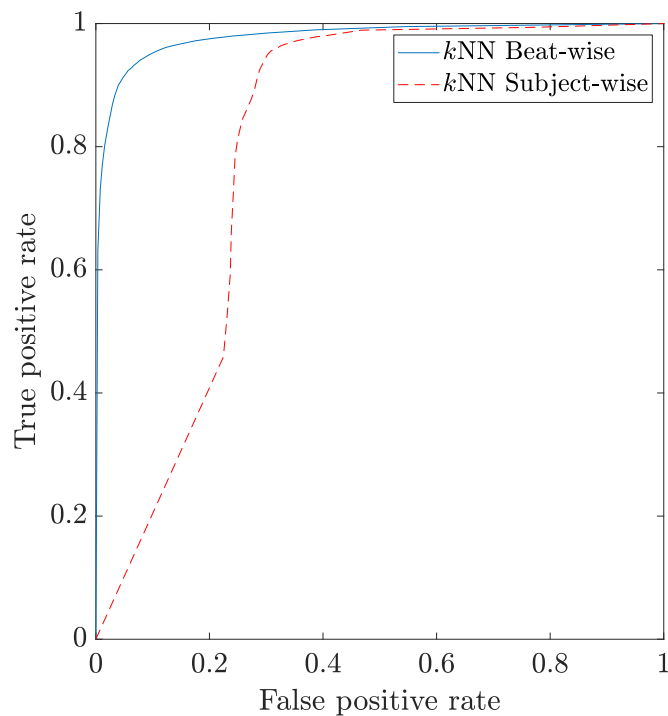
Figure 5.4. ROC curves for the beat-wise and subject-wise test results using the classification framework.

5.4   Discussion

Robust discrimination between the two-class problem of ischemic beat and normal beat detection is of critical importance in the observation of ischemic episodes and subsequent diagnosis of myocardial ischemia. In the current study, an interpretable classification model is proposed based on a correspondence based template adaptation feature extraction technique and a kNN classifier. In the proposed work, the template signal was generated by averaging the signal length across the entire recording beat-by-beat. The beats were extracted based on a set interval, where each QRS point was considered to be the central sample of the cardiac cycle. This is not dissimilar to other template adaptation methods (Schmidt *et al.*, 2014).

Previously, template adaptation has been studied and applied in ECG literature for the extraction of morphological features (Baumert *et al.*, 2012; Karisik and Baumert, 2021; Schmidt *et al.*, 2014). Furthermore, it provides an interpretable and observable approach to the feature extraction process. In this work, the extraction method permits for the incorporation of human knowledge by manual delineation of the template beat; automatic methods also exist and have been utilized in earlier works (Schmidt *et al.*, 2014, 2018a). Manual selection was utilized in this work due to the complex nature of beat morphologies

pertaining to ischemic beats. In our framework, the feature extraction method employs a parameterisation to impose smooth deformations in the form of splines. The application of a parameterised grid with smooth properties prevents unrealistic template adaptations. We employed a further restriction on the deformation process by using a sparse grid of 2 control points. The feature extraction method in this work utilizes a non-binary correspondence matrix to achieve an appropriate template adaptation. The imposition of a non-binary matrix permits for the adaptation and interpolation of points across signals with low sample rates (250 Hz in this work). It was previously observed in Karisik and Baumert (2021) that persistent features such as the R-peak approach correspondence values of close to 1. Lastly, a regularisation parameter is incorporated into the template adaptation cost function to prevent adaptations that represent undesirable movement of the control points. This is common practice in the image and point-set registration domain.

The classification algorithm that this work applies is amongst the most simplistic and commonly employed in data processing and automation literature. kNN classification is an effective and interpretable algorithm which provides a strong foundation for clinical adoption. This is an important characteristic of the selected algorithm since many classification models are capable of producing state-of-the-art results but lack interpretability. An additional advantage of using kNN classification stems from the fact that the method only contains a single hyper-parameter, k. Thus, the design process merely consists of selecting an appropriate distance function in conjunction with a data-driven value of k. In this work, a correlation based distance function was found to yield the best results when compared against: euclidean, cityblock, chebychev, minkowski, cosine and mahalanobis distances. The simple design process of a kNN makes it easily adaptable for the purpose of future datasets and improvements.

The results presented by the current framework are better than those obtained by methods which have utilized the same subset of the European ST-T Database and the same updated beat-by-beat annotations. The European ST-T is a standard database employed for the purpose of myocardial ischemia. Our work demonstrated better results in terms of both sensitivity and specificity compared to all previous comparable works (Papaloukas *et al.*, 2001, 2002b,a; Goletsis *et al.*, 2003, 2004; Exarchos *et al.*, 2006, 2007; Tsipouras *et al.*, 2007). Additionally, we evaluated our work in a subject-wise manner to provide a more representative estimate of the framework's performance. This has not been standard reporting procedure previously and was raised in a recent review of myocardial ischemia and myocardial infarction classification systems (Ansari *et al.*, 2017). It should be noted that our

work demonstrates a bias toward classifying ischemic beats when evaluated in a subject-wise manner. This is observable in the ROC curve, for the subject-wise case in Fig. 5.4, where a true positive rate is only attainable with a relatively high false positive rate ($\sim$20%); however, this trend does not continue and a high true positive rate can be achieved with only an incremental percentage change from the aforementioned false positive rate offset. Furthermore, there seems to be an element of variance between the validation set and test set sensitivity. This apparent decrease in performance occurs due to two reasons: (a) there is no leakage of data between the intra-channel training/validation and testing sets when ischemic classification methods are evaluated in a subject-wise manner, (b) the limited size of the training set consists of an insufficient set of sample data (limited variability) to guarantee generalization. However, it is important to note that a less severe form of data leakage still exists with our improved validation approach. This arises from the inter-channel leakage caused by employing data from different channels of the same patient across both the training and validation sets; that is, the two channels are derived from the same cardiac vector. Lastly, a more complex method for the validation (in a subject-wise manner) of the proposed framework, such as leave-one-out cross validation, was not employed due to the difficulty in generating a balanced split of the data between normal and ischemic beats across folds. This is an important limitation to note pertaining to the dataset employed for the evaluation of the current work and previously proposed methods. The development of an improved dataset addressing this limitation is of critical importance for future works and for widespread adoption of automated ischemic beat classification techniques.

The performance of the method can be improved in several ways. Firstly, more advanced QRS detection could be applied. Better performing and more robust methods have been employed since the release of the utilized algorithm (Tompkins and Afonso, 1993). The QRS-detection system used was employed to provide a fair comparison with the previously proposed algorithms; thus, serving to limit the amount of design variability in the classification process. Secondly, modern ECG recorders could be employed for the recording of the data with a higher sampling rate. Modern recorders produce less noisy signals with higher resolution. Additionally, the method could be adapted to consider additional arrythmias and cardiac conditions. Algorithmically, an improved template generation method could be utilized which includes beat-by-beat alignment before averaging, as observed in Schmidt *et al.* (2014, 2018b). Lastly, the incorporation of clinical information containing patient health history and lifestyle characteristics could be included as input features to the model.

5.5   Conclusion

We introduced a novel technique for the detection of ischemic cardiac beats in the ECG. The approach utilized a correspondence based template adaptation method for feature extraction combined with a kNN classifier. The application of a correspondence based matrix technique for the extraction of complex morphological features proved to be a successful approach. The interpretable nature of the framework may make clinical adoption easier.

The proposed method discriminated between ischemic and normal cardiac sequences at a greater rate than previously proposed works. This suggests that the proposed method has potential to be applied in a clinical setting or modern monitoring systems, e.g. wearables. Although, the method produced state-of-the-art results, further testing and evaluation is needed on modern recording devices and across a large clinical study where more robust cross-validation techniques can be employed.

Acknowledgment

A Long Short-Term Memory Network to Classify Myocardial Infarction Using Vectorcardiographic Ventricular Depolarization and Repolarization

The content of this chapter is a modified version of the publication:

Karisik, F. and Baumert. M (2019), 'A Long Short-Term Memory Network to Classify Myocardial Infarction Using Vectorcardiographic Ventricular Depolarization and Repolarization', *2019 Computing in Cardiology (CinC)*, pp. 1–4.

6

Abstract

QT interval variability has indicated diagnostic and prognostic value in myocardial infarction. Furthermore, research has suggested that vectorcardiogram has superior diagnostic capabilities compared to electrocardiogram in myocardial infarction. In this study, vectorcardiographic ventricular depolarization and repolarization were utilized to discriminate myocardial infarction patients from control subjects. In summary, 147 vectorcardiogram recordings (78 MI vs. 69 Control) were assessed. For each recording, sixty beats were extracted using the 2DSW algorithm. An inhomogeneous three-dimensional template adaptation scheme was applied across each QRS-loop and T-loop, respectively, to capture subtle morphological changes between cardiac cycles. Training was performed on a regularized two-layer long short-term memory network. The framework yielded classification results against test set data with an overall 93.2% accuracy, 91.7% sensitivity and 95.5% specificity. In conclusion, the use of template adapted VCG and a recurrent neural network has demonstrated promising results in MI classification.

6.1   Introduction

Myocardial infarction (MI) is a cardiac event in which the myocardium is deprived of sufficient blood supply, resulting in irreversible damage. MI has been linked to a plethora of cardiac conditions including tachycardia and sudden cardiac death (SCD) (Bhar-Amato *et al.*, 2017); thus, highlighting the broader health implications of MI. Traditionally, MI has been assessed analyzing the standard 12-lead electrocardiogram (ECG). However, research has suggested that vectorcardiogram (VCG) holds superior diagnostic value in MI diagnosis (Pérez Riera *et al.*, 2007; Chou, 1986). The primary advantage of VCG is that phasic changes are more clearly identifiable (Chou, 1986).

Recent investigations have reported that increased beat-to-beat QT variability (QTV) contains information related to sudden cardiac death and other diseases (Baumert *et al.*, 2016a). Robust measurement of QTV requires the detection of the QRS onset and T-wave offset. Due to subtle morphological changes across cardiac cycles and low wave amplitude, the detection of the T-wave offset is a difficult task. However, recent template

adaptation techniques have demonstrated significant improvements in QTV measurement (Schmidt *et al.*, 2014, 2018a). Resultantly, the inclusion of the entire T-wave in analysis of ventricular depolarization and repolarization has been recommended (Baumert *et al.*, 2016a). Furthermore, template adaptation techniques have been recommended for QTV analysis. Although template adaptation techniques have demonstrated state-of-the-art performance across ECG applications (Baumert *et al.*, 2012; Starc and Schlegel, 2006), little emphasis has been placed on VCG. Thus, we employ a recently proposed three-dimensional template adaptation technique for pre-processing VCG. The adapted cardiac data are fed into a long short-term memory (LSTM) network for classification. Therefore, in this work we aim to incorporate both the reported advantages of VCG in MI and, template adaptation in QTV measurement for the classification of MI.

Previous machine learning literature has focused on utilizing various combinations of the 12-lead ECG to discriminate between MI patients and healthy subjects. Furthermore, existing efforts have employed a series of machine learning and deep learning methods to perform classification. A brief overview of the proposed techniques that have employed robust system validation against the PTB database via hold-out or K-fold methods is provided. Several ECG based techniques have been proposed. Acharya *et al.* (2017) reported the use of a convolutional neural network (CCN) on a single beat for each patient. Zhou *et al.* (2011) proposed feeding a support vector machine polynomial for approximating coefficients of the ST segment. Further investigation by Arif *et al.* (2012) described a K-nearest neighbour classifier utilizing time domain features, namely: T-wave amplitude, ST segment deviation and Q-wave amplitude. In Sharma *et al.* (2015), the authors introduced a multiscale energy and eigenspace approach for the discrimination of MI and control subjects. Similarly, existing methods have employed VCG based methods. Yang (2011) proposed the use of multiscale recurrence quantification across linear discriminant analysis, quadratic discriminant analysis and kNN. Further investigation by the same group proposed the use of VCG and logistic regression (Yang *et al.*, 2013). The aforementioned works have produced state-of-the-art results, however, have neglected to consider long-term dependencies via the use of recurrent neural networks. The performance of the prior algorithms is provided in the Results section of this study.

6.2   Methodology

In this section, we briefly describe the proposed classification framework. The described method employs template adaptation for the pre-processing of data and an LSTM network

for the classification component. VCG data extraction is performed via two-dimensional signal warping (Schmidt *et al.*, 2014). Similarly, for both the QRS complex and T-wave, template VCG loop alignment is performed via inhomogeneous template adaptation. The beat-to-beat template data are processed as raw inputs by an RNN. Classification is performed using a standard LSTM framework. The classifier employs a softmax activation function combined with a cross-entropy loss function.

6.2.1 Template Adaptation

Procrustes analysis is a statistical shape alignment technique employed to globally match spatial data. In this work, we utilize Procrustes analysis to globally rotate and translate the reference template, Y_r, to the target data, Y_t. An independent Procrustes analysis is performed on each VCG lead to account for varying temporal-shifts across different projections of the same cardiac cycle. Mathematically, the optimal rotation (R) and translation (T) can be obtained by minimizing the below equation using linear least squares:

$$Y_g = R(Y_r) + T. \tag{6.1}$$

Next, the three-lead globally adapted VCG template, Y_g, is parameterized. Free-from deformation is a computer graphics technique utilized to parameterize three-dimensional data to a lattice of control points. In this work, for each cardiac cycle we parameterize the globally adapted template to the minimum bounding rectangular prism containing the template and the target data. For a given sample, Y_g^a, the three-dimensional point can be parameterized to control point, P_{ijk}, by the following:

$$x_{ijk} = \sum_{i=0}^{l} \binom{l}{i}(1-s)^{l-i}s^i \times \sum_{j=0}^{m} \binom{m}{j}(1-t)^{m-j}t^j \times \sum_{k=0}^{n} \binom{n}{k}(1-u)^{n-k}u^k, \tag{6.2}$$

where s, t and u denote the embedding rectangular prism localized coordinate system. In the interest of conciseness, we do not expand on how to obtain the value of s, t and u for each three-dimensional sample, instead we refer the reader to the original works by Sederberg and Parry (1986). Parameterizing each three-dimensional sample of Y_g to the control point lattice yields a matrix of FFD weights, X. Mathematically, the parameterization can be expressed as:

$$Y_g = XV, \tag{6.3}$$

where V denotes an 8×3 matrix of the control point coordinates. To obtain a locally adapted template, Y_f, a linear least squares optimization can be performed across the embedding control points:

$$Y_f = (X^T X)^{-1} X^T Y_t. \tag{6.4}$$

Subsequently, the template adaptation is described by:

$$Y_f = X V_f, \tag{6.5}$$

where V_f denotes the optimal control point locations. However, such a formulation is unable to robustly capture subtle non-linearities in morphology, thus, the simple linear least squares regression is extended to a kernel ridge regression (KRR). In the kernelized non-parametric extension of the linear least squares solution, the described inhomogeneous template adaptation technique becomes:

$$f^*(Y_t, \Lambda) = K(K + c_1 \Lambda)^{-1} Y_t, \tag{6.6}$$

where K represents the kernelized FFD weights matrix and Λ the noise estimation regularization matrix, respectively. The kernel function applied to the FFD weights matrix X is the Gaussian kernel:

$$k(x, x') = exp(\frac{|x - x'|^2}{2\sigma^2}), \tag{6.7}$$

where σ denotes the kernel width. The kernel width determines the length of the wiggles in the Gaussian kernel function. Lastly, the noise estimation model used in this technique is based on a simple differentiator model:

$$\Lambda_a = Y_{t_a} - Y_{t_{a-1}}, \tag{6.8}$$

where Λ_a denotes the ath diagonal entry in the $N \times N$ regularization matrix and Y_{t_a} the ath sample of the current VCG cycle, respectively. The regularization term is a square diagonal matrix containing the estimated lambda values. A differentiator noise model is employed to capture outliers in the data, which for the case of VCG can significantly differ between samples. This concludes the three-dimensional template adaptation description. In the ensuing section the employed RNN is described.

6.2.2 Classification

LSTM

In this work, we propose the use of a LSTM network to discriminate between myocardial infarction patients and control subjects. LSTM networks belong to the recurrent neural network family and were developed to overcome two key limitations of traditional RNN networks - the vanishing gradient problem and the long-term dependency problem (Hochreiter and Schmidhuber, 1997). RNNs are networks with a feedback mechanism, which allow for information to persist (Olah, 2015). This inherent ability to retain information across multiple time-steps makes RNNs a powerful tool in time-series classification problems. A brief overview of an LSTM layer is provided based on Fig. 6.1.
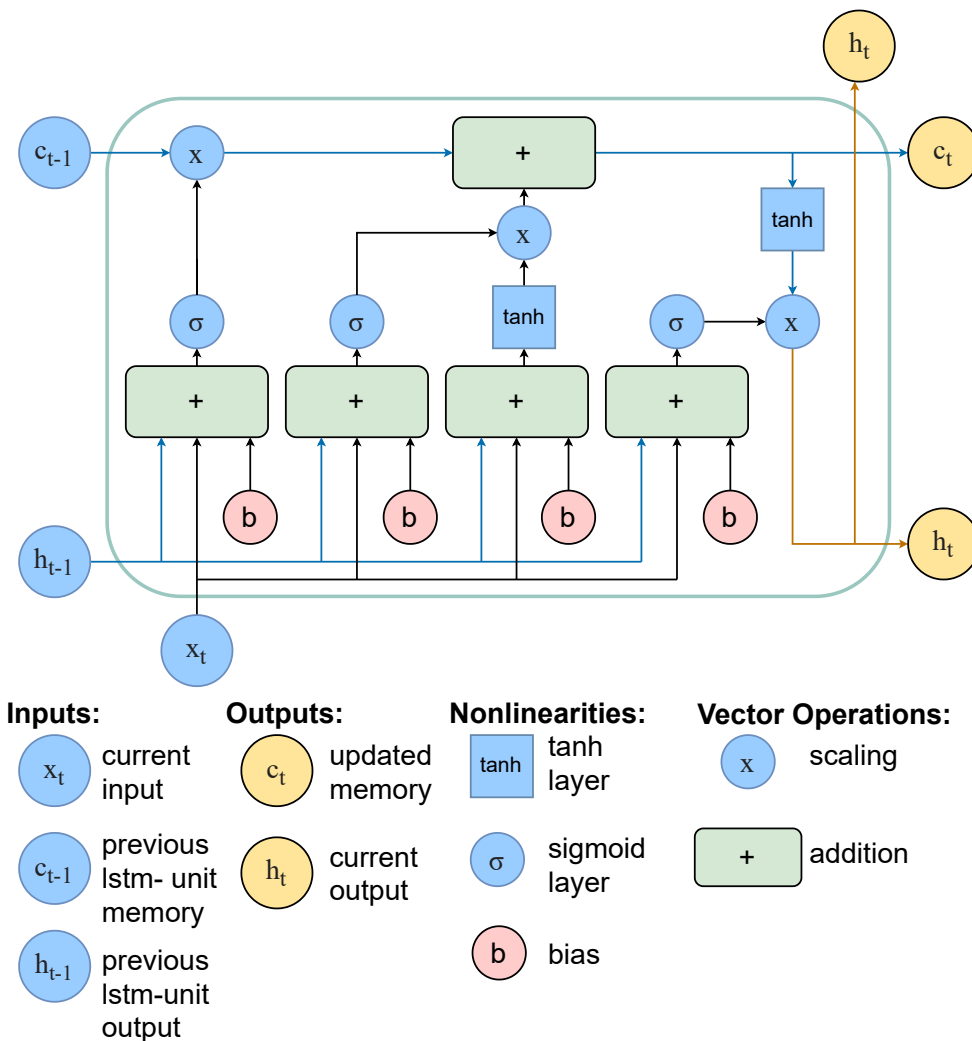
Figure 6.1. LSTM flow diagram.

The primary component of an LSTM is the cell state, denoted by the uppermost horizontal line in Fig. 6.1. Information flows directly across the cell state chain, passing through two linear manipulations (Olah, 2015). As such, LSTMs are able to add or remove information to the cell state, c_{t-1}, which is regulated by the network gates (Hochreiter and Schmidhuber, 1997). Gates consist of a standard sigmoid layer combined with a pointwise multiplication operation. Each gate outputs a value between zero and one, thus controlling the amount of information to be transferred for the corresponding component (Olah, 2015). In Fig. 6.1, the leftmost sigmoid layer determines what information to discard from the cell state by incorporating information from the current time step, x_t, and the previous hidden state, h_{t-1}. A result of 1 instructs the system to retain all information in the cell state and a value of 0 to discard all information, respectively (Olah, 2015). The next step is a two-fold process which determines what new information to store in the cell state. Firstly, the centre sigmoid layer identifies which values to update, whilst the leftmost tanh layer outputs a vector of new candidate values. The vector multiplication of these two layers determines the amount of new information to capture (Olah, 2015). Next, the cell state is updated to forget information previously deemed to be unnecessary. Updated information is incorporated via vector addition. Lastly, the neural network output is determined by a two-step process. A sigmoid layer decides what part of the cell to output; whilst, a tanh clamping operation is performed on the cell state and multiplied by the output of the rightmost sigmoid gate. Thus, only information that is determined relevant is output as h_t.

Network Architecture

Table 6.1 describes the implemented network architecture. The input to the network consists of a 3-dimensional matrix containing sixty beats for each VCG recording. The classification architecture contains two LSTM layers, one dropout layer and one fully-connected layer. The dropout layer serves as a regularization term in the network to prevent overfitting. Dropout regularization excludes a percentage of terms for each update in the backpropagation step of training the network. A constant dropout rate of 5% was used in this work. The output layers consist of the standard softmax activation function combined with a cross-entropy loss function. The softmax activation function is commonly employed in literature as it produces probabilities pertaining to each class, from which the maximum estimated probability can be selected to produce the final prediction. Similarly, cross-entropy is primarily employed in classification tasks as it has demonstrated superior performance (Goodfellow *et al.*, 2016). Network design selections can be observed in Table 6.2.

Table 6.1. Network architecture.

Layer	Layer Type	Size
1	VCG Inputs	3×time steps
2	LSTM	2
3	LSTM	28
4	Dropout	28
5	Fully-Connected	28
6	Outputs	2

Table 6.2. Network design selections.

Design Selection	Value
Learning Rate	0.075
L2 Regularization	0.000001
Optimizer	Adam

6.3 Results

The performance of the proposed method was statistically evaluated using accuracy, sensitivity and specificity measures. Based on the proposed classification architecture, the system achieved 93.2% accuracy, 91.7% sensitivity and 95.5% specificity. A 5-fold cross-validation was employed to evaluate the network with an 70/30 percent split between the model selection and independent test data. Table 6.3 illustrates the performance of the proposed method relative to existing classification techniques employing a robust validation approach (hold-out of K-fold). The confusion matrix across the test set data can be observed in Table 6.4. Additionally, the receiver operating characteristic curve with the optimal operating point is depicted in Fig. 6.2.
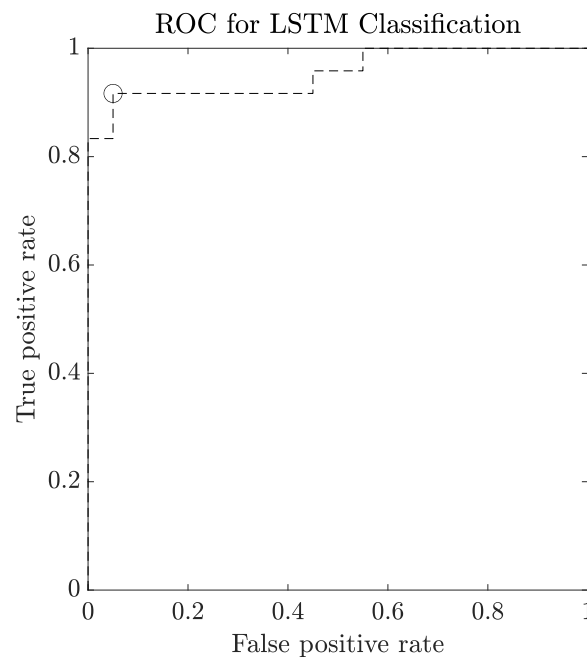
Figure 6.2. ROC curve for the proposed classification framework with the optimal operating point highlighted (circle).

Table 6.3. Performance comparison of current method against existing techniques.

Author	Sensitivity	Specificity
Acharya *et al.* (2017)	95.5%	94.2%
Zhou *et al.* (2011)	98.7%	96.6%
Arif *et al.* (2012)	99.6%	99.1%
Sharma *et al.* (2015)	93.0%	99.0%
Yang (2011)	96.5%	75.0%
(Yang *et al.*, 2013)	86.8%	92.5%
Current Method	91.7%	95.5%

Table 6.4. Confusion matrix across PTB database test set.

		Predicted		
		MI	**C**	**sum**
True	**MI**	20 (45.50%)	2 (4.55%)	22
	C	1 (2.27%)	21 (47.73%)	22
	sum	21	23	44

6.4 Discussion

Classification of myocardial infarction patients is an important task for healthcare monitoring. The current study investigates this task by providing an end-to-end classification system capable of capturing dynamic changes in VCG. Our work focuses on pre-processing data by template adaptation, in an effort to accurately capture morphological changes between cardiac cycles. This provides a benefit over traditional signal processing techniques, such as Fourier filtering, as template adaptation attempts to preserve morphology amongst noise. Additionally, two-dimensional signal warping, a state-of-the-art delineation method for ECG is employed. This technique provides robust extraction of both the QRS-complex and T-wave. By employing an accurate ECG delineation technique, the onset and offset of VCG loops can be robustly extracted; thus, minimising the effect of noisy isoelectric line samples being included in the three-dimensional template adaptation step.

Existing literature has neglected to evaluate the performance of LSTM networks in myocardial infarction classification. LSTMs are a natural application for studying dynamic changes in biomedical signals as they are capable of capturing long term dependencies between time steps. This is particularly important in ECG analysis as beat-to-beat variability has been demonstrated to contain important diagnostic information. Thus, in classification applications for ECG and VCG, the employment of RNNs is a sensible choice due to the complex interrelations manifesting across serial recordings. Observing Table 6.3 and Table 6.4, promising results have been reported across this study. The performance of the proposed framework is comparable to several state-of-the art algorithms which have previously employed an appropriate validation scheme against the PTB database (Acharya *et al.*, 2017; Zhou *et al.*, 2011; Arif *et al.*, 2012; Yang, 2011; Sharma *et al.*, 2015). Compared to the

first VCG study employing the same database (Yang, 2011), the proposed network demonstrated improved specificity (95.5% vs 75.0%) and slightly reduced sensitivity (91.7% vs 96.5%). Similarly, the performance of the proposed method indicated a comparable but improved performance (sensitivity-91.7%, specificity-95.5% vs sensitivity-86.8%, specificity-92.5%) relative to a study employing logistic regression (Yang *et al.*, 2013). Thus, suggesting that a balanced and high performance classifier can be attained via VCG classification. Furthermore, relative to the remaining studies (12-lead ECG) in Table 6.3, the proposed framework demonstrated lower, but comparable, sensitivity. Additionally, the specificity of the proposed framework was comparable to most ECG based methods and only marginally higher compared to one study (Acharya *et al.*, 2017). Although the preliminary results are promising, further hyper-parameter tuning is required to implement a more robust LSTM classifier. The necessity for robust hyper-parameter tuning via search methods is important as it permits the identification of an optimal network architecture within a discretely bounded domain.

Due to the relatively small number of recordings in the PTB database, the training and evaluation of the proposed classifier are inherently sensitive to incorrect classification. The performance of neural network methods vastly improves with a significant training set, and robust training practices. This is evident in our analysis as two misdiagnosed myocardial infarction patients across twenty-two total samples significantly impacted the sensitivity results. A large database of recordings would be required to adequately train and assess the performance of the current method and existing frameworks. Lastly, it is of interest to mention that due to the small size of the employed database and the number of studies undertaken across it, a form of data leakage exists. This occurs as each study is effectively attempting to produce improved results across overlapping test sets. This devalues the significance of the test set results as re-training of a model has occurred with the intent of improving test performance.

6.5   Conclusion

In this study, a diagnostic assessment of VCG ventricular depolarization and repolarization in MI patients was performed via machine learning. To account for complex beat-to-beat spatio-temporal behaviour of VCG data, a three-dimensional inhomgeneous template adaptation technique was employed. Discrimination of control subjects and MI patients was performed using an LSTM network. The results suggest that the proposed analysis of VCG

depolarization and repolarization may be a suitable method in MI patient diagnostics. Future analysis ought to look at extending training and validation with an increased complexity level in network architecture, via a grid search. Furthermore, training and testing should be performed across a large-scale database to evaluate the generalization of the proposed framework.

Evaluation of Ventricular Repolarization Variability in Patients With Nonischemic Dilated Cardiomyopathy

The content of this chapter is a modified version of the publication:

Schmidt, M., Karisik, F., Zausender, S., Linke, A., Malberg, H. and Baumert. M (2021), 'Evaluation of Ventricular Repolarization Variability in Patients With Nonischemic Dilated Cardiomyopathy From Vectorcardiography *2021 Computing in Cardiology (CinC)*, pp. 1–4.

7

Abstract

To investigate the predictive value of ventricular repolarization variability (VRV) in patients with nonischemic dilated cardiomyopathy (CM), we analyzed the Defibrillator in Non-Ischemic Cardiomyopathy Treatment Evaluation trial (DEF-INITE). The Telemetric and Holter ECG Warehouse (THEW) dataset, E-HOL-03-0401-017, contains 393 recordings from 236 patients. All patients had a left ventricular ejection fraction $< 36\%$ and were randomized to receiving standard medical therapy with or without an ICD. 24h-Holter 3-lead (Frank lead system) ECGs were performed at enrolment and subsequently within a 5 year follow-up period. The all-cause mortality during the follow-up period was 4.8 %. We analyzed three-dimensional variability of the T-loop using inhomogeneous three-dimensional template adaptation. Similarly, single lead analysis was performed by employing two-dimensional signal warping. To assess the predictive value of the proposed VRV parameters, Kaplan-Meier survival curves of baseline Holter ECGs were calculated. Our results demonstrated a significant association to survival ($P < 0.01$ by the log-rank test) for the T wave amplitude corrected QT interval variability index ($cQTV_i$). The low $cQTV_i$ group showed no mortality for the entire observation period. We found no associations between $cQTV_i$ groups and patient-specific parameters. Based on the Kaplan-Meier results, an extended survival analysis was performed using the Cox proportional hazards model. However, statistical significance was not observed. This can likely be attributed to the small study-size and breach of the proportional hazards assumption across input variables.

7.1   Introduction

Non-ischemic cardiomyopathy describes a broad set of diseases of the myocardium related to mechanical and/or electrical dysfunction, excluding those caused by ischemic factors, such as: myocardial ischemia and myocardial infarction (Bluemke, 2010). Research of static variables has previously been employed to study ischemic and non-ischemic CM. Markers such as fragmented QRS have indicated significant prognostic capabilities in patients who receive an ICD for primary or secondary prevention of SCD (Das *et al.*, 2010).

Additional works by Cho *et al.* (2021) found that inferior fragmented QRS may be predictive of ventricular arrythmias in patients with non-ischemic CM. Similarly, studies evaluating CM cohorts using ventricular lability have received some attention. Berger *et al.* (1997) evaluated QTV_i across a database of 83 dilated CM patients and 60 control subjects. The authors found that dilated CM is linked to an increased QT interval variability compared to normal subjects in both ischemic and non-ischemic patients (CM - 60.4$\pm$63.1 versus healthy - 25.7$\pm$24.8 ms^2); concluding that dilated CM leads to temporal lability in ventricular repolarisation. Further works have evaluated low-risk patients with non-ischemic dilated CM. The authors concluded that patients with non-ischemic CM and preserved HRV have an excellent prognosis and thus may not necessarily require ICD therapy (Rashba *et al.*, 2006). Furthermore, ventricular repolarization variability (VRV) has demonstrated predictive value for mortality in patients with ischemic heart disease (El-Hamad *et al.*, 2020), where the mode of death is likely malignant ventricular arrhythmia (Baumert *et al.*, 2016a). However, the potential for risk stratification in patients with nonischemic cardiomyopathy requires further investigation (Baumert *et al.*, 2016a).

QT interval variations of the surface electrocardiogram (ECG) reflect beat-to-beat fluctuations of ventricular repolarization. Previous studies have shown temporal VRV, as indicated by an increased QT interval variability (QTV), is associated with cardiac mortality (Baumert *et al.*, 2016a; Schmidt *et al.*, 2018b). However, measuring subtle beat-to-beat changes in QT interval remains challenging. Although novel QTV techniques have improved sensitivity and robustness (Baumert *et al.*, 2012; Schmidt *et al.*, 2014), conventional QTV measures still lack in insightful QTV description (Baumert *et al.*, 2016a). More recent techniques are able to capture VRV from vectorcardiography (VCG) (Karisik and Baumert, 2019) and thus offer new descriptive features for the characterization of ventricular repolarization. Thus, in this study we investigate the predictive value of VRV for all-cause mortality in patients with nonischemic dilated cardiomyopathy. We analyzed the Defibrillator in Non-Ischemic Cardiomyopathy Treatment Evaluation trial (DEFINITE) to evaluate: 1) the applicability of new methods to characterize VRV using the VCG and 2) to investigate the predictive value of VRV parameters for risk stratification of all-cause mortality.

7.2   Methodology

In this section we briefly describe the data and algorithmic frameworks employed for VRV assessment. Template adaptation methods are employed for all parameter extraction. For

detailed mathematical descriptions of the methods employed in this study, the reader is referred to Karisik and Baumert (2019); Schmidt *et al.* (2018a).

7.2.1 VRV Quantification

To quantify VRV, we analyzed three-dimensional variability of the T-loop using inhomogeneous three-dimensional template adaptation (Karisik and Baumert, 2019). Inhomogeneous three-dimensional template adaptation is performed via a global-to-local adaptation scheme. Templates of interest are first globally translated, scaled and rotated using Procrustes analysis. Subsequently, local adaptation is performed using a kernel ridge regression formulation to capture subtle morphological changes. To account for complex noise behaviour encountered in quasi-periodic data, the framework employs an adaptive noise model. VRV was evaluated across the T-loop using two parameters: 1) mean-loop-length (MLL) and 2) distance variability (DV). MLL is calculated as the sum of the distances between adjacent points for a given loop. DV contains the set of Euclidean distances between corresponding samples of the template loop and the adapted template loop.

Similarly, single-lead QTV measurement was performed by the iterative two-dimensional signal warping method (i2DSW) (Schmidt *et al.*, 2014, 2018a). Analysis was undertaken on the bipolar Z lead (pseudo-orthogonal) because it inherently contains a high T wave amplitude, thus maximizing the signal-to-noise ratio (Schmidt *et al.*, 2016). i2DSW was employed to account for subtle inhomogeneous shape variations of the ECG waveform across time and amplitude (Schmidt *et al.*, 2014, 2018a). The algorithm automatically generates a template beat with common features of interest (e.g. the PQ, QRS or QT intervals and amplitude related information) based on ensemble averaging of selected beats. To adapt the template, a 2D mesh of warping points are superimposed on the data. Subsequently, warping points are shifted across both time and amplitude to minimize a Euclidean cost function between the template and target data, resulting in the adapted template. The adapted template contains temporal and spatial information pertaining to annotated points of interest; in this work, the QT interval and T wave amplitude were considered. An automatic beat rejection proposed by (Schmidt *et al.*, 2014) was applied to exclude noisy cardiac cycles. Standard QTV parameters were employed, namely: standard deviation of QT intervals (SDQT) and QT interval variability index (QTV_i) (Berger *et al.*, 1997). To account for the inverse relationship between QTV and the T wave amplitude, we calculated the T wave amplitude-corrected QTV measures of SDQT (cSDQT) and QTV_i ($cQTV_i$). All parameters

Table 7.1. Characteristics of DEFINITE patients (THEW data) at baseline. Percentages are in normal brackets and ranges are in square brackets. Left ventricular ejection fraction (LVEF) and New York Heart Association (NYHA) classifications are included.

		Therapy	
Characteristic		Standard	ICD
Patients		103 (44 %)	132 (56 %)
Sex	male	70 (30 %)	98 (42 %)
	female	33 (14 %)	34 (14 %)
Age, yr	mean	58.0 [22-80]	58.3 [26-82]
NYHA	I	25 (11 %)	41 (17 %)
	II	56 (24 %)	70 (30 %)
	III	22 (9 %)	21 (9 %)
LVEF, %	mean	21.8 [10-36]	20.6 [9-35]

were calculated from five minute epochs throughout the 24-h Holter ECGs. To characterize daily VRV we calculated the median, maximum quantile (highest 95 %) and minimum quantile (lowest 5 %).

7.2.2 Data

The Telemetric and Holter ECG Warehouse (THEW) dataset, E-HOL-03-0401-017, was employed for analysis in this study (Couderc *et al.*, 2007). This dataset contains 393 recordings from 236 patients of the DEFINITE study (67 women, age: 60 ± 14 years; 168 men, age: 58 ± 12 years; 1 record not specified). All patients had a left ventricular ejection fraction $< 36\%$ and were randomized to receiving standard medical therapy with or without an ICD (see Tab. 7.1). 24h-Holter 3-lead (Frank lead system) ECGs were performed at enrolment and within a 5-year follow-up period. The data were sampled at 500 Hz and an amplitude resolution of 1 μV (Rashba *et al.*, 2006); the all-cause mortality during the follow-up period was 4.8%.

7.3 Results

To assess the predictive value of VRV parameters, Kaplan-Meier survival curves of baseline Holter ECGs were obtained for the trichotomized median, min and max of SDQT, QTV_i, cS-DQT, $cQTV_i$, MLL_T, DV_{mean}, and DV_{sd}. Significant parameters were further investigated for their correlations with patient-specific characteristics to show their independent value. Additionally, Spearman's correlation analysis was performed to provide a clearer understanding of the relationships between the analyzed parameters. Lastly, to evaluate the multivariate

predictive potential of significant VRV parameters, the Cox proportional hazards model was employed. To assess the validity of the model, the proportional hazards assumption was tested across input variables.
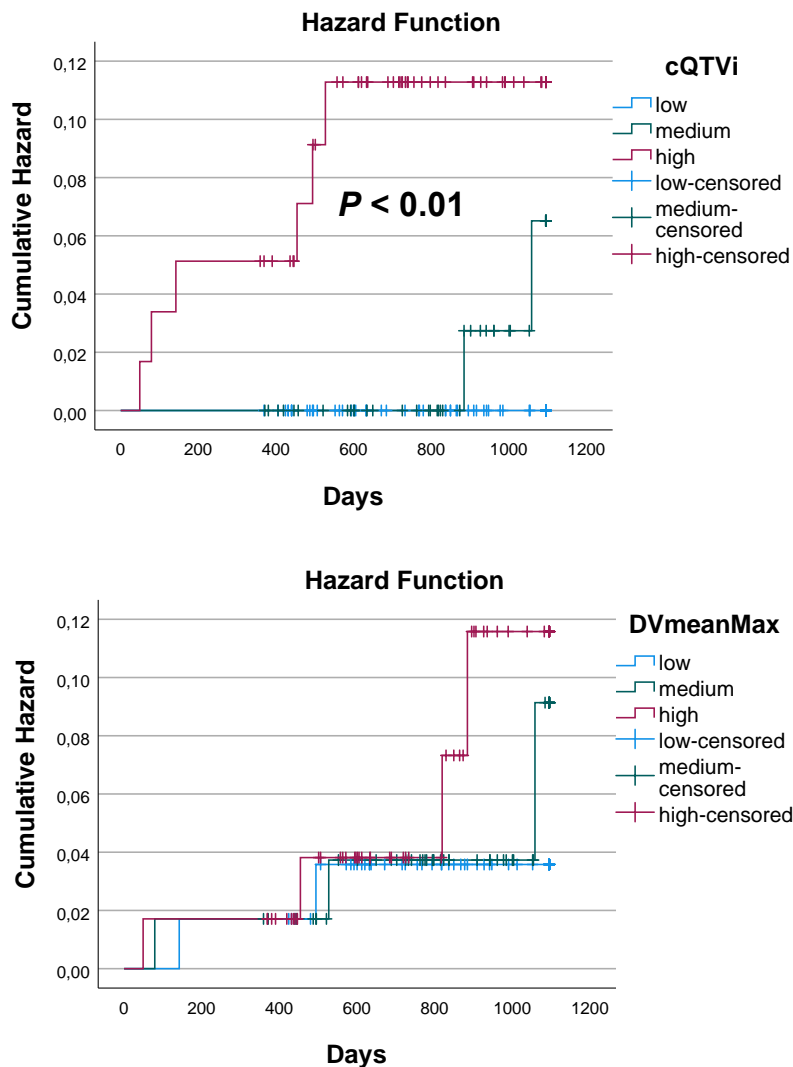
Figure 7.1. Hazard functions of Kaplan–Meier survival analysis; estimated hazard of DEFINITE patients for trichotomized $cQTV_i$ (left) and trichotomized $DV_{mean}Max$ (right). The last observations of a patient are marked in the curves with a cross (censored data).

Kaplan-Meier survival analysis shows significant association between survival and $cQTV_i$ ($P < 0.01$ by the log-rank test; Fig. 7.1). At year one, the mortality was zero in the low and the medium $cQTV_i$ group and 5.0 % in the group with high $cQTV_i$. After 2 years, it was 0.0 % in the low and the medium $cQTV_i$ group and 10.7 % in the group with high $cQTV_i$. At the end of survival estimation (after 3 years) $cQTV_i$ was 0.0 % in the low $cQTV_i$ group, 6.3 % in the medium $cQTV_i$ group and 10.7 % in the group with high $cQTV_i$. No further prediction parameters were found to achieve statistical significance. However, a similar qualitative

Table 7.2. Patient characteristics according to trichotomized $cQTV_i$ for sex, age, therapy, NYHA class, and LVEF at baseline. Ranges are shown in square brackets.

| | | | $cQTV_i$ | |
		low	medium	high
Sex	male	41	44	46
	female	18	15	15
Age, yr	mean	56.8	60.8	57.4
		[26-82]	[27-80]	[22-81]
Therapy	Standard	23	27	29
	ICD	36	32	31
NYHA	I	18	14	16
	II	32	33	32
	III	9	12	12
LVEF, %	mean	20.8	22.0	20.0
		[10-34]	[10-35]	[9-34]
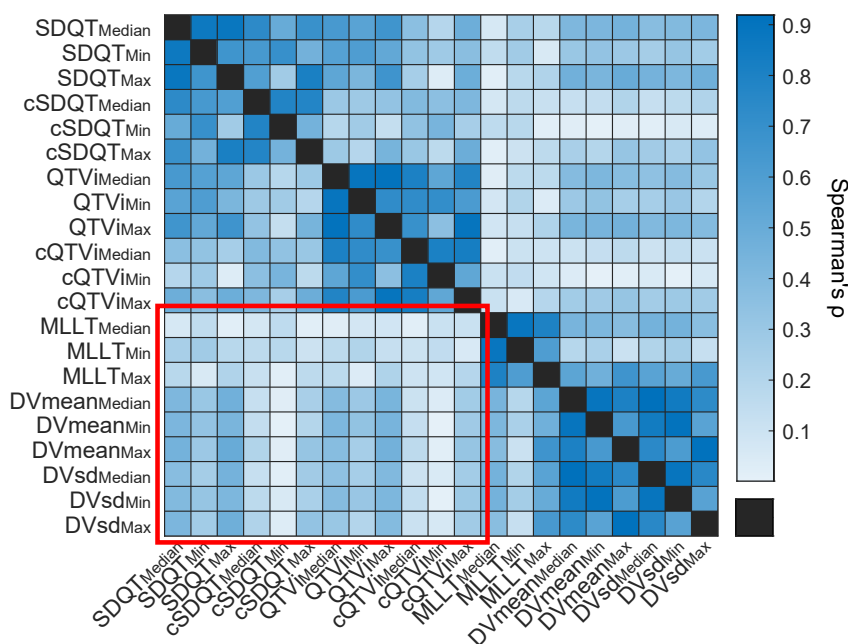
Figure 7.2. Correlation analysis between single lead ECG (SDQT, cSDQT, QTV_i, $cQTV_i$) and VCG (MLL_T, DV_{mean}, DV_{sd}) VRV parameters (highlighted in red). Absolute values of Spearman's ρ are shown.

trend was observed in QTV_i and the maximum of DV_{mean}. Table 7.2 shows the patient-specific characteristics of the trichotomized $cQTV_i$. No statistically significant differences were found between $cQTV_i$ groups with respect to sex, age, therapy, NYHA class, and LVEF. Correlation analysis results between the studied parameters can be observed in Fig. 7.2. A moderate relationship ($|\rho| > 0.3$) is observable between DV_{mean} and DV_{sd} (median, min and max) with SDQT and QTV_i (median and max). The largest observed correlation

Table 7.3. Likelihood ratio test values for Cox model.

Variable	Sex	Therapy	Age	cQTV$_i$	LVEF	NYHA
P	0.518	0.789	0.168	0.986	0.979	0.444
					$\dfrac{\text{global}}{P}$	0.812

($|\rho| > 0.5$) is between SDQT (max) and DV$_{\text{mean}}$ (max). Additionally, it is worth noting that the relationship between the VCG parameters and the single channel parameters are reduced after T wave amplitude correction.

Multivariate analysis of survival was performed using the Cox proportional hazards model to further assess the predictive value of cQTV$_i$. The survival probability curve can be observed in Fig. 7.3. Cox regression was performed by including sex, age, therapy, NYHA, LVEF and cQTV$_i$ as input parameters. However, using the likelihood ratio test, statistical significance was not observed ($P = 0.812$). Furthermore, statistical significance was not observed for any single parameter using Cox-regression. The statistical significance results for Cox regression can be observed in Table 7.3. The proportional hazards assumption for each covariate included in the Cox regression model was assessed using scaled Schoenfeld residuals to test for independence between residuals and time. Statistical significance was not observed for sex, therapy, age and NYHA. Conversely, cQTV$_i$ and LVEF were found to be statistically significant, thus, suggesting a breach of the proportional hazards assumption (see Fig. 7.4).
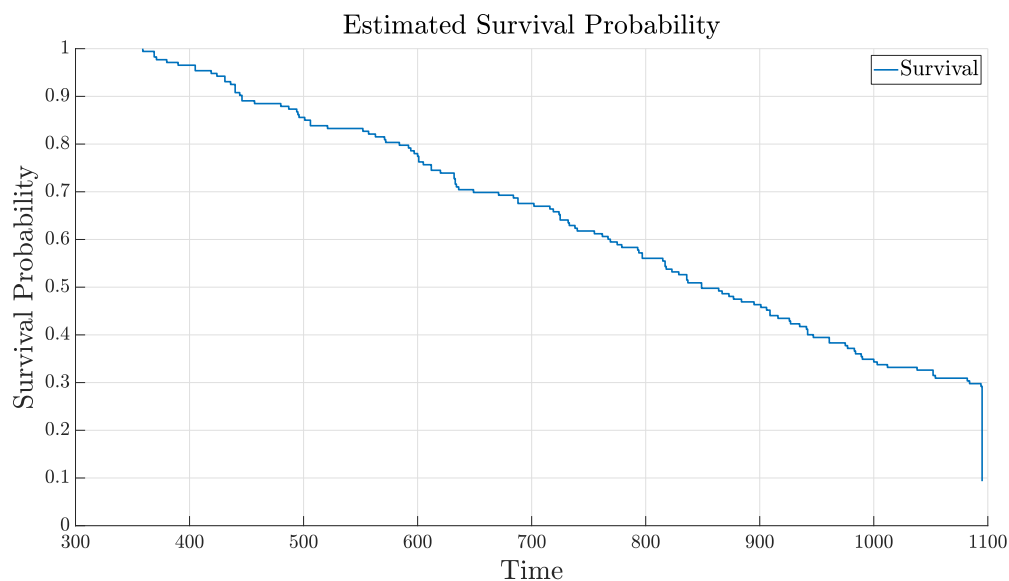
Figure 7.3. Hazard function of Cox model survival analysis with input parameters sex, therapy, age, cQTV$_i$, LVEF and NYHA.
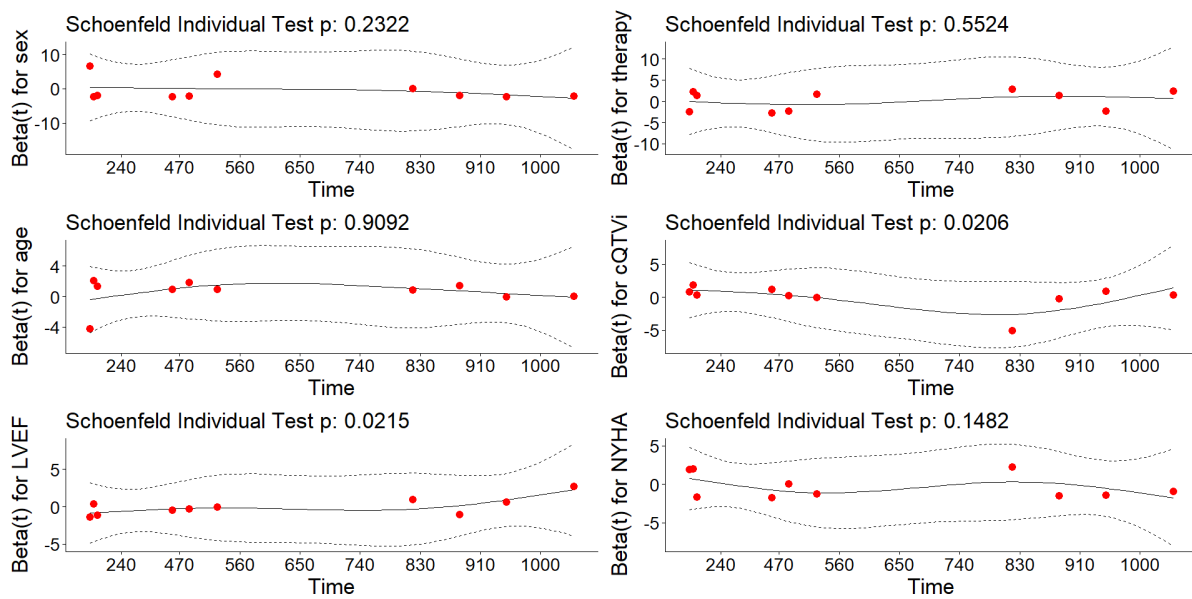
Figure 7.4. Schoenfeld residual curves for input parameters to Cox model. $P < 0.05$ provides evidence suggesting that the proportional hazards assumption has not been met.

7.4   Discussion

The present study provides an analysis of the predictive value of VRV in non-ischemic cardiomyopathy. Quantification was performed using robust template adaptation methods for VCG and single-lead ECG. The current work explored the use of dynamic geometric features in three-dimensional ECG for risk stratification. Qualitative analysis demonstrated similar predictive potential to $cQTV_i$ for the maximum of the DV_{mean}, however, statistical significance was not observed. Thus, a more comprehensive study with a larger number of end-points would be required to robustly assess the potential of geometric three-dimensional features in survival analysis.

In the single-lead analysis statistical significance was observed for $cQTV_i$ ($P < 0.01$ by the log-rank test). This result aligns with earlier works by Berger *et al.* (1997), wherein the authors reported an increased QT interval variability for non-ishemic dilated CM patients relative to healthy subjects. In our Kaplan-Meier analysis, the low $cQTV_i$ group showed zero mortality for the entire observation period. Furthermore, no significant association was found between the $cQTV_i$ groups and patient-specific parameters; thus, providing support that this non-invasive prognostic parameter may provide additional information for risk estimation. In the low $cQTV_i$ group, 36 patients received an ICD implantation (see Tab. 7.2). Observing the survival analysis presented in this study, the risk mortality of the low $cQTV_i$

group was zero. Thus, providing preliminary evidence that implantation may provide additional risks for patients.

To assess the predictive ability of $cQTV_i$ in conjunction with patient characteristics, we employed the Cox proportional hazards model. Multivariate regression was performed with sex, age, therapy, $cQTV_i$, NYHA and LVEF as input parameters. The analysis did not yield statistical significance using the likelihood ratio test (globally: $P = 0.812$). The lack of statistical significance can likely be attributed in part to two reasons. Firstly, the proposed study is limited by the few end-points available. Secondly, results suggest that two out of the six input parameters do not meet the proportional hazards assumption, namely: $cQTV_i$ and LVEF. This breach of assumptions can quantitatively be observed in Fig. 7.4, where $cQTV_i$ and LVEF yielded Schoenfeld individual P value results below < 0.05. Furthermore, the global Schoenfeld P value was found to be statistically significant ($P < 0.05$), thus suggesting that the model does not meet the proportional hazards assumption. Qualitatively, this can be observed in in Fig. 7.4. Visual inspection of $cQTV_i$ residuals demonstrates a non-stationary relationship against time.

7.5   Conclusion

In this study, we used two techniques to quantify VRV. Analysis was performed across VCG and on a single derivative basis. Our initial Kaplan-Meier analysis provides some evidence that patients with non-ischemic cardiomyopathy and a high $cQTV_i$ have a significantly higher all-cause mortality relative to patients with low $cQTV_i$. However, multivariate survival analysis using the Cox model does not support this finding. This can likely be attributed to the small number of end-points observed in this database and a breach of the proportional hazards assumption. Further investigation ought to be undertaken across a more comprehensive database to decisively determine whether VRV can contribute to a treatment decision.

Acknowledgments

Conclusion

THIS chapter summarizes the conclusions of this dissertation and highlights the original contributions of each chapter. Additionally, potential future directions are discussed.

8

8.1   Conclusion and thesis summary

Previous works in the analysis of ventricular repolarisation and depolarisation lability have provided valuable insight and promising results. In particular, template adaptation methods have demonstrated state-of-the art performance. However, previous frameworks have neglected to evaluate the VCG as an inhomogeneous process and the ECG as a correspondence based registration process; thus, discarding a significant amount of morphological information in VCG and limiting the generalisation capabilities of deformations in ECG. Furthermore, analysis of cardiac diseases, namely - myocardial infarction, myocardial ischemia and non-ischemic CM, has largely neglected to employ such techniques to capture subtle beat-to-beat information. In this thesis, an inhomogeneous template adaptation technique for the analysis of VCG is proposed in conjunction with a probability-based system for ECG feature extraction. Moreover, these methods are extended for the analysis of the aforementioned cardiac conditions. Correspondence-based template adaptation was used to study myocardial infarction and myocardial ischemia in ECG. Similarly, three-dimensional template adaptation was used to study myocardial infarction and VRV in non-ischemic CM. Thus, the proposed systems present novel and highly accurate methods for the study of myocardial diseases.

Ventricular repolarisation lability is an area of great clinical interest as increased beat-to-beat variability has been observed in a variety of cardiac diseases. However, the process of manually inspecting markers is a laborious, expensive and biased process. In Chapter 3, a framework capable of capturing subtle beat-to-beat morphological variations in VCG via template adaptation is presented. The system combines data parametrisation via FFD with a computationally efficient kernel ridge regression formulation to obtain an optimal transformation for each beat. Additionally, the system employs accurate VCG loop extraction by incorporating state-of-the-art QRS and T-wave delineation (two-dimensional signal warping). The analysis adopts previously proposed geometric features for the evaluation of ventricular repolarisation lability. Against simulated data, the method demonstrated significantly higher accuracy across both varying morphology and SNR compared to standard methods. Similarly, in the assessment of myocardial infarction the method yielded improved performance compared to traditional VCG methods. Lastly, the adaptive nature of the method demonstrated qualitative capabilities in other biomedical applications (limb movement). Thus, the proposed method presents a novel, computationally efficient and accurate technique for the evaluation of three-dimensional quasi-periodic data.

The ECG is considered a quasi-periodic process between cycles, thus features can subtly deviate from their temporal location between beats. To further the modes of study for feature measurement in cardiac diseases via template adaptation, a novel correspondence-based technique was developed in Chapter 4. The proposed system employs an adapted form of registration for the delineation of common ECG features (e.g. - QT-interval). Correspondences are assumed to be non-binary and the data are mapped by a FFD parametrisation. By transforming the data as a mathematically smooth process and allowing non-binary correspondences between samples of the template and target data, temporal interpolation was permitted. Furthermore, by formulating the process as an iterative gradient-descent based method, varying degrees of signal morphology and variation can be captured. The framework demonstrated state-of-the-art performance across simulated data and annotated clinical data for measuring QTV. Furthermore, in QTV analysis of myocardial infarction the method confirmed an increased QTV in diseased patients compared to healthy subjects. Lastly, an extended analysis was performed against simulated PPG, where the proposed and unadjusted framework demonstrated superior performance in dicrotic notch measurement compared to a previously proposed method. Hence, the novel correspondence based template adaptation introduces an accurate and mathematically robust system for analysing ECG and PPG.

Myocardial ischemia is a highly-prevalent cardiac condition and a pre-cursor to various other diseases including myocardial infarction. Previous research efforts have proposed numerous promising ischemic beat detection systems. However, such works have either neglected to utilise an ischemic beat-specific set of annotations or valid cross-validation for their proposed frameworks. In this thesis, an interpretable and robust framework for the detection of ischemic beats in ECG is proposed. Appropriate cross-validation is performed via a hold-out method to provide an unbiased and more representative measure of algorithm performance against unseen data. The method employs the correspondence-based template adaptation method developed in Chapter 4 in conjunction with a kNN classifier. The selected classifier is amongst the most commonly used in machine learning literature and is highly interpretable. The proposed system demonstrated superior performance against the annotated database when evaluated in a beat-wise manner, and similarly when evaluated in a statistically robust subject-wise manner. Therefore, the introduced framework presents an interpretable and accurate method for the detection of ischemic beats.

In Chapter 6, a novel LSTM network for the detection of myocardial infarction is presented. The method utilises the three-dimensional template adaptation process described in Chapter 3 to perform beat-to-beat extraction and pre-processing of input VCG data. The framework showed promising results, approaching the performance of state-of-the-art classifiers, and is comparable to the few other works that have employed VCG. The inherent advantage of the classification scheme employed is that it utilises an LSTM network. This type of RNN is capable of capturing temporal relations across samples. Additionally, in Chapter 7 an analysis of VRV in non-ischemic patients was performed using $cQTV_i$ and geometric VCG features. The study presents some evidence, that ventricular repolarisation features of lability in VCG qualitatively illustrate predictive prowess using Kaplan-Meier survival analysis. However, multivariate survival analysis did not support these findings, thus, further investigation is required to establish VRV in risk stratification.

8.2 Future directions

Although computationally efficient and accurate, the developed three-dimensional system in Chapter 3 is dependent on temporal synchronisation by means of two-dimensional signal warping. To overcome this limitation, the morphological transformation of the proposed system could be reformulated as a three-dimensional correspondence-based system. Although this would come at a computational cost, due to the requirement for gradient-descent based optimisation, it would offer an independent solution. Additionally, the system was only evaluated against ventricular repolarisation (the T-loop) and thus future research should incorporate ventricular depolarisation (the QRS-loop). Furthermore, future works ought to consider employing the technique across larger datasets, for which ventricular repolarisation and depolarisation lability have not been exhaustively studied.

In Chapter 4, where a correspondence based template adaptation method is proposed, a key drawback of the method is that it requires template and target data to be of equal length. Thus, a pre-processing step is necessary where data are interpolated to the length of the template by stretching or shrinking. This could be addressed by introducing slack variables in the optimisation process. Furthermore, the system is semi-automated, for quality assurance purposes pertaining to template annotations in this thesis. However, in future research this could be automated using similar methods to (Schmidt *et al.*, 2014, 2018a). To attain finer resolution adaptations, a more complex regularisation scheme could be employed. This could draw from machine learning literature in the form of drop-out regularisation. Alternatively, a custom regularisation which penalises the displacement between

neighbouring samples could be employed; although this would come at a computational cost. Additionally, the use of AWGN is prone to producing optimistic results as it does not accurately reflect noise observed in ECG. Thus, a more comprehensive analysis of algorithm performance against improved noise sources should be performed. Lastly, validation of the proposed method ought to be extended across a large database containing extensive clinical annotations.

Chapter 5 introduced a robust and appropriately validated framework for myocardial ischemia. Although the reported results were promising, the specificity of the system would require improvement for clinical studies. Firstly, this could be refined by algorithmic improvements. A more complex classifier could be employed, however, this is a delicate balancing act with precision often coming at the cost of interpretability in machine learning. Secondly, if the current kNN classifier were to be maintained, a significantly larger training set would be beneficial. This would require the development or attainment of a large annotated database for ischemic beat detection. Furthermore, any such database ought to be annotated according to current best medical practice. It is worth noting, the annotated dataset employed in this work is outdated, as the definition of myocardial ischemia has been updated since its inception.

The proposed classification system in Chapter 6 presents the first work on LSTM networks in myocardial infarction analysis. From a pre-processing standpoint, the system utilises the three-dimensional template adaptation network proposed in this thesis, and could thus benefit from the aforementioned improvements from that end. From a classification standpoint, improvements could be made by training across a more complex network architecture, as the proposed method employed only three layers with a small number of LSTM cells in the first two layers. Additionally, in Chapter 7, where VRV is analysed in non-ischemic CM patients, a more comprehensive set of VCG features could be hand-crafted for the analysis of ventricular repolarisation lability. Additionally, dynamic ventricular depolarisation features could be included in future studies to provide a more detailed analysis. Lastly, due to the small number of end-points in the DEFINITE study, a larger database ought to be analysed to establish VRV metrics for risk stratification.

Appendix A

Beat-to-Beat Analysis of Vectorcardiogram by Inhomogeneous Template Adaptation

The content of this chapter is a modified version of the publication:

Karisik, F., Schmidt, M. and Baumert. M (2019), 'Beat-to-Beat Analysis of Vectorcardiogram by Inhomogeneous Template Adaptation', *2019 41st Annual International Conference of the IEEE Engineering in Medicine and Biology Society (EMBC)*, pp. 83–86.

Abstract

Increased QT interval variability in ECG has demonstrated value for the assessment of ventricular depolarization and repolarization lability. More recently, vectorcardiogram based analysis has shown similar promise. In this study, we describe an inhomogeneous template adaptation technique for vectorcardiogram using a global-to-local adaptation scheme. The proposed framework was employed across the PTB database to assess ventricular depolarization and repolarization lability in VCG. The results demonstrated statistical significance between control subjects and MI patients.

A.1   Introduction

The QT interval represents the sequence between the onset of the Q-wave and the offset of the T-wave in a cardiac cycle of the electrocardiogram (ECG). This segment of the ECG corresponds to the global ventricular depolarization and repolarization activity. Elevated beat-to-beat QT interval variability (QTV) has been observed in various cardiac diseases and sudden cardiac death (Baumert *et al.*, 2016a; Piccirillo *et al.*, 2007). Additionally, an elevated QTV has been linked to cardiac sympathetic activity (Baumert *et al.*, 2011b). Similarly, research has suggested the potential relationship between QTV with T-wave amplitude and morphology (Baumert *et al.*, 2016a; Hasan *et al.*, 2012b). Thus, QTV analysis has demonstrated important relationships.

The vectorcardiogram (VCG) represents cardiac electrical activity as a single dipole (Chou, 1986). The magnitude and orientation of the dipole are represented by a three-dimensional spatial vector. During sinus rhythm and in a structurally normal heart, the recorded magnitude and direction are represented by three-dimensional loops. VCG analysis holds an inherent advantage over conventional 12-lead ECG analysis because phasic changes are more clearly identifiable (Chou, 1986). Furthermore, clinically, VCG has been reported to provide improved diagnostic sensitivity in myocardial infarction patients (Pérez Riera *et al.*, 2007); however, beat-to-beat changes in VCG are not well understood.

Recently, dynamic VCG features have been assessed to study ventricular depolarization and repolarization lability in myocardial infarction (MI) patients (Hasan *et al.*, 2012a). Statistical analysis reported by Hasan *et al.* (2012a) established significance between control

subjects and MI patients, where, the authors employed homogeneous template adaptation to quantify variability. However, an important consideration in QT interval analysis is the detection of subtle inhomogeneous changes across time, which Hasan *et al.* (2012a) neglected to account for. Thus, in this work we aim to propose a method for the quantification of VCG lability using an inhomogeneous method.

Template adaptation methods have yielded state-of-the art performance in QTV measurement (Baumert *et al.*, 2012; Schmidt *et al.*, 2014, 2018a). Traditional ECG template adaptation methods rely on homogeneous shifting and stretching of data to minimize some objective function. By annotating template data, the QT interval can easily be obtained after the adaptation process. More recently, Schmidt *et al.* (2014) introduced a method for inhomogeneous adaptation of ECG. This method is able to account for complex morphological variations occurring beat-to-beat. Drawing from inhomogeneous template adaptation for ECG, we propose an inhomogeneous template adaptation for VCG. The proposed framework is applied across the PTB database to study differences between control subjects and MI patients using ventricular depolarization and repolarization lability. Adaptations of previously employed VCG features (Hasan *et al.*, 2012a) are employed to perform QT interval quantification. Subsequently, analysis is performed across the feature results to test for statistical significance between groups.

A.2 Methodology

In this section we describe the proposed approach for template adaptation of quasi-periodic three-dimensional data. The framework follows a global-to-local adaptation scheme. Data are first adapted globally using Procrustes analysis. Next, a local adaptation is performed using kernel ridge regression (KRR) with a simple noise model. The proposed framework flowchart can be observed in Fig. A.1.

A.2.1 Procrustes Analysis

Procrustes analysis is a statistical shape analysis technique used to homogeneously align data (Gower and Dijksterhuis, 2004). Global alignment consists of translation, rotation, scaling and reflection. In this work, we solely employ global translation and rotation via Procrustes analysis. Optimal global translation and rotation between the VCG template and a given VCG loop can be expressed as an optimization problem to obtain the rotation

Figure A.1. Flowchart of the proposed framework flowing from left to right.

component, R, and the translation component, T, in the below equation:

$$Y_g = R(Y_r) + T, \tag{A.1}$$

where Y_g denotes the globally adapted template and Y_r represents the original template.

A.2.2 Free-Form Deformation Parameterization

Free-form deformation (FFD) is a technique for deforming geometric data in a free-form manner (Sederberg and Parry, 1986). Data are embedded to a three-dimensional parallelepiped, defined by a lattice of control points, where each embedded data point is parameterized to the lattice. This process is employed to obtain a linear relationship between the embedded data points and control points. The relationship between any embedded data point x, and control point of the lattice P_{ijk}, can be obtained by evaluating the following

tri-variate Bernstein polynomial:

$$x_{ijk} = \sum_{i=0}^{l} \binom{l}{i}(1-s)^{l-i}s^i \times \sum_{j=0}^{m} \binom{m}{j}(1-t)^{m-j}t^j \times \sum_{k=0}^{n} \binom{n}{k}(1-u)^{n-k}u^k. \qquad \text{(A.2)}$$

The s, t and u values describe the given data sample in the lattice space. For brevity, we skip the description on how to obtain s, t and u. The mathematical description can be found in Sederberg and Parry (1986) with a pseudo-code implementation in Procházková (2017). By virtue of FFD, the globally-adapted template vectorcardiogram, Y_g (containing n samples), can be embedded by a parallelepiped of p control points in three-dimensions. Mathematically, this can be expressed by:

$$Y_g = XV, \qquad \text{(A.3)}$$

where X denotes the $n \times p$ weights matrix of the embedded samples, and V denotes the $p \times 3$ geometric coordinates of the control points. Now, imagine we wish to obtain a linear least squares (LLS) adaptation of the globally adapted template to a target beat, Y_t; that is, obtain the optimal location of the control points. This optimization can be described by:

$$V_f = (X^T X)^{-1} X^T V C G_t, \qquad \text{(A.4)}$$

such that,

$$Y_f = XV_f. \qquad \text{(A.5)}$$

Although pragmatic, this formulation is highly susceptible to outliers and, thus, incapable of robustly capturing subtle morphological changes. To address this limitation, we propose the use of a non-parametric model - kernel ridge regression.

A.2.3   Kernel Ridge Regression & Noise Estimation

Kernel ridge regression is a kernel-based extension of ridge regression. Ridge regression is a regularized variation of the standard LLS approximation. Thus, the inhomogeneous template adaptation step can be expressed as a KRR process:

$$f^*(Y_t, \Lambda) = K(K + c_1 \Lambda)^{-1} Y_t, \qquad \text{(A.6)}$$

where, c_1 denotes a scalar multiplying factor and $K = k(x, x')$ represents a kernel function with weight inputs, x, belonging to X_{ijk}. Under this formulation, the covariance matrix is

Figure A.2. An example of 15 raw (black) VCG T-loop cycles (left) and the corresponding adapted data (right) for an MI patient. Green denotes the original template and red the adapted template.
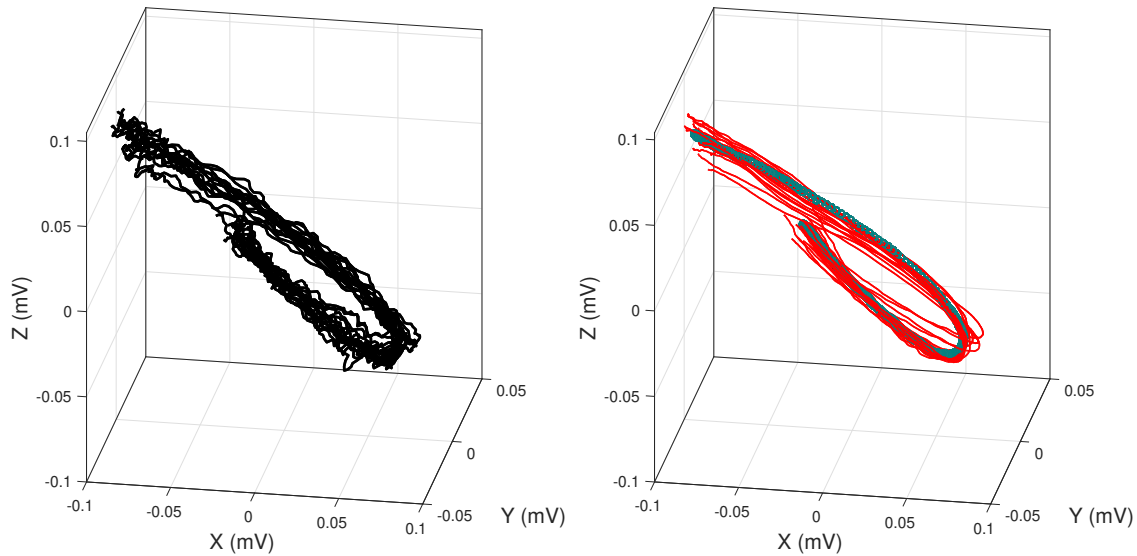
Figure A.3. An example of 15 raw (black) VCG T-loop cycles (left) and the corresponding adapted data (right) for a control subject. Green denotes the original template and red the adapted template.

transformed by a kernel function that is not limited to a finite dimensional space. In this work, we employ a Gaussian kernel function to exploit smoothness properties inherent to this transformation (Hofmann *et al.*, 2008). Mathematically, the Gaussian kernel function can be expressed as:

$$k(x, x') = exp(\frac{|x - x'|^2}{2\sigma^2}),$$ (A.7)

where σ denotes the kernel width.

To account for the varying signal-to-noise ratio of VCG, a simple noise model is incorporated via an adaptive regularization term. We employ a non-stationary noise estimation model where each entry of the diagonal matrix λ is estimated as the difference between samples. For an $n \times n$ diagonal matrix, Y_t, the ath diagonal entry can be obtain by:

$$\Lambda_a = Y_{t_a} - Y_{ta-1}. \tag{A.8}$$

Fig. A.2 and Fig. A.3 depict adaptation results across fifteen beats for an MI patient and control subject, respectively.

A.2.4 Template Generation & Features

Beat-to-beat delineation of the QRS-loop and T-loop was performed using two-dimensional signal warping (Schmidt *et al.*, 2014). For each loop, interpolation was performed to match the length of the given cardiac segment to the respective mean length. Next, the template loops were generated for each patient by averaging across beats for the respective recording and loop. To evaluate the proposed method in assessing ventricular depolarization and repolarization lability, several variations of previously proposed VCG features were evaluated, namely: mean-loop-length (MLL) and distance variability (DV) (Hasan *et al.*, 2012a). MLL is defined as the distance summation between sequential samples. DV is defined as the vector containing the Euclidean distances between corresponding points in the adapted loop and template loop. In our analysis, we translated the adapted template to the original template. Global realignment was performed to ensure the DV features were robust to translation caused by motion and respiration artefacts. Furthermore, we normalized each loop by the squared sum of its eigenvalues. This was performed to account for the various physiological amplitudes present.

A.2.5 Data

In this study we employed the PTB diagnostic ECG database, which is freely available on Physionet (Goldberger *et al.*, 2000). We used the VCG (Frank lead system) leads available in the database. In detail, 79 myocardial infarction patients (22 female, mean age 63 ± 12 years; 57 male, mean age 57 ± 10 years) and 69 control subjects (17-female, 42 ± 18 years; 52 male, 40 ± 13 years) were analyzed. Beat-to-beat analysis was performed using the described inhomogeneous three-dimensional template adaptation.

Table A.1. QRS-loop and T-loop features in the control and MI groups.

Feature	Control Subjects	MI Patients	p-value
MLL_{QRS}	10.8 ± 4.1	13.9 ± 5.9	< 0.0005
MLL_T	10.5 ± 5.4	19.6 ± 11.2	< 0.0001
$DV_{QRS}\,(std)$	1.2 ± 0.5	1.6 ± 0.9	< 0.0100
$DV_T\,(std)$	1.1 ± 0.7	2.2 ± 1.4	< 0.0001
$DV_{QRS}\,(mean)$	2.4 ± 1.3	3.3 ± 1.6	< 0.0005
$DV_T\,(mean)$	2.6 ± 1.3	5.1 ± 3.5	< 0.0001

The results from our analysis are shown in Table A.1. The features were considered statistically significant for $p < 0.05$ (using the unpaired student t-test). All values were expressed as mean $\pm$ standard deviation. The beat-to-beat VCG features were obtained for both the myocardial infarction patients and the control subjects. Beat-to-beat variability was calculated as the standard deviation of the given ECG features.

A.3   Results

Observing Table A.1, the mean-loop-length of the QRS-loop (MLL_{QRS}) was found to be statistically lower in control subjects compared to the MI group. Similarly, the mean-loop-length of the T-Loop (MLL_T) was found to be statistically lower in control subjects compared to the MI group. The point-to-point distance variability features were found to be statistically lower in control subjects compared to the MI group for the QRS-loop. Similarly, for the T-loop, the DV features were found to be statistically lower in control subjects compared to MI patients.

A.4   Discussion

In this study, we introduced a novel framework for inhomogeneous template adaptation of VCG. Our proposed method applies a global-to-local adaptation scheme. The proposed framework presents an efficient system by avoiding expensive iterative optimization methods. Data are optimally translated and rotated using Procrustes analysis, which permits for the data to be described by localized paramterization weights (FFD). FFD yields a linear descriptor of the embedded shape, which is then adapted using a kernel ridge regression formulation. Adaptation results can be observed in Fig. A.2 and Fig. A.3, where subtle and smooth deformation of the template can be observed across fifteen beats. Although the proposed method has demonstrated promising results, a more robust non-stationary

noise estimation ought to be employed for the regularization term in the KRR formulation. Autoregressive noise estimation could be one such area of investigation.

Statistical results across the PTB database indicate that both the beat-to-beat MLL of the QRS-loop and T-loop may hold value in the assessment of MI patients. Similar results were observed for the DV features. The preliminary results of this investigation suggest that further VCG features ought to be investigated for the study of ventricular depolarization and repolarization lability. Future research could explore time-series shape analysis. Furthermore, sensitivity analysis ought to be performed against a synthetic database for the presented features and any subsequently proposed features. Any such assessment should include sufficient ST-segment changes.

A.5   Conclusion

The proposed inhomogeneous three-dimensional template adaptation method demonstrated the ability to detect morphological variations in VCG. We evaluated the PTB database using the proposed method and observed statistical significance between control subjects and MI patients. Thus, the proposed framework may be useful in the study of ventricular depolarization and repolarization in VCG.

Bibliography

Abend, W., Bizzi, E., and Morasso, P. (1982). 'Human arm trajectory formation', *Brain*, **105**(1), pp. 331– 348.

Acar, B., and Koymen, H. (1999). 'SVD-based on-line exercise ECG signal orthogonalization', *IEEE Transactions on Biomedical Engineering*, **46**(3), pp. 311–321.

Acar, B., Yi, G., Hnatkova, K., and Malik, M. (1999). 'Spatial, temporal and wavefront direction characteristics of 12-lead T-wave morphology', *Medical and Biological Engineering and Computing*, **37**(5), pp. 574–584.

Acharya, U. R., Fujita, H., Oh, S. L., Hagiwara, Y., Tan, J. H., and Adam, M. (2017). 'Application of deep convolutional neural network for automated detection of myocardial infarction using ECG signals', *Information Sciences*, **415-416**, pp. 190–198.

Afonso, V. X., Tompkins, W. J., Nguyen, T. Q., and Luo, S. (1999). 'ECG beat detection using filter banks', *IEEE Transactions on Biomedical Engineering*, **46**(2), pp. 192–202.

Ahmad, Z., Tabassum, A., Guan, L., and Khan, N. M. (2021). 'ECG Heartbeat Classification Using Multimodal Fusion', *IEEE Access*, **9**, pp. 100615–100626.

Allen, J., Zheng, D., Kyriacou, P. A., and Elgendi, M. (2021). 'Photoplethysmography (PPG): state-of-the-art methods and applications', *Physiological Measurement*, **42**(10), 100301.

Almeida, R., Gouveia, S., Rocha, A. P., Pueyo, E., Martínez, J. P., and Laguna, P. (2006). 'QT variability and HRV interactions in ECG: Quantification and reliability', *IEEE Transactions on Biomedical Engineering*, **53**(7), pp. 1317–1329.

Alpert, J. S., Thygesen, K., Antman, E., and Bassand, J. P. (2000). 'Myocardial infarction redefined–a consensus document of The Joint European Society of Cardiology/American College of Cardiology Committee for the redefinition of myocardial infarction.', *Journal of the American College of Cardiology*, **36**(3), pp. 959–969.

Andreotti, F., Riedl, M., Himmelsbach, T., Wedekind, D., Zaunseder, S., Wessel, N., and Malberg, H. (2013). 'Maternal signal estimation by Kalman Filtering and Template Adaptation for fetal heart rate extraction', *Computing in Cardiology Conference (CinC)*, pp. 193–196.

Ansari, S., Farzaneh, N., Duda, M., Horan, K., Andersson, H. B., Goldberger, Z. D., Nallamothu, B. K., and Najarian, K. (2017). 'A Review of Automated Methods for Detection of Myocardial Ischemia and Infarction Using Electrocardiogram and Electronic Health Records.', *IEEE reviews in biomedical engineering*, **10**, pp. 264–298.

Arif, M., Malagore, I. A., and Afsar, F. A. (2012). 'Detection and localization of myocardial infarction using K-nearest neighbor classifier.', *Journal of medical systems*, **36**(1), pp. 279–289.

Astrom, M., Santos, E. C., Sornmo, L., Laguna, P., and Wohlfart, B. (2000). 'Vectorcardiographic loop alignment and the measurement of morphologic beat-to-beat variability in noisy signals', *IEEE Transactions on Biomedical Engineering*, **47**(4), pp. 497–506.

Atiga, W. L., Fananapazir, L., McAreavey, D., Calkins, H., and Berger, R. D. (2000). 'Temporal repolarization lability in hypertrophic cardiomyopathy caused by beta-myosin heavy-chain gene mutations.', *Circulation*, **101**(11), pp. 1237–1242.

Avbelj, V., Trobec, R., and Gersak, B. (2003). 'Beat-to-beat repolarisation variability in body surface electrocardiograms.', *Medical & biological engineering & computing*, **41**(5), pp. 556–560.

Bailey, J. J., Berson, A. S., Garson, A., Horan, L. G., Macfarlane, P. W., Mortara, D. W., and Zywietz, C. (1990). 'Recommendations for standardization and specifications in automated electrocardiography: Bandwidth and digital signal processing. A report for health professionals by an ad hoc Writing Group of the Committee on electrocardiography and Cardiac Electrophysi', *Circulation*, **81**(2), pp. 730–739.

Baumert, M., Lambert, E., Vaddadi, G., Sari, C. I., Esler, M., Lambert, G., Sanders, P., and Nalivaiko, E. (2011a). 'Cardiac repolarization variability in patients with postural tachycardia syndrome during graded head-up tilt', *Clinical Neurophysiology*, **122**(2), pp. 405–409.

Baumert, M., Porta, A., Vos, M. A., Malik, M., Couderc, J. P., Laguna, P., Piccirillo, G., Smith, G. L., Tereshchenko, L. G., and Volders, P. G. (2016a). 'QT interval variability in body surface ECG: measurement, physiological basis, and clinical value: position statement and consensus guidance endorsed by the European Heart Rhythm Association jointly with the ESC Working Group on cardiac cellular electroph', *Europace*, **18**(6), pp. 925–944.

Baumert, M., Schlaich, M. P., Nalivaiko, E., Lambert, E., Sari, C. I., Kaye, D. M., Elser, M. D., Sanders, P., and Lambert, G. (2011b). 'Relation between QT interval variability and cardiac sympathetic activity in hypertension', *AJP: Heart and Circulatory Physiology*, **300**(4), pp. H1412–H1417.

Baumert, M., Schmidt, M., Zaunseder, S., and Porta, A. (2016b). 'Effects of ECG Sampling Rate on QT Interval Variability Measurement', *Biomed. Signal Process. Control*, **25**(Supplement C), pp. 159–164.

Baumert, M., Smith, J., Catcheside, P., McEvoy, R. D., Abbott, D., Sanders, P., and Nalivaiko, E. (2008). 'Variability of QT interval duration in obstructive sleep apnea: an indicator of disease severity.', *Sleep*, **31**(7), pp. 959–956.

Baumert, M., Starc, V., and Porta, A. (2012). 'Conventional QT variability measurement vs. template matching techniques: comparison of performance using simulated and real ECG', *PLoS ONE*, **7**(1), 18.

Bayliss, W. M., Starling, E. H., and Sharpey-Schafer, E. A. (1892). 'V. On the electromotive phenomena of the mammalian heart', *Proceedings of the Royal Society of London*, **50**(302-307), pp. 211–214.

Bayoumy, K., Gaber, M., Elshafeey, A., Mhaimeed, O., Dineen, E. H., Marvel, F. A., Martin, S. S., Muse, E. D., Turakhia, M. P., Tarakji, K. G., and Elshazly, M. B. (2021). 'Smart wearable devices in cardiovascular care: where we are and how to move forward', *Nature Reviews Cardiology*, **18**(8), pp. 581–599.

Becker, D. E. (2006). 'Fundamentals of electrocardiography interpretation', *Anesthesia progress*, **53**(2), pp. 53–64.

Ben-Haim, S. A., Becker, B., Edoute, Y., Kochanovski, M., Azaria, O., Kaplinsky, E., and Palti, Y. (1991). 'Beat-to-beat electrocardiographic morphology variation in healed myocardial infarction.', *The American journal of cardiology*, **68**(8), pp. 725–728.

Berger, R. D., Kasper, E. K., Baughman, K. L., Marban, E., Calkins, H., and Tomaselli, G. F. (1997). 'Beat-to-beat QT interval variability: Novel evidence for repolarization lability in ischemic and nonischemic dilated cardiomyopathy', *Circulation*, **96**(5), pp. 1557–1565.

Berson, A. S., and Pipberger, H. V. (1967). 'Electrocardiographic distortions caused by inadequate high-frequency response of direct-writing electrocardiographs', *American Heart Journal*, **74**(2), pp. 208–218.

Besl, P. J., and McKay, N. D. (1992). 'A Method for Registration of 3-D Shapes', *IEEE Transactions on Pattern Analysis and Machine Intelligence*, **14**(2), pp. 239–256.

Bhar-Amato, J., Davies, W., and Agarwal, S. (2017). 'Ventricular arrhythmia after acute myocardial infarction: 'the perfect storm'', *Arrhythmia & Electrophysiology Review*, **6**(3), pp. 134–139.

Bluemke, D. A. (2010). 'MRI of nonischemic cardiomyopathy', *AJR. American journal of roentgenology*, **195**(4), pp. 935–940.

Bonnet, M., Tancer, M., Uhde, T., and Yeragani, V. K. (2005). 'Effects of caffeine on heart rate and QT variability during sleep.', *Depression and anxiety*, **22**(3), pp. 150–155.

Bookstein, F. L. (1989). 'Principal Warps: Thin-Plate Splines and the Decomposition of Deformations', *IEEE Transactions on Pattern Analysis and Machine Intelligence*, **11**(6), pp. 567 – 585.

Bousseljot, R., Kreiseler, D., and Schnabel, A. (1995). 'Nutzung der EKG-signaldatenbank CARDIODAT der PTB über das internet', *Biomedizinische Technik*, **40**(2), pp. 317–318.

Cabasson, A., Meste, O., and Vesin, J.-M. (2012). 'Estimation and modeling of QT-interval adaptation to heart rate changes.', *IEEE transactions on bio-medical engineering*, **59**(4), pp. 956–965.

Carney, R. M., Freedland, K. E., Stein, P. K., Watkins, L. L., Catellier, D., Jaffe, A. S., and Yeragani, V. K. (2003). 'Effects of depression on QT interval variability after myocardial infarction.', *Psychosomatic medicine*, **65**(2), pp. 177–180.

Castaneda, D., Esparza, A., Ghamari, M., Soltanpur, C., and Nazeran, H. (2018). 'A review on wearable photoplethysmography sensors and their potential future applications in health care', *International journal of biosensors & bioelectronics*, **4**(4), pp. 195–202.

Channer, K., and Morris, F. (2002). 'ABC of clinical electrocardiography: Myocardial ischaemia', *BMJ (Clinical research ed.)*, **324**(7344), pp. 1023–1026.

Charlton, P. H., Mariscal Harana, J., Vennin, S., Li, Y., Chowienczyk, P., and Alastruey, J. (2019). 'Modeling arterial pulse waves in healthy aging: a database for in silico evaluation of hemodynamics and pulse wave indexes.', *American journal of physiology. Heart and circulatory physiology*, **317**(5), pp. H1062–H1085.

Cho, H.-w., Lee, H., Lee, H. J., Shin, D. G., Park, J.-K., Lee, J. M., Oh, J., Kang, S.-M., Shim, S. S., Kim, Y., Lee, H.-J., Kim, Y. J., Joung, B., and Park, J. (2021). 'Inferior Fragmented QRS as a New Predictor of Ventricular Arrhythmias in Patients With Nonischemic Cardiomyopathy', *JACC: Cardiovascular Imaging*, **14**(1), pp. 296–298.

Chou, T.-C. (1986). 'When is the vectorcardiogram superior to the scalar electrocardiogram?', *Journal of the American College of Cardiology*, **8**(4), pp. 791–799.

Chui, H., and Rangarajan, A. (2003). 'A new point matching algorithm for non-rigid registration', *Computer Vision and Image Understanding*, **89**(2), pp. 114 – 141.

Clark, V. L., and Kruse, J. A. (1990). 'Clinical Methods: The History, Physical, and Laboratory Examinations', *JAMA*, **264**(21), pp. 2808–2809.

Correa, R., Arini, P. D., Correa, L. S., Valentinuzzi, M., and Laciar, E. (2014). 'Novel technique for ST-T interval characterization in patients with acute myocardial ischemia.', *Computers in biology and medicine*, **50**, pp. 49–55.

Couderc, J.-P., Zareba, W., McNitt, S., Maison-Blanche, P., and Moss, A. J. (2007). 'Repolarization Variability in the Risk Stratification of MADIT II Patients', *Europace*, **9**(9), pp. 717–723.

Crum, W. R., Hartkens, T., and Hill, D. L. G. (2004). 'Non-rigid image registration: theory and practice', *The British Journal of Radiology*, **77**(2), pp. 140–153.

Cuomo, S., Marciano, F., Migaux, M. L., Finizio, F., Pezzella, E., Losi, M. A., and Betocchi, S. (2004). 'Abnormal QT interval variability in patients with hypertrophic cardiomyopathy: can syncope be predicted?', *Journal of electrocardiology*, **37**(2), pp. 113–119.

Das, M. K., Maskoun, W., Shen, C., Michael, M. A., Suradi, H., Desai, M., Subbarao, R., and Bhakta, D. (2010). 'Fragmented QRS on twelve-lead electrocardiogram predicts arrhythmic events in patients with ischemic and nonischemic cardiomyopathy', *Heart Rhythm*, **7**(1), pp. 74–80.

Dean, L. (2005). '*Blood groups and red cell antigens*', Vol. 2, NCBI Bethesda.

DeFilippis, A. P., Chapman, A. R., Mills, N. L., de Lemos, J. A., Arbab-Zadeh, A., Newby, L. K., and Morrow, D. A. (2019). 'Assessment and Treatment of Patients With Type 2 Myocardial Infarction and Acute Nonischemic Myocardial Injury', *Circulation*, **140**(20), pp. 1661–1678.

Dower, G. E., Machado, H. B., and Osborne, J. A. (1980). 'On deriving the electrocardiogram from vectoradiographic leads.', *Clinical cardiology*, **3**(2), pp. 87–95.

Dubois, R., Maison-Blanche, P., Quenet, B., and Dreyfus, G. (2007). 'Automatic ECG wave extraction in long-term recordings using Gaussian mesa function models and nonlinear probability estimators', *Computer Methods and Programs in Biomedicine*, **88**(3), pp. 217–233.

Dunbar, S. B., Khavjou, O. A., Bakas, T., Hunt, G., Kirch, R. A., Leib, A. R., Morrison, R. S., Poehler, D. C., Roger, V. L., and Whitsel, L. P. (2018). 'Projected Costs of Informal Caregiving for Cardiovascular Disease: 2015 to 2035: A Policy Statement From the American Heart Association', *Circulation*, **137**(19), pp. 558–577.

Duvenaud, D. K. (2014). *Automatic Model Construction with Gaussian Processes*, PhD thesis.

Dyson, F. (2007). 'Our Biotech Future'.

Edenbrandt, L., and Pahlm, O. (1988). 'Vectorcardiogram synthesized from a 12-lead ECG: superiority of the inverse Dower matrix.', *Journal of electrocardiology*, **21**(4), pp. 361–367.

El-Hamad, F. J., Bonabi, S. Y., Müller, A., Steger, A., Schmidt, G., and Baumert, M. (2020). 'Augmented Oscillations in QT Interval Duration Predict Mortality Post Myocardial Infarction Independent of Heart Rate', *Frontiers in Physiology*, **11**, 1442.

Exarchos, T. P., Papaloukas, C., Fotiadis, D. I., and Michalis, L. K. (2006). 'An association rule mining-based methodology for automated detection of ischemic ECG beats', *IEEE Transactions on Biomedical Engineering*, **53**(8), pp. 1531–1540.

Exarchos, T. P., Tsipouras, M. G., Exarchos, C. P., Papaloukas, C., Fotiadis, D. I., and Michalis, L. K. (2007). 'A methodology for the automated creation of fuzzy expert systems for ischaemic and arrhythmic beat classification based on a set of rules obtained by a decision tree', *Artificial Intelligence in Medicine*, **40**(3), pp. 187–200.

Floater, M. S., Kós, G., and Reimers, M. (2005). 'Mean value coordinates in 3D', *Computer Aided Geometric Design*, **22**(7), pp. 623–631.

Frank, E. (1956). 'An Accurate, Clinically Practical System For Spatial Vectorcardiography', *Circulation*, **13**(5), pp. 737–749.

Fye, W. B. (1994). 'A history of the origin, evolution, and impact of electrocardiography.', *The American journal of cardiology*, **73**(13), pp. 937–949.

García, J., Åström, M., Mendive, J., Laguna, P., and Sörnmo, L. (2003). 'ECG-based detection of body position changes in ischemia monitoring', *IEEE Transactions on Biomedical Engineering*, **50**(6), pp. 677–685.

García, J., Sörnmo, L., Olmos, S., and Laguna, P. (2000a). 'Automatic detection of ST-T complex changes on the ECG using filtered RMS difference series: application to ambulatory ischemia monitoring.', *IEEE transactions on bio-medical engineering*, **47**(9), pp. 1195–1201.

García, J., Wagner, G., Sörnmo, L., Olmos, S., Lander, P., and Laguna, P. (2000b). 'Temporal evolution of traditional versus transformed ECG-Based indexes in patients with induced myocardial ischemia', *Journal of Electrocardiology*, **33**(1), pp. 37–47.

Gil, E., Bailón, R., Vergara, J. M., and Laguna, P. (2010). 'PTT Variability for Discrimination of Sleep Apnea Related Decreases in the Amplitude Fluctuations of PPG Signal in Children', *IEEE Transactions on Biomedical Engineering*, **57**(5), pp. 1079–1088.

Gold, S., Rangarajan, A., Lu, C.-P., Pappu, S., and Mjolsness, E. (1998). 'New algorithms for 2D and 3D point matching: pose estimation and correspondence', *Pattern Recognition*, **31**(8), pp. 1019–1031.

Goldberger, A. L., Amaral, L. A., Glass, L., Hausdorff, J. M., Ivanov, P. C., Mark, R. G., Mietus, J. E., Moody, G. B., Peng, C. K., and Stanley, H. E. (2000). 'PhysioBank, PhysioToolkit, and PhysioNet: components of a new research resource for complex physiologic signals.', *Circulation*, .

Goldberger, A. L., Amaral, L. A. N., Glass, L., Hausdorff, J. M., Ivanov, P. C., Mark, R. G., Mietus, J. E., Moody, G. B., Peng, C.-K., and Stanley, H. E. (2012). 'PhysioBank, PhysioToolkit, and PhysioNet', *Circulation*, .

Goletsis, Y., Papaloukas, C., Fotiadis, D. I., Likas, A., and Michalis, L. K. (2003). 'A multicriteria decision based approach for ischaemia detection in long duration ECGs', *4th International IEEE EMBS Special Topic Conference on Information Technology Applications in Biomedicine, 2003.*, IEEE, pp. 173–176.

Goletsis, Y., Papaloukas, C., Fotiadis, D. I., Likas, A., and Michalis, L. K. (2004). 'Automated ischemic beat classification using genetic algorithms and multicriteria decision analysis.', *IEEE transactions on bio-medical engineering*, **51**(10), pp. 1717–1725.

Goodfellow, I., Bengio, Y., and Courville, A. (2016). '*Deep learning*', MIT press.

Gower, J. C., and Dijksterhuis, G. B. (2004). '*Procrustes Problems*', Oxford University Press, Oxford.

Grote, L., and Zou, D. (2017). 'Chapter 167 - Pulse Wave Analysis During Sleep', Elsevier, pp. 1624–1632.

Gu, W. B., Poon, C. C. Y., and Zhang, Y. T. (2008). 'A novel parameter from PPG dicrotic notch for estimation of systolic blood pressure using pulse transit time', *2008 5th International Summer School and Symposium on Medical Devices and Biosensors*, pp. 86–88.

Guillem, M. S., Climent, A. M., Bollmann, A., Husser, D., Millet, J., and Castells, F. (2009). 'Limitations of Dower's inverse transform for the study of atrial loops during atrial fibrillation.', *Pacing and clinical electrophysiology : PACE*, **32**(8), pp. 972–980.

Guillem, M. S., Sahakian, A. V., and Swiryn, S. (2008). 'Derivation of orthogonal leads from the 12-lead electrocardiogram. Performance of an atrial-based transform for the derivation of P loops.', *Journal of electrocardiology*, **41**(1), pp. 19–25.

Han, L., and Tereshchenko, L. G. (2010). 'Lability of R- and T-wave peaks in three-dimensional electrocardiograms in implantable cardioverter defibrillator patients with ventricular tachyarrhythmia during follow-up', *Journal of Electrocardiology*, **43**(6), pp. 577–582.

Hasan, M. A., Abbott, D., and Baumert, M. (2012a). 'Beat-to-Beat Vectorcardiographic Analysis of Ventricular Depolarization and Repolarization in Myocardial Infarction', *PLoS ONE*, **7**(11), pp. 1–10.

Hasan, M. A., Abbott, D., and Baumert, M. (2012b). 'Relation between beat-to-beat qt interval variability and t-wave amplitude in healthy subjects', *Annals of Noninvasive Electrocardiology*, **17**(3), pp. 195–203.

Hasan, M. A., Abbott, D., and Baumert, M. (2013). 'Beat-to-beat QT interval variability and T-wave amplitude in patients with myocardial infarction', *Physiological Measurement*, **34**(9), pp. 1075–1083.

Hasan, M. A., and Abbott, D. (2016). 'A review of beat-to-beat vectorcardiographic (VCG) parameters for analyzing repolarization variability in ECG signals', *Biomedizinische Technik*, **61**(1), pp. 3–17.

Hekkanen, J. J., Kenttä, T. V., Haukilahti, M. A. E., Rahola, J. T., Holmström, L., Vähätalo, J., Tulppo, M. P., Kiviniemi, A. M., Pakanen, L., Ukkola, O. H., Junttila, M. J., Huikuri, H. V., and Perkiömäki, J. S. (2020). 'Increased Beat-to-Beat Variability of T-Wave Heterogeneity Measured From Standard 12-Lead Electrocardiogram Is Associated With Sudden Cardiac Death: A Case–Control Study', *Frontiers in Physiology*, **11**.

Hill, D. L. G., Batchelor, P. G., Holden, M., and Hawkes, D. J. (2001). 'Medical image registration', *Physics in Medicine and Biology*, **46**(3), pp. R1–R45.

Hinton, G. E., Srivastava, N., and Swersky, K. (2012). 'Neural Networks for Machine Learning Lecture 6a Overview of mini-batch gradient descent.', *COURSERA: Neural Networks for Machine Learning*, .

Hiromoto, K., Shimizu, H., Mine, T., Masuyama, T., and Ohyanagi, M. (2006). 'Correlation between beat-to-beat QT interval variability and impaired left ventricular function in patients with previous myocardial infarction', *Annals of noninvasive electrocardiology : the official journal of the International Society for Holter and Noninvasive Electrocardiology, Inc*, **11**(4), pp. 299–305.

Hochreiter, S., and Schmidhuber, J. (1997). 'Long short-term memory', *Neural Computation*, **9**(8), pp. 1735–1780.

Hofmann, T., Schölkopf, B., and Smola, A. J. (2008). 'Kernel methods in machine learning', *Annals of Statistics*, **36**(3), pp. 1171–1220.

Huang, B., and Kinsner, W. (2002). 'ECG frame classification using dynamic time warping', *IEEE CCECE2002. Canadian Conference on Electrical and Computer Engineering. Conference Proceedings*, Vol. 2, pp. 1105–1110.

Huang, H.-C., Lin, L.-Y., Yu, H.-Y., and Ho, Y.-L. (2009). 'Risk stratification by T-wave morphology for cardiovascular mortality in patients with systolic heart failure.', *Europace : European pacing, arrhythmias, and cardiac electrophysiology : journal of the working groups on cardiac pacing, arrhythmias, and cardiac cellular electrophysiology of the European Society of Cardiology*, **11**(11), pp. 1522–1528.

Huang, X., Paragios, N., and Metaxas, D. N. (2006). 'Shape registration in implicit spaces using information theory and free form deformations', *IEEE Transactions on Pattern Analysis and Machine Intelligence*, **28**(8), pp. 1303–1318.

Israel, C. W. (2014). 'Mechanisms of sudden cardiac death', *Indian heart journal*, **66 Suppl 1**(Suppl 1), pp. S10–S17.

Jager, F., Moody, G. B., and Mark, R. G. (1998). 'Detection of transient ST segment episodes during ambulatory ECG monitoring.', *Computers and biomedical research, an international journal*, **31**(5), pp. 305–322.

Jowett, N. I., Turner, A. M., Cole, A., and Jones, P. A. (2005). 'Modified electrode placement must be recorded when performing 12-lead electrocardiograms', *Postgraduate Medical Journal*, **81**(952), pp. 122–125.

Kachuee, M., Fazeli, S., and Sarrafzadeh, M. (2018). 'ECG Heartbeat Classification: A Deep Transferable Representation', *2018 IEEE International Conference on Healthcare Informatics (ICHI)*, pp. 443–444.

Karisik, F., and Baumert, M. (2019). 'Inhomogeneous Template Adaptation of Temporal Quasi-Periodic Three-Dimensional Signals', *IEEE Transactions on Signal Processing*, **67**(23), pp. 6067–6077.

Karisik, F., and Baumert, M. (2021). 'Template Adaptation of 2D Quasi-Periodic Data Using a Soft-Assign Localized Correspondence Matrix', *IEEE Transactions on Signal Processing*, **69**, pp. 826–836.

Karsikas, M., Noponen, K., Tulppo, M., Huikuri, H. V., and Seppänen, T. (2009). 'Beat-to-beat variation of three-dimensional QRS-T angle measures during exercise test', *2009 36th Annual Computers in Cardiology Conference (CinC)*, pp. 125–128.

Kenttä, T., Karsikas, M., Kiviniemi, A., Tulppo, M., Seppänen, T., and Huikuri, H. V. (2010). 'Dynamics and Rate-Dependence of the Spatial Angle between Ventricular Depolarization and Repolarization Wave Fronts during Exercise ECG', *Annals of Noninvasive Electrocardiology*, **15**(3), pp. 264–275.

Keogh, E. J., and Pazzani, M. J. (2001). 'Derivative Dynamic Time Warping'.

Klabunde, R. E. (2012). '*Cardiovascular physiology concepts*', 2nd edn, Lippincott Williams & Wilkins, Baltimore.

Kléber, A. G., Janse, M. J., van Capelle, F. J., and Durrer, D. (1978). 'Mechanism and time course of S-T and T-Q segment changes during acute regional myocardial ischemia in the pig heart determined by extracellular and intracellular recordings.', *Circulation research*, **42**(5), pp. 603–613.

Kligfield, P., Gettes, L. S., Bailey, J. J., Childers, R., Deal, B. J., Hancock, E. W., van Herpen, G., Kors, J. A., Macfarlane, P., Mirvis, D. M., Pahlm, O., Rautaharju, P., and Wagner, G. S. (2007). 'Recommendations for the Standardization and Interpretation of the Electrocardiogram', *Circulation*, **115**(10), pp. 1306–1324.

Knight, P. A. (2008). 'The sinkhorn-knopp algorithm: Convergence and applications', *SIAM Journal on Matrix Analysis and Applications*, **30**(1), pp. 261–275.

Kors, J. A., Van Herpen, G., Sittig, A. C., and Van Bemmel, J. H. (1990). 'Reconstruction of the Frank vectorcardiogram from standard electrocardiographic leads: diagnostic comparison of different methods', *European Heart Journal*, **11**(12), pp. 1083–1092.

Koschke, M., Boettger, M. K., Schulz, S., Berger, S., Terhaar, J., Voss, A., Yeragani, V. K., and Bär, K.-J. (2009). 'Autonomy of autonomic dysfunction in major depression.', *Psychosomatic medicine*, **71**(8), pp. 852–860.

Kumar, A., and Singh, M. (2016). 'Ischemia detection using Isoelectric Energy Function', *Computers in Biology and Medicine*, **68**, pp. 76–83.

Laguna, P., Cortés, J. P. M., and Pueyo, E. (2016). 'Techniques for Ventricular Repolarization Instability Assessment From the ECG', *Proceedings of the IEEE*, **104**(2), pp. 392–415.

Laguna, P., Jané, R., and Caminal, P. (1994). 'Automatic detection of wave boundaries in multilead ECG signals: validation with the CSE database.', *Computers and biomedical research, an international journal*, **27**(1), pp. 45–60.

Laguna, P., Mark, R. G., Goldberg, A., and Moody, G. B. (1997). 'A database for evaluation of algorithms for measurement of QT and other waveform intervals in the ECG', *Computers in Cardiology 1997*, pp. 673–676.

Lek, S., and Park, Y. S. (2008). 'Artificial Neural Networks', Academic Press, Oxford, pp. 237–245.

Lewis, T. (1909). 'REPORT CXIX. AURICULAR FIBRILLATION: A COMMON CLINICAL CONDITION', *British medical journal*, **2**(2552), 1528.

Li, B. N., Dong, M. C., and Vai, M. I. (2010). 'On an automatic delineator for arterial blood pressure waveforms', *Biomedical Signal Processing and Control*, **5**(1), pp. 76–81.

Lin, C.-Y., Lin, L.-Y., and Chen, P.-C. (2007). 'Analysis of T-wave morphology from the 12-lead electrocardiogram for prediction of long-term prognosis in patients initiating haemodialysis.', *Nephrology, dialysis, transplantation : official publication of the European Dialysis and Transplant Association - European Renal Association*, **22**(9), pp. 2645–2652.

Lui, H. W., and Chow, K. L. (2018). 'Multiclass classification of myocardial infarction with convolutional and recurrent neural networks for portable ECG devices', *Informatics in Medicine Unlocked*, **13**, pp. 26–33.

Lyon, A., Mincholé, A., Martínez, J. P., Laguna, P., and Rodriguez, B. (2018). 'Computational techniques for ECG analysis and interpretation in light of their contribution to medical advances.', *Journal of the Royal Society, Interface*, **15**(138), 20170821.

Maglaveras, N., Stamkopoulos, T., Diamantaras, K., Pappas, C., and Strintzis, M. (1998a). 'ECG pattern recognition and classification using non-linear transformations and neural networks: A review', *International Journal of Medical Informatics*, **52**(1), pp. 191–208.

Maglaveras, N., Stamkopoulos, T., Pappas, C., and Strintzis, M. (1998b). 'ECG processing techniques based on neural networks and bidirectional associative memories', *Journal of Medical Engineering & Technology*, **22**(3), pp. 106–111.

Maiseli, B., Gu, Y., and Gao, H. (2017). 'Recent developments and trends in point set registration methods', *Journal of Visual Communication and Image Representation*, **46**, pp. 95–106.

Marquardt, D. W., and Snee, R. D. (1975). 'Ridge regression in practice', *American Statistician*, **29**(1), pp. 3–20.

Martinez, J. P., Almeida, R., Olmos, S., Rocha, A. P., and Laguna, P. (2004). 'A wavelet-based ECG delineator: evaluation on standard databases', *IEEE Transactions on Biomedical Engineering*, **51**(4), pp. 570–581.

Martínez, J. P., Olmos, S., Wagner, G., and Laguna, P. (2006). 'Characterization of repolarization alternans during ischemia: time-course and spatial analysis.', *IEEE transactions on bio-medical engineering*, **53**(4), pp. 701–711.

Mayol, B. (2019). 'Nancy articulated humanoid under Matlab'.

Middleton, P. M., Tang, C. H. H., Chan, G. S. H., Bishop, S., Savkin, A. V., and Lovell, N. H. (2011). 'Peripheral photoplethysmography variability analysis of sepsis patients.', *Medical & biological engineering & computing*, **49**(3), pp. 337–347.

Miranda, J. G. V., Daneault, J. F., Vergara-Diaz, G., Torres, Â. F. S. d. O. e., Quixadá, A. P., Fonseca, M. d. L., Vieira, J. P. B. C., dos Santos, V. S., da Figueiredo, T. C., Pinto, E. B., Peña, N., and Bonato, P. (2018). 'Complex Upper-Limb Movements Are Generated by Combining Motor Primitives that Scale with the Movement Size', *Scientific Reports*, **8**(1), pp. 1–11.

Moody, G. B., and Mark, R. G. (2001). 'The impact of the MIT-BIH arrhythmia database.', *IEEE engineering in medicine and biology magazine : the quarterly magazine of the Engineering in Medicine & Biology Society*, **20**(3), pp. 45–50.

Morris, F., and Brady, W. J. (2002). 'Acute myocardial infarction — Part I Hyperacute T waves', *BMJ*, **324**(7341), pp. 831–834.

Murabayashi, T., Fetics, B., Kass, D., Nevo, E., Gramatikov, B., and Berger, R. D. (2002). 'Beat-to-beat QT interval variability associated with acute myocardial ischemia', *Journal of Electrocardiology*, **35**(1), pp. 19–25.

Neumaier, A. (1998). 'Solving Ill-Conditioned and Singular Linear Systems: A Tutorial on Regularization', *SIAM Review*, **40**(3), pp. 636–666.

Nikus, K., Birnbaum, Y., Eskola, M., Sclarovsky, S., Zhong-Qun, Z., and Pahlm, O. (2014). 'Updated Electrocardiographic Classification of Acute Coronary Syndromes', *Current Cardiology Reviews*, **10**(3), pp. 229–236.

Nowbar, A. N., Gitto, M., Howard, J. P., Francis, D. P., and Al-Lamee, R. (2019). 'Mortality From Ischemic Heart Disease', *Circulation: Cardiovascular Quality and Outcomes*, **12**(6), e005375.

Olah, C. (2015). 'Understanding LSTM networks'.

Oliveira, F. P. M., and Tavares, J. M. R. S. (2014). 'Medical image registration: a review', *Computer methods in biomechanics and biomedical engineering*, **17**(2), pp. 73–93.

Orrego, D. A., Becerra, M. A., and Delgado-Trejos, E. (2012). 'Dimensionality reduction based on fuzzy rough sets oriented to ischemia detection.', *Annual International Conference of the IEEE Engineering in Medicine and Biology Society. IEEE Engineering in Medicine and Biology Society. Annual International Conference*, **2012**, pp. 5282–5285.

Pan, J., and Tompkins, W. J. (1985). 'A real-time QRS detection algorithm.', *IEEE transactions on bio-medical engineering*, **32**(3), pp. 230–236.

Papadimitriou, S., Mavroudi, S., Vladutu, L., and Bezerianos, A. (2001). 'Ischemia detection with a self-organizing map supplemented by supervised learning.', *IEEE transactions on neural networks*, **12**(3), pp. 503–515.

Papaloukas, C., Fotiadis, D. I., Liavas, A. P., Likas, A., and Michalis, L. K. (2001). 'A knowledge-based technique for automated detection of ischaemic episodes in long duration electrocardiograms.', *Medical & biological engineering & computing*, **39**(1), pp. 105–112.

Papaloukas, C., Fotiadis, D. I., Likas, A., and Michalis, L. K. (2002a). 'An expert system for ischemia detection based on parametric modeling and artificial neural networks', *Proc. Eur. Med. Biol. Eng. Conf*, pp. 742–743.

Papaloukas, C., Fotiadis, D. I., Likas, A., and Michalis, L. K. (2002b). 'An ischemia detection method based on artificial neural networks.', *Artificial intelligence in medicine*, **24**(2), pp. 167–178.

Papaloukas, C., Fotiadis, D. I., Likas, A., Stroumbis, C. S., and Michalis, L. K. (2002c). 'Use of a novel rule-based expert system in the detection of changes in the ST segment and the T wave in long duration ECGs.', *Journal of electrocardiology*, **35**(1), pp. 27–34.

Park, J., Pedrycz, W., and Jeon, M. (2012). 'Ischemia episode detection in ECG using kernel density estimation, support vector machine and feature selection', *Biomedical engineering online*, **11**, 30.

Pelaez, J. I., Dona, J. M., Fornari, J. F., and Serra, G. (2014). 'Ischemia classification via ECG using MLP neural networks', *International Journal of Computational Intelligence Systems*, **7**(2), pp. 344–352.

Pérez Riera, A. R., Uchida, A. H., Ferreira Filho, C., Meneghini, A., Ferreira, C., Schapacknik, E., Dubner, S., and Moffa, P. (2007). 'Significance of vectorcardiogram in the cardiological diagnosis of the 21st century', *Clinical Cardiology*, **30**(7), pp. 319–323.

Perkiömäki, J. S., Hyytinen-Oinas, M., Karsikas, M., Seppänen, T., Hnatkova, K., Malik, M., and Huikuri, H. V. (2006). 'Usefulness of T-wave loop and QRS complex loop to predict mortality after acute myocardial infarction.', *The American journal of cardiology*, **97**(3), pp. 353–360.

Peyvandi, M. Y. E. H. (2017). '*Deterministic Annealing: A Variant of Simulated Annealing and its Application to Fuzzy Clustering*', IntechOpen, Rijeka.

Piccirillo, G., Magrì, D., Matera, S., Magnanti, M., Torrini, A., Pasquazzi, E., Schifano, E., Velitti, S., Marigliano, V., Quaglione, R., and Barillà, F. (2007). 'QT variability strongly predicts sudden cardiac death in asymptomatic subjects with mild or moderate left ventricular systolic dysfunction: A prospective study', *European Heart Journal*, **28**(11), pp. 1344–1350.

Pimentel, M. A. F., Johnson, A. E. W., Charlton, P. H., Birrenkott, D., Watkinson, P. J., Tarassenko, L., and Clifton, D. A. (2017). 'Toward a Robust Estimation of Respiratory Rate From Pulse Oximeters', *IEEE Transactions on Biomedical Engineering*, **64**(8), pp. 1914–1923.

Pluim, J. P. W., Maintz, J. B. A., and Viergever, M. A. (2003). 'Mutual-Information-Based Registration of Medical Images : A Survey', , **22**(8), pp. 986–1004.

Pohl, R., and K Yeragani, V. (2001). 'QT interval variability in panic disorder patients after isoproterenol infusions.', *The international journal of neuropsychopharmacology*, **4**(1), pp. 17–20.

Pollehn, T. (2002). 'The electrocardiographic differential diagnosis of ST segment depression', *Emergency Medicine Journal*, **19**(2), pp. 129–135.

Pomerleau, F., Colas, F., and Siegwart, R. (2015). 'A Review of Point Cloud Registration Algorithms for Mobile Robotics', *Foundations and Trends in Robotics*, **4**(1), pp. 1–104.

Porta, A., Baselli, G., Lambardi, F., Cerutti, S., Antolini, R., Del Greco, M., Ravelli, F., and Nollo, G. (1998). 'Performance assessment of standard algorithms for dynamic R-T interval measurement: comparison between R-Tapex and R-Tend approach', *Medical and Biological Engineering and Computing*, **36**(1), pp. 35–42.

Porta, A., Girardengo, G., Bari, V., George Jr, A. L., Brink, P. A., Goosen, A., Crotti, L., and Schwartz, P. J. (2015). 'Autonomic control of heart rate and QT interval variability

influences arrhythmic risk in long QT syndrome type 1', *Journal of the American College of Cardiology*, **65**(4), pp. 367–374.

Porta, A., Tobaldini, E., Guzzetti, S., Furlan, R., Montano, N., and Gnecchi-Ruscone, T. (2007). 'Assessment of cardiac autonomic modulation during graded head-up tilt by symbolic analysis of heart rate variability', *American Journal of Physiology-Heart and Circulatory Physiology*, **293**(1), pp. H702–H708.

Porthan, K., Viitasalo, M., Jula, A., Reunanen, A., Rapola, J., Väänänen, H., Nieminen, M. S., Toivonen, L., Salomaa, V., and Oikarinen, L. (2009). 'Predictive value of electro-cardiographic QT interval and T-wave morphology parameters for all-cause and cardio-vascular mortality in a general population sample.', *Heart rhythm*, **6**(8), pp. 1202–1208.

Prasad, K., and Gupta, M. M. (1979). 'Phase-invariant signature algorithm: a noninvasive technique for early detection and quantification of ouabain-induced cardiac disorders.', *Angiology*, **30**(11), pp. 721–732.

Presedo, J., Vila, J., Barro, S., Palacios, F., Ruiz, R., Taddei, A., and Emdin, M. (1996). 'Fuzzy modelling of the expert's knowledge in ECG-based ischaemia detection', *Fuzzy Sets and Systems*, **77**(1), pp. 63–75.

Procházková, J. (2017). 'Free Form Deformation Methods – the Theory and Practice', , **1**(1), pp. 1276–1282.

Ramírez, J., Orini, M., Tucker, J. D., Pueyo, E., and Laguna, P. (2017). 'Variability of Ventricular Repolarization Dispersion Quantified by Time-Warping the Morphology of the T-Waves', *IEEE Transactions on Biomedical Engineering*, **64**(7), pp. 1619–1630.

Ramírez, J., van Duijvenboden, S., Aung, N., Laguna, P., Pueyo, E., Tinker, A., Lambiase, P. D., Orini, M., and Munroe, P. B. (2019). 'Cardiovascular Predictive Value and Genetic Basis of Ventricular Repolarization Dynamics', *Circulation: Arrhythmia and Electrophysiology*, **12**(10), e007549.

Rangarajan, A., Gold, S., and Mjolsness, E. (1996). 'A Novel Optimizing Network Architecture with Applications', *Neural Computation*, **8**(5), pp. 1041–1060.

Ranjith, P., Baby, P. C., and Joseph, P. (2003). 'ECG analysis using wavelet transform: application to myocardial ischemia detection', *ITBM-RBM*, **24**(1), pp. 44–47.

Rashba, E. J., Estes, N. A. M., Wang, P., Schaechter, A., Howard, A., Zareba, W., Couderc, J.-P., Perkiomaki, J., Levine, J., and Kadish, A. (2006). 'Preserved Heart Rate Variability Identifies Low-risk Patients With Nonischemic Dilated Cardiomyopathy: Results From the Definite Trial', *Heart Rhythm*, **3**(3), pp. 281–286.

Ravensbergen, H. J. C., Walsh, M. L., Krassioukov, A. V., and Claydon, V. E. (2012). 'Electrocardiogram-based predictors for arrhythmia after spinal cord injury.', *Clinical autonomic research : official journal of the Clinical Autonomic Research Society*, **22**(6), pp. 265–273.

Rincón, F., Recas, J., Khaled, N., and Atienza, D. (2011). 'Development and Evaluation of Multilead Wavelet-Based ECG Delineation Algorithms for Embedded Wireless Sensor Nodes', *IEEE Transactions on Information Technology in Biomedicine*, **15**(6), pp. 854–863.

Rohlf, F. J., and Slice, D. (1990). 'Extensions of the Procrustes Method for the Optimal Superimposition of Landmarks', *Systematic Biology*, **39**(1), pp. 40–59.

Roth, G. A., Mensah, G. A., Johnson, C. O., Addolorato, G., Ammirati, E., Baddour, L. M., ..., and Fuster, V. (2020). 'Global Burden of Cardiovascular Diseases and Risk Factors, 1990-2019: Update From the GBD 2019 Study', *Journal of the American College of Cardiology*, **76**(25), pp. 2982–3021.

Rueckert, D., Frangi, A., and Schnabel, J. (2001). 'Automatic Construction of 3D Statistical Deformation Models Using Non-rigid Registration', *Medical Image Computing and Computer-Assisted Intervention – MICCAI*, **2208**(8), pp. 77–84.

Salvador, S., and Chan, P. (2007). 'Toward accurate dynamic time warping in linear time and space', *Intelligent Data Analysis*, **11**, pp. 561–580.

Sameni, R., Clifford, G. D., Jutten, C., and Shamsollahi, M. B. (2007). 'Multichannel ECG and noise modeling: Application to maternal and fetal ECG signals', *Eurasip Journal on Advances in Signal Processing*, **2007**(1), pp. 1–14.

Sampson, M., and McGrath, A. (2015). 'Understanding the ECG. Part 1: Anatomy and physiology', *British Journal of Cardiac Nursing*, **10**(11), pp. 548–554.

Sarker, I. H. (2021). 'Machine Learning: Algorithms, Real-World Applications and Research Directions', *SN Computer Science*, **2**(3), 160.

Sathya, R., and Abraham, A. (2013). 'Comparison of supervised and unsupervised learning algorithms for pattern classification', *International Journal of Advanced Research in Artificial Intelligence*, **2**(2), pp. 34–38.

Schafer, R. W. (2011). 'What Is a Savitzky-Golay Filter? [Lecture Notes]', *IEEE Signal Processing Magazine*, **28**(4), pp. 111–117.

Schlegel, T. T., Kulecz, W. B., Feiveson, A. H., Greco, E. C., DePalma, J. L., Starc, V., Vrtovec, B., Rahman, M. A., Bungo, M. W., Hayat, M. J., Bauch, T., Delgado, R., Warren, S. G., Núñez-Medina, T., Medina, R., Jugo, D., Arheden, H., and Pahlm, O. (2010). 'Accuracy of advanced versus strictly conventional 12-lead ECG for detection and screening of coronary artery disease, left ventricular hypertrophy and left ventricular systolic dysfunction', *BMC Cardiovascular Disorders*, **10**(1), 28.

Schmidt, M., Baumert, M., Malberg, H., and Zaunseder, S. (2016). 'T Wave Amplitude Correction of QT Interval Variability for Improved Repolarization Lability Measurement', *Front. Physiol.*, **7**, 216.

Schmidt, M., Baumert, M., Malberg, H., and Zaunseder, S. (2018a). 'Iterative two-dimensional signal warping—Towards a generalized approach for adaption of one-dimensional signals', *Biomedical Signal Processing and Control*, **43**(1), pp. 311–319.

Schmidt, M., Baumert, M., Penzel, T., Malberg, H., and Zaunseder, S. (2018b). 'Nocturnal ventricular repolarization lability predicts cardiovascular mortality in the Sleep Heart Health Study', *American Journal of Physiology-Heart and Circulatory Physiology*, **316**(3), pp. 495–505.

Schmidt, M., Baumert, M., Porta, A., Malberg, H., and Zaunseder, S. (2014). 'Two-dimensional warping for one-dimensional signals—conceptual framework and application to ECG processing', *IEEE Transactions on Signal Processing*, **62**(21), pp. 5577–5588.

Schölkopf, B., Luo, Z., and Vovk, V. (2013). '*Empirical inference. Festschrift in honor of Vladimir N. Vapnik*', Springer.

Sederberg, T. W., and Parry, S. R. (1986). 'Free-form deformation of solid geometric models', *Proceedings of the 13th annual conference on Computer graphics and interactive techniques - SIGGRAPH '86*, **20**(4), pp. 151–160.

Shaffer, F., and Ginsberg, J. P. (2017). 'An Overview of Heart Rate Variability Metrics and Norms', *Frontiers in Public Health*, **5**.

Sharma, L. N., Tripathy, R. K., and Dandapat, S. (2015). 'Multiscale Energy and Eigenspace Approach to Detection and Localization of Myocardial Infarction', *IEEE Transactions on Biomedical Engineering*, **62**(7), pp. 1827–1837.

Shimokawa, H., and Yasuda, S. (2008). 'Myocardial ischemia: current concepts and future perspectives.', *Journal of cardiology*, **52**(2), pp. 67–78.

Smetana, P., Batchvarov, V. N., Hnatkova, K., Camm, A. J., and Malik, M. (2004). 'Ventricular gradient and nondipolar repolarization components increase at higher heart rate.', *American journal of physiology. Heart and circulatory physiology*, **286**(1), pp. H131–6.

Sörnmo, L. (1998). 'Vectorcardiographic loop alignment and morphologic beat-to-beat variability.', *IEEE transactions on bio-medical engineering*, **45**(12), pp. 1401–1413.

Sörnmo, L., and Laguna, P. (2006). 'Electrocardiogram (ECG) Signal Processing'.

Stamkopoulos, T., Diamantaras, K., Maglaveras, N., and Strintzis, M. (1998). 'ECG analysis using nonlinear PCA neural networks for ischemia detection', *IEEE Transactions on Signal Processing*, **46**(11), pp. 3058–3067.

Starc, V., and Schlegel, T. T. (2006). 'Real-time multichannel system for beat-to-beat QT interval variability', *Journal of Electrocardiology*, **39**(4), pp. 358–367.

Steenbergen, C., and Frangogiannis, N. G. (2012). 'Chapter 36 - Ischemic Heart Disease', Academic Press, Boston/Waltham, pp. 495–521.

Stephenson, A., Adams, J. W., and Vaccarezza, M. (2017). 'The vertebrate heart: an evolutionary perspective', *Journal of Anatomy*, **231**(6), pp. 787–797.

Strang, G. (2016). '*Introduction to Linear Algebra*', Wellesley-Cambridge Press.

Sur, S., Han, L., and Tereshchenko, L. G. (2013). 'Comparison of sum absolute QRST integral, and temporal variability in depolarization and repolarization, measured by dynamic vectorcardiography approach, in healthy men and women', *PloS one*, **8**(2), pp. e57175–e57175.

Taddei, A., Distante, G., Emdin, M., Pisani, P., Moody, G. B., Zeelenberg, C., and Marchesi, C. (1992). 'The European ST-T database: standard for evaluating systems for the analysis of ST-T changes in ambulatory electrocardiography.', *European heart journal*, **13**(9), pp. 1164–1172.

Team, K. (2020). 'Keras documentation: RMSprop'.

Tereshchenko, L. G., Han, L., Cheng, A., Marine, J. E., Spragg, D. D., Sinha, S., Dalal, D., Calkins, H., Tomaselli, G. F., and Berger, R. D. (2010). 'Beat-to-beat three-dimensional ECG variability predicts ventricular arrhythmia in ICD recipients', *Heart rhythm*, **7**(11), pp. 1606–1613.

Thygesen, K., Alpert, J. S., Jaffe, A. S., Chaitman, B. R., Bax, J. J., Morrow, D. A., and White, H. D. (2018). 'Fourth Universal Definition of Myocardial Infarction (2018)', *Circulation*, **138**(20), pp. e618–e651.

Thygesen, K., Alpert, J. S., Jaffe, A. S., Simoons, M. L., Chaitman, B. R., and White, H. D. (2012). 'Third Universal Definition of Myocardial Infarction', *Circulation*, **126**(16), pp. 2020–2035.

Thygesen, K., Alpert, J. S., White, H. D., Jaffe, A. S., Apple, F. S., Galvani, M., ..., and Al-Attar, N. (2007). 'Universal definition of myocardial infarction: Kristian Thygesen, Joseph S. Alpert and Harvey D. White on behalf of the Joint ESC/ACCF/AHA/WHF Task Force for the Redefinition of Myocardial Infarction', *European Heart Journal*, **28**(20), pp. 2525–2538.

Tomasi, G., Van Den Berg, F., and Andersson, C. (2004). 'Correlation optimized warping and dynamic time warping as preprocessing methods for chromatographic data', *Journal of Chemometrics*, **18**(5), pp. 231–241.

Tompkins, W. J., and Afonso, V. X. (1993). 'Biomedical Digital Signal Processing: C-Language Examples and Laboratory Experiments for the IBM PC, chapter 12', *Enlgewood Cliffs, NJ: Prentice-Hall*, pp. 236–264.

Tseng, Y.-L., Lin, K.-S., and Jaw, F.-S. (2016). 'Comparison of Support-Vector Machine and Sparse Representation Using a Modified Rule-Based Method for Automated Myocardial Ischemia Detection', *Computational and Mathematical Methods in Medicine*, .

Tsipouras, M. G., Voglis, C., and Fotiadis, D. I. (2007). 'A Framework for Fuzzy Expert System Creation—Application to Cardiovascular Diseases', *IEEE Transactions on Biomedical Engineering*, **54**(11), pp. 2089–2105.

Vähätalo, J. H., Huikuri, H. V., Holmström, L. T. A., Kenttä, T. V., Haukilahti, M. A. E., Pakanen, L., Kaikkonen, K. S., Tikkanen, J., Perkiömäki, J. S., Myerburg, R. J., and

Junttila, M. J. (2019). 'Association of Silent Myocardial Infarction and Sudden Cardiac Death', *JAMA Cardiology*, **4**(8), pp. 796–802.

Vemuri, B. C., Huang, S., Sahni, S., Leonard, C. M., Mohr, C., Gilmore, R., and Fitzsimmons, J. (1998). 'An efficient motion estimator with application to medical image registration', *Medical Image Analysis*, **2**(1), pp. 79–98.

Vintsyuk, T. K. (1968). 'Speech discrimination by dynamic programming', *Cybernetics*, .

Vogel, B., Claessen, B. E., Arnold, S. V., Chan, D., Cohen, D. J., Giannitsis, E., Gibson, C. M., Goto, S., Katus, H. A., Kerneis, M., Kimura, T., Kunadian, V., Pinto, D. S., Shiomi, H., Spertus, J. A., Steg, P. G., and Mehran, R. (2019). 'ST-segment elevation myocardial infarction', *Nature Reviews Disease Primers*, **5**(1), 39.

Vrtovec, B., Starc, V., and Starc, R. (2000). 'Beat-to-beat QT interval variability in coronary patients.', *Journal of electrocardiology*, **33**(2), pp. 119–125.

Vullings, H. J. L. M., Verhaegen, M. H. G., and Verbruggen, H. B. (1998). 'Automated ECG segmentation with dynamic time warping', *Proceedings of the 20th Annual International Conference of the IEEE Engineering in Medicine and Biology Society. Vol.20 Biomedical Engineering Towards the Year 2000 and Beyond*, pp. 163–166.

Wagner, G. S., Macfarlane, P., Wellens, H., Josephson, M., Gorgels, A., Mirvis, D. M., Pahlm, O., Surawicz, B., Kligfield, P., Childers, R., and Gettes, L. S. (2009). 'AHA/ACCF/HRS Recommendations for the Standardization and Interpretation of the Electrocardiogram', *Circulation*, **119**(10), pp. e262–e270.

Waks, J. W., and Buxton, A. E. (2018). 'Risk Stratification for Sudden Cardiac Death After Myocardial Infarction.', *Annual review of medicine*, **69**, pp. 147–164.

Walker, H Kenneth and Hall, W Dallas and Hurst, J. W. (1990). '*Clinical methods: the history, physical, and laboratory examinations*'.

Waller, A. D. (1887). 'A Demonstration on Man of Electromotive Changes accompanying the Heart's Beat', *The Journal of physiology*, **8**(5), pp. 229–234.

Wang, A., Yang, L., Liu, C., Cui, J., Li, Y., Yang, X., Zhang, S., and Zheng, D. (2015). 'Athletic Differences in the Characteristics of the Photoplethysmographic Pulse Shape: Effect of Maximal Oxygen Uptake and Maximal Muscular Voluntary Contraction', *BioMed Research International*, **2015**, 752570.

Yang, H. (2011). 'Multiscale recurrence quantification analysis of spatial cardiac vectorcardiogram signals.', *IEEE transactions on bio-medical engineering*, **58**(2), pp. 339–347.

Yang, H., Bukkapatnam, S. T., and Komanduri, R. (2012). 'Spatiotemporal representation of cardiac vectorcardiogram (VCG) signals', *BioMedical Engineering Online*, **11**(1), pp. 1–15.

Yang, H., Kan, C., Liu, G., and Chen, Y. (2013). 'Spatiotemporal Differentiation of Myocardial Infarctions', *IEEE Transactions on Automation Science and Engineering*, **10**(4), pp. 938–947.

Yeragani, V. K., and Kumar, H. V. (2000). 'Heart period and QT variability, hostility, and type-A behavior in normal controls and patients with panic disorder.', *Journal of psychosomatic research*, **49**(6), pp. 401–407.

Yeragani, V. K., Pohl, R., Balon, R., Jampala, V. C., and Jayaraman, A. (2002). 'Twenty-four-hour QT interval variability: increased QT variability during sleep in patients with panic disorder.', *Neuropsychobiology*, **46**(1), pp. 1–6.

Zaza, A., Malfatto, G., and Schwartz, P. J. (1991). 'Sympathetic modulation of the relation between ventricular repolarization and cycle length.', *Circulation Research*, **68**(5), pp. 1191–1203.

Zhang, Z. (2016). 'Introduction to machine learning: k-nearest neighbors', *Annals of translational medicine*, **4**(11), 218.

Zhou, J., Chang, P., Lin, J., and Wu, Y. (2011). 'Myocardial infarction classification using polynomial approximation and principal component analysis', *International Conference on Computer Engineering and Technology, 3rd (ICCET 2011)*, pp. 689–699.

Zifan, A., Moradi, M., Saberi moghadam, S., and Towhidkhah, F. (2005). 'Automated ECG Segmentation Using Piecewise Derivative Dynamic Time Warping', *Int. J. Biolog. Med. Sci.*, **1**(3).

Zipes, D. P., and Wellens, H. J. J. (1998). 'Sudden Cardiac Death', *Circulation*, **98**(21), pp. 2334–2351.

Zywietz, C., Wagner, G., and Scherlag, B. (1986). 'Sampling rate of ECGs in relation to measurement accuracy', *Computerized Interpretation of the Electrocardiogram. New York, NY: Engineering Foundation*, pp. 122–125.